DESIGN AND ANALYSIS OF A CONSTANT ENVELOPE-MULTICARRIER MODULATION SCHEME FOR MULTI-USER SYSTEM BASED ON MMWAVE MIMO FOR 5G COMMUNICATION SYSTEM

Chrianus Kyaruzi Kajuna
EE300-0002/16

A thesis submitted to Pan African University Institute for Basic Sciences, Technology and Innovation in partial fulfillment of the requirements for the award of the degree of Master of Science in Electrical Engineering (Telecommunication Engineering)

June 2018

DECLARATION

This work is my original work and has never been presented for a degree in any other university.

Signature ……. Date 23/01/2018

Chrianus Kyaruzi Kajuna

This Thesis has been submitted for examination with approval as University Supervisors

Signature …… Date 23/01/2018

Prof. Claudio Sacchi

UNITN, Italy

Signature ……. Date……

Dr. Kibet Langat

JKUAT, Kenya

DEDICATION

I dedicate this work to my son Jayson Kajuna and my brothers, Mr. James Kajuna, Mr. Dezidery Kajuna, and Mr. Deus Kajuna for their incredible moral support through my entire academic career.

ACKNOWLEDGEMENT

Firstly, I recognize God's blessings toward good health and wellbeing enabling me to complete this work. Secondly, I would like to express my sincere gratitude to my supervisors Prof. Claudio Sacchi, and Dr. Kibet Langat for their immense support and motivation toward selecting the area of research, setting up the research system and troubleshooting the system in the right way.

Finally, I offer my sincere thanks to African Union, and JICA for providing financial support. Again much gratitude to Jomo-Kenyatta University of Agriculture and Technology, and Pan-African University staff for their assistance toward accomplishing my research is highly appreciated. Lastly I acknowledge my classmates for their significant supports and advice that made me to have hope of completing my research work.

TABLE OF CONTENTS

LIST OF TABLES

LIST OF FIGURES

LIST OF ABBREVIATIONS AND ACRONYMS

1G	First Generation
2G	Second Generation
3G	Third Generation
4G	Fourth Generation
5G	Fifth Generation
AE	Antenna Elements
AWGN	Additive White Gaussian Noise
AoA	Angle of Arrival
AoD	Angle of Depression
BER	Bit-Error-Rate
BLAST	Bell Labs Layered Space Time
BS	Base station
CCDF	Complementary Cumulative Distribution Function
CDF	Cumulative Distribution Function
CDMA	Code Division Multiple access
CE	Constant Envelope
CE-OFDM	Constant Envelope Orthogonal Frequency Division Multiplexing
CE-SCFDMA	Constant Envelope-Single Carrier-Frequency Division Multiple access
CFO	Carrier Frequency Offset
CSI	Channel System Information

CP	Cyclic Prefix
D-BLAST	Diagonal Bell Labs Layered Space Time
DFT	Discrete Fourier Transform
DM	Dispersion Matrix
DMT	Diversity-Multiplexing Trade-off
EHF	Extremely High Frequency
FD	Frequency Domain
FDE	Frequency Domain Equalizer
FFT	First Fourier Transform
GA	Genetic Algorithm
GSM	Global System for Mobile Communications
HPA	High Power Amplifier
IBO	Input-Back-Off
ICI	Inter-Channel Interference
IDFT	Inverse Discrete Fourier Transform
IFFT	Inverse First Fourier Transform
i.i.d	independent and identically distributed
ISD	Inter Cite Distance
ISI	Inter-Symbol Interference
LDC	Linear Dispersion Coding
LEO	Low Earth Orbit
LMDS	Local Microwave Distribution Service
LMS	Land Mobile Satellite

LOS	Line-Of-Site
MC	Multicarrier
MIMO	Multiple Input Multiple Output
MRRC	Maximum Receiver Ratio Combining
MU-MIMO	Multi User Multiple Input Multiple Output
ML	Maximum Likelihood
mmWave	Millimeter Wave
MMSE	Minimum Mean Square Error
NLOS	Non Line-Of-Site
OBO	Output-Back-Off
OFDM	Orthogonal Frequency Division Multiplexing
OOB	Out of Band Power
PAPR	Peak-to-Average Power Ratio
PA	Power Amplifier
PHY	Physical
PTS	Partial Transmit Sequence
PM	Phase Modulation
QAM	Quadrature Amplitude Modulation
QoS	Quality of Service
RF	Radio Frequency
SC-FDE	Single Carrier Frequency Domain Equalizer
SD	Symbol Detector
SHF	Supper High Frequency

SLM	Selective Mapping
SM	Spatial Modulation
SISO	Single Input Single Output
SSCM	Spatial Correlation Channel Model
SSK	Space Shift Keying
SSPA	Solid State Power Amplifier
ST	Space Time
STBC	Space Time Block Coding
STC	Space Time Coding
STSK	Space Time shift keying
SMUX	Spatial multiplexing
SM-MIMO	Spatial Modulation Multiple Input Multiple Output
SNR	Signal-to-Noise Ratio
SU-MIMO	Single User Multiple Input Multiple Output
TDMA	Time Division Multiple Access
TWTA	Travelling-Wave Tube Amplifier
UE	User Equipment
V-BLAST	Vertical Bell Labs Layered Space Time
WCDMA	Wideband Coding Division Multiple Access
ZF	Zero- Forcing

ABSTRACT

The Orthogonal Frequency Division Multiplexing (OFDM) used in 4G has been suggested for application in 5G with modification to avoid high signal amplitude fluctuations which causes the problem of peak-to-average power ratio (PAPR). The presence of high PAPR influences OFDM sensitivity to nonlinear distortion caused by the transmitter's power amplifier (PA). In the absence of power back-off, which is the reduced output power when the input power is decreased, the system experiences spectral broadening, intermodulation distortion and performance degradation. The efficiency of PA is reduced with increase in back- off, therefore, this is a particular problem for mobile battery device due to limit in its power resources. A new mitigation technique for PAPR is the use of constant envelope multicarrier.

The Constant Envelope Orthogonal Frequency Division Multiplexing (CE-OFDM) scheme reduces PAPR to 0 dB in which the signal is transmitted with saturating amplifiers without amplitude distortion and spectral regrowth. The CE-OFDM has only been investigated in single input single output (SISO) scheme, with transmission in millimeter wave (mmWave) frequencies (E-band frequencies) 71-76GHz and 81-86GHz channels to provide enough bandwidth that can overcome the growing demands of communication. However, SISO systems have limited capacity and throughput. To mitigate against this for 5G application, Multiple Input Multiple Output (MIMO) is required. The recent new type of MIMO introduced by Sugiura et al. called Space Time Shift Keying (STSK) is capable of achieving high diversity-multiplexing tradeoff (DMT) as compared to other types MIMO.

In this work, the STSK CE-OFDM in mmWave transmission has been designed.

The transmission performance analysis was done by comparing the Bit-Error-Rate (BER) against Signal-to-Noise-Ratio (SNR) in a dense urban environment for small cell backhaul technology in the absence of phase noise effects. The simulation analysis was carried out with respect to line of sight (LOS) for Uplink transmission in 73GHz mmWave channel, with 2×2 antenna system and STSK configuration being adapted from previous work. The results show that STSK CE-OFDM in mmWave channel experiences a decrease in BER as the modulation index (MI) increases. In addition, the STSK CE-OFDM outperforms the STSK OFDM when a non-linear power amplifier is adopted.

Generally, the designed STSK CE-OFDM system is recommended for uplink communication due its ability of consuming low power since it has 0 dB PAPR. The application of this system to uplink communication will increase the battery life and minimize the communication cost to the end user.

CHAPTER ONE

INTRODUCTION

1.1 Background

The exponential demand in wireless communication services has influenced the improvement in innovation of cellular communication network. The evolution of mobile communication has been a progressive event since 1970s with the introduction of First Generation (1G) mobile network that used FDMA and was used for voice signal only with less robustness. This was followed by second generation (2G) in 1990s and Third generation (3G) followed thereafter. Each evolution has been an improvement of the other. Thus, 2G was able to accommodate voice and data with digital transmission mechanism and employs Time Division Multiple Access (TDMA) and Code Division Multiple Access (CDMA). It was based on Global System for Mobile Communications (GSM) standards. The 3G differs from the earlier generations due to its ability of using packet switching transmission scheme, with improved service such as allowing internet and mobile telephone customers to use audio, graphics and video streaming applications [1]. It was based on Wideband (CDMA) modulation scheme with the widespread availability of good quality coverage and improved speed and greater network capacity. In 4G, better performance was noted due to improved Quality of Service (QoS). It also used Orthogonal frequency multiplexing (OFDM) as the modulation scheme, with improved features such as orthogonal sub-carrier which mitigate the inter symbol interference (ISI) compared to previous generations. However, due to the growing demands for cellular services, 4G has been found to be limited in terms of capacity, speed, and coverage. This has resulted in

increased research to overcome these challenges [1][2]. The next Fifth Generation (5G) is expected to offer solutions to these problems encountered in the 4G. A new modulation scheme with application Massive Multiple Input Multiple Output and mmWave technology has been proposed in the literature as one of the technique to alleviate these challenges [3]. Under this 5G, information is expected to be shared "*anywhere and anytime for anyone and anything*". To achieve such information sharing, MIMO, millimeter wave and small cell technology have been investigated and adopted for communication improvement [4].

1.1.1 Multiple Input Multiple Output (MIMO)

MIMO technology refers to simultaneous transmission of multiple data streams from transmitters to receivers. MIMO technology can significantly improve system performance in coverage, capacity, and user data rates by neutralizing the effect of multipath fading [5]. MIMO technology uses multiple "smart" transmitter and receiver antenna with an added "spatial diversity" to overcome multipath effects that increases performance and range significantly. Also the throughput of the channel increases due to use of multiple antennas [6]. Using multiple antennas results in a smaller probability of error which increases the system performance. In addition, multiple antennas can be used to increase the transmission rate. Massive MIMO in Uplink scenario has the ability of radiating maximum energy to a required point that lead to high array gain which is facilitated by coherent combination[7]. In downlink scenario, the base station BS radiates energy into spatial direction where user equipment is located. Therefore, the transmitter power for each user is reduced since negligible power is lost. The two main objectives for MIMO are summarized as follows[8]:

1.1.1.1 Spatial diversity in MIMO system

The wireless communications normally are affected by multipath fading. Therefore, to ensure proper communication through air, this problem should be taken care of. Spatial diversity basically eradicates channel fading by transmitting multiple signal copies across multiple independent paths. This process implies that the when the same information is sent through different paths the received signal with be channel fading free with a sense that when there is a signal power loss in one path then that losses will be compensated by other signal received from different path. The spatial diversity approaches infinite when the number of transmit or receive approach to infinite and that situation make the channel to behave as AWGN channel. Thus improves the signal to noise ratio of the channel [8-9].

1.1.1.2 Spatial multiplexing in MIMO system

This is another means of combating the fading effect of the channel by increasing the data throughputs. The spatial multiplexing is capable of increasing the transmission rates (through puts) while maintaining the same bandwidth and power expenses. In spatial multiplexing the receiver is assumed to have knowledge of the what happened at the transmitter. For example, for two transmit and two receive antennas system, a bit stream is split into half-bit stream in which they simultaneous modulated and transmitted to both antennas. Since the channel information (CI) is known, then the receiver can recover the original bit stream by combining the individual bit streams. The different bit streams enable to carry different data. Thus the data rate increases as the number of transmit or receive antennas increases.

These two goals have been the crucial areas for achieving better MIMO technology capable of supporting the requirements for future communication [12]. To achieve the above

objectives, Space-Time coding has attracted a great attention due its capability of achieving the extreme possible diversity. The space-time codes (STC) provide a diversity gain equal to the product of the number of transmit (*N*) and receive antennas (*M*), while Spatial multiplexing provides better multiplexing gain. The example of STC is spatial modulation (SM) which is rich in diversity. However, spatial multiplexing (SMUX) is a better choice for high rate systems operating at relatively high Signal-to-Noise-Ratio (SNRs) while space-time coding is more appropriate for transmitting at relatively low rates and low SNRs. The example of SMUX technology is Bell Labs Layered Space-Time (BLAST) architectures [13].

1.1.2 MIMO System Model

MIMO system with transmit antennas N_t and receive antennas N_r, as shown in Figure 1.1. The signal matrix transmitted is $N_t \times 1$ column matrix of x where x_i is the *i*-th component; transmitted from antenna i. Assuming the channel is a Gaussian channel, in such a way that elements of x are considered to be independent and identically distributed (i.i.d.). Gaussian variables. Since channel is unknown at the transmitter, then each transmitted antenna is assumed to have equal powers of E_s/N_t where E_s represents total transmitted power without regarding the number of transmit antenna. The channel matrix H is an $N_r \times N_t$ complex matrix. The fading coefficient from the *i*-th transmit to *j*-th receive antenna is represented by component $h_{i,j}$ of the matrix[4-5][8].

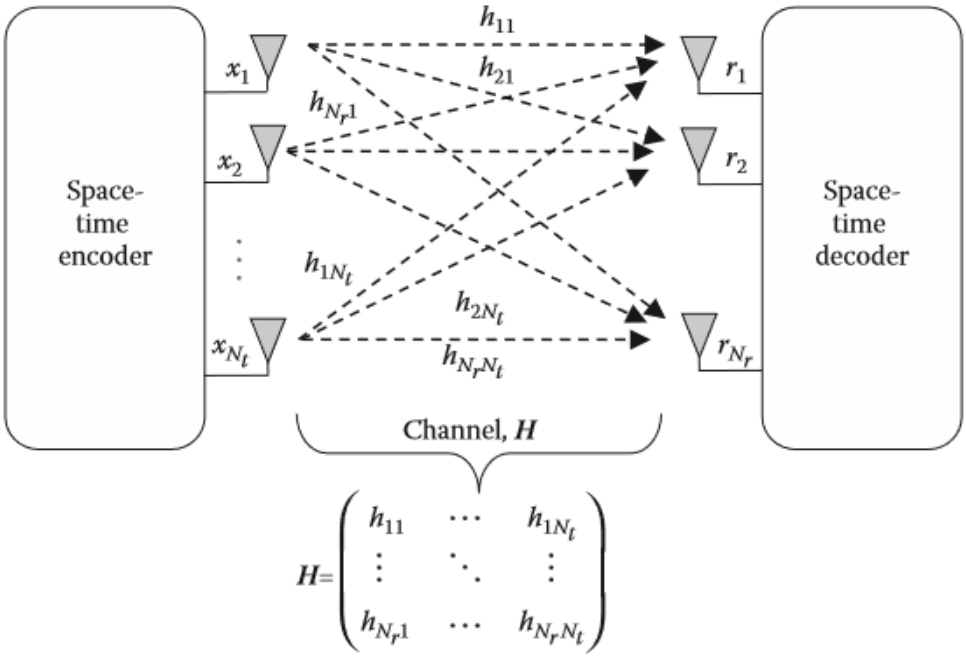

Figure 1.1: block diagram for MIMO system

When the signal attenuation, and gain are neglected the system is normalized with received power for each receive antennas equal to the total transmitted power. Therefore, the received signal is expressed as N_r *x 1* matrix and can be denoted as $\mathbf{r}$, where each component refers to a receive antenna and can be expressed as [9] [12];

$$\boldsymbol{r} = \boldsymbol{Hx} + \boldsymbol{n} \qquad \textbf{(}1.1\textbf{)}$$

The equation (1.1) can be written in the form of a matrix as shown below in equation (1.2)

$$\begin{pmatrix} r_1 \\ r_2 \\ \vdots \\ r_{N_r} \end{pmatrix} = \begin{pmatrix} h_{11} & \dots & h_{1,N_t} \\ \vdots & \ddots & \vdots \\ h_{N_r,1} & \dots & h_{N_r,N_t} \end{pmatrix} \begin{pmatrix} x_1 \\ \vdots \\ \vdots \\ x_{N_t} \end{pmatrix} + \begin{pmatrix} n_1 \\ \vdots \\ \vdots \\ n_{N_r} \end{pmatrix} \qquad \textbf{(}1.2\textbf{)}$$

Where $\boldsymbol{n}$ is noise at the receiver with the size of $N_r \times 1$. However, the required MIMO technology to support next generation must be able to exploit both spatial diversity and

spatial multiplexing gain concurrently. MIMO technology involves two scenarios which are; Single User MIMO(SU-MIMO) and Multi user MIMO(MU-MIMO) [8].

Single user MIMO **(**SU-MIMO) this happen when more data is needed to be sent to one user. It involves transmitting multiple streams of data from multiple antennas to a single user. In this scenario the spatial dimension is limited by number of antennas acceptable on mobile device. MU-MIMO is the MIMO system in which data is needed to be sent to many users. This involves simultaneous independent transmission of data using multiple antenna at the transmitter and independent reception using multiple antenna at the receiver. Their main differences between the two MIMO system is that, the SU-MIMO experiences limited throughput, and limited capacity unlike MU-MIMO [4-5].

There are a number of advantages of application of MU-MIMO over conventional MIMO [9]- [11].

❖ Huge spectral efficiency and high communication reliability.

Ability of MU-MIMO of providing large multiplexing gain which depend on the increase in number of transmitter antenna and receiver antenna facilitate the achievement of high diversity with order of the number of the transmitter antenna. Thus the increase the number of transmitter and receiver antenna lead to increase in spectral efficiency and enhance the communication reliability.

❖ High energy efficiency.

MU-MIMO in Uplink scenario has ability of radiating maximum energy to required point this lead to high array again which is facilitated by coherent combining. Therefore, the transmitter power for each user is reduced since negligible power is lost. At downlink scenario the base station BS radiates energy into spatial direction

where user equipment is located. example, with massive antenna arrays, the radiated power can be reduced by the order of magnitude or more that lead to achieve of high energy efficiency. For fixed users, the double increase in the number of transmitter antenna while reducing the transmit power by two, the original spectral efficiency can be maintained hence the radiated energy efficiency is doubled.

❖ Simple signal processing

MU-MIMO is capable of using excessive transmitter antenna over receiver which allows the favorable propagation environment. Thus the channel vectors between the transmitter and the receiver is nearly orthogonal. Therefore, the effect of interference can be eliminated by employing simple linear processing technique.

However, the advantage of MU-MIMO comes with several expenses such as

❖ Multiuser interference: since involves many users, it experiences significant performance degradation because of interference between users. Therefore, to handle these cases the interference cancellation or reduction mechanism should be applied such as maximum likelihood multiuser detection, dirty paper coding technique or alignment of interferences. However, these reduction techniques are complex.

❖ Channel state information is required: in order to maximize the spatial multiplexing, gain the transmitter and the receiver should have knowledge of the channel. In higher mobility scenario this process is difficult since it requires accurate and timely acquisition of CSI.

❖ User scheduling: Scheduling increases the expenses due to several users being served at same time-frequency resource

1.1.3 Millimeter Wave Communication

The millimeter wave (mmWave) refers to the wave with longer wavelength than infrared waves or x-rays but shorter than radio wave or microwave. It is electromagnetic spectrum corresponds to radio band frequencies that ranges from 30GHz to 300GHz. It is referred as the Extremely High Frequency (EHF). However, the super high frequency band with frequency range from 3GHz to 30GHz experiences the same properties with the EHF band. This makes the overall frequency band for mmWave to fall in the range from 3GHz to 300GHz with wavelength range 1mm to 100mm [3]. It has been standardized as the physical layer (PHY) for 5G[3]. The utilization of mm Wave in 5G technology has several advantages. These include, enough spectrum which facilitate use of large antenna arrays as many as 8 to 256 elements and 9 to 24 in link budget at both transmitter and receiver ends. It also provides sub-millisecond latency which makes the network smart and intelligent. The figure 1.2 shows different radio frequency spectrum distribution by International Telecommunication Union (ITU). This distribution is in every country [3].

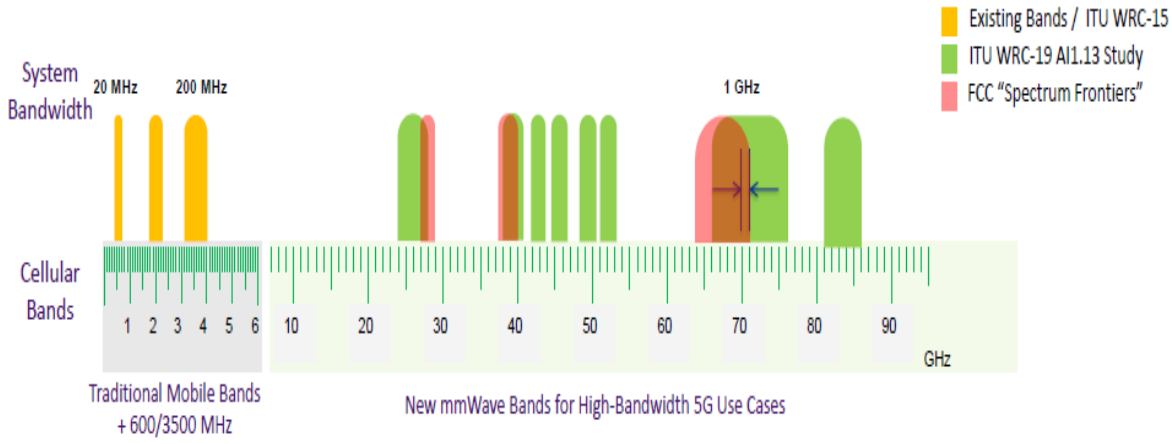

Figure 1.2: mmWave Spectrum [3]

According to ITU-R regulation, there are several frequency bands such as 28GHz band, which is called Local Microwave distribution service (LMDS) band, 38GHz band identified as useful for fixed microwave services, and provide point-to-point microwave operation specifically backhaul services. Another band is called 60GHz band, which is unlicensed band. This band experiences large absorption effect of Oxygen but less effect to cellular communication in small area of less than 200m. The E-band at 71GHz-76GHz, 81GHz-86GHz is licensed and useful for mobile communication since the oxygen attenuation is less than that of 60 GHz band. Rain attenuation can highly affect the communication in the E-band unless it is applied in small cell cellular networks. The last band is 92GHz –95GHz which is an unlicensed band [3][20].

1.1.4 Small Cell Technology

The term '*small cell'* the collective term used to describe several different types of cells, including femtocells, picocells, microcells, metrocells, and ruralcells. Small cell technology is the low-powered radios (i.e. maximum output of 10W) with a range of coverage and capacity of 100 – 200m inter site distance (ISD) [21].

The 5G is expected to apply small cell technology that can facilitate the increase in data traffic volume, spectral efficiency, and energy and cost reduction. The traffic volume per mobile for 5G technology is expected to be 1000x higher, 10-100x devices interconnection, 10-100x data rate and 10x power saving battery as well as 5x reduced end to end delay. This can be achieved with the combination of MIMO technology and mmWave operating in small cell. The size of the cell will limit effect on performance due to factor such as multipath, rain effect which is measured per kilometer [21].

1.1.5 Backhaul technology

Backhaul refers to the transportation of information between the wireless access points to the public network, or the Internet in case of a Wireless LAN. The backhaul small cell is the technology that facilitate better coverage and capacity for small cell technology.

In 5G technologies, the small call backhaul technology has been investigated and proved to be a good communication strategy[22]. To ensure the integrity and proper information flow within the cell to a core network, backhaul technology is applied. Therefore, in small cell, backhaul guarantees the required throughput. The following are the advantages of backhaul system in small cell technology[23]:

i. It reduces the latency to small sub-millisecond or less that can facilitate two-way gaming.
ii. It provides support where there is no direct communication connection (LOS).
iii. It connects several small cells within intra distance of 30 to 300 within small geographic area of few kilometers.
iv. It guarantees the high throughput hundreds of Mbps to tens of connected small cells.

1.2 Problem statement

The limitations of Fourth generation (4G) cellular network are its inability to overcome exponential growth of demands of high data rate, coverage and capacity to accommodate growing number of users. These problems are attributed to multicarrier modulation scheme used in 4G which is OFDM. The envelope fluctuation of OFDM modulation requires high power amplifier input back-off (IBO) which lead to high power consumption. This will also lead to a decrease in spectral efficiency resulting in poor coverage with respect to the

demand. In addition, OFDM is a good candidate in supporting 5G technology with some modifications required. The multicarrier waveform with almost constant envelope, low spectral occupancy, and high capability of exploiting diversity in the frequency domain is needed. This will be able to overcome the limitation of 4G cellular network. Different research has been done on constant envelope Orthogonal Frequency Division Multiplexing (CE-OFDM) primarily proposed by Thomason et al. [24] and Constant envelope Single carrier frequency multiple access for satellite communication by Claudio et al [25] both implemented is a single input single output system. Better performance has been shown in [25] with almost the same performance features as in [24] both with 0dB Peak to Average Power ratio (PAPR) and improved features than conventional OFDM. However, CE-OFDM has not been investigated for multiple user management in the Uplink. The effect of high PAPR in OFDM affects the performance of power amplifier. Because of this problem in OFDM, its application becomes limited in the Uplink communication since mobile handsets need a scheme that can support long life power battery while maintaining its performance.

1.3 Objective of the study

1.3.1 General objective

The main objective is to design and analyze a constant envelope-multicarrier modulation scheme for multi-user system based on mmWave MIMO for 5G communication system.

1.3.2 Specific objectives

i. To investigate the performance of STSK OFDM on mmWave Transmission with different signal detection scheme.

ii. To design constant envelope OFDM MIMO space Time shift Keying based on mm Wave Transmission.

iii. To analyze performance of CE-OFDM STSK against OFDM STSK based on mm Wave Transmission for uplink scenario.

1.4 Justification

This thesis is the extension of the design suggested in [28] to be implemented in multi user system specifically using the Space Time shift keying (STSK) Multiple Input Multiple Output system. This will aid in maximizing the throughput, coverage and reduced power consumption with improved diversity gain and multiplexing gain for uplink mobile communication. The constant envelope Orthogonal Frequency Division multiplexing in MIMO system implemented in millimeter wave channel, proved to be a good candidate for uplink for 5G mobile communication technology requirements. Orthogonal Frequency Division Multiplexing used in 4G and proposed to be used in 5G has been noticed to have weakness such as high side lobe with high PAPR. Therefore, the constant envelope OFDM based on millimeter wave transmission channel with Space Time Shift Keying MIMO can improve performance in Uplink communication in small cell backhaul in dense urban areas.

1.5 Scope of study

The focus of the work is in designing a new waveform for uplink mobile communication implemented in multi user system. The Space Time Shift Keying Constant Envelope Orthogonal Frequency Division Multiplexing (STSK CE-OFDM) was implemented under millimetre Wave channel. In this work only lower modulation order of 4QAM has been investigated under preferable trade-off dispersion matrix of Q equal to 4. The performance

of STSK OFDM mmWave channel has been investigated using different signal detection mechanism. These detection mechanisms are Maximum likelihood detection and other liner signal detection such as Minimum Mean Square Error and Zero forcing detection mechanism. The investigation of performance of Space Time Shift Keying CE-OFDM and Space Time Shift Keying OFDM was done only for uncoded signal. This work only focused on transmission without involving the hardware effect on the system (phase noise). Furthermore, this work has demonstrated tremendous performance of the new MIMO modulation System. The results are analysed and discussed in two channel states; Additive White Gaussian Noise (AWGN), and dispersive mmWave channel under Line of Sight (LOS) condition. The effect of power amplifier to nonlinearity property is considered with Gallium Nitride (GaN) amplifier. Finally, the 2x2 antenna configuration was considered for this work.

1.6 Organization of the thesis

In this thesis Space Time Shift Keying MIMO system has been studied in detail and used to implement the constant envelope OFDM STSK MIMO scheme. The organization of the thesis is presented as follows.

Chapter 1: This section covers the background of the study, the problem statement supported by objectives, then finally justification and scope of the study.

Chapter 2: This cover the literature review and brief understanding the STSK OFDM, CE-OFDM and transmission of millimetre wave.

Chapter 3: covers the methodology with simulation flow and block diagram of the novel design.

Chapter 4: covers the results and discussion of the results of the study.

Chapter 5: The conclusion of the thesis and recommendation for further works is presented in this chapter.

1.7 Note on publication

A paper entitled ‘Space Time Shift Keying (STSK) MIMO based on Constant Envelope multicarrier multiple accesses in different antenna configuration under AWGN channel”, has been published in the **International Journal of Applied Engineering Research**. The paper is based on some part of research work presented in this thesis and the rest of the work is in process to be published. This paper was the basis of the design of the study which only analysed the performance at different modulation indices. A copy of the published paper is attached in the appendix II and can be cited as shown below:

C. Kajuna, C. Sacchi, K. Langat, T.F. Rahman, “Space Time Shift Keying (STSK) MIMO based on Constant Envelope multicarrier multiple access in different antenna configuration under AWGN channel,” International Journal of Applied Engineering Research (IJAER), Vol.24, no.12, pp 15848 – 15854, 2017.

CHAPTER TWO

LITERATURE REVIEW

There has been growing research on the next generation of wireless communication including the 5G, and its enabling technologies. The aims of these researches are to have a wireless communications system that provides high data rates, very low latency, and increase in base station capacity, and improved quality of service (QoS) as compared to the current 4G LTE networks. Some of these research includes work in Orthogonal Frequency Division Multiplexing (OFDM), Constant Envelope Orthogonal Frequency Division Multiplexing (CE-OFDM) [24], MIMO systems, Millimeter wave transmission and Space Time Shift Keying (STSK) MIMO. This chapter provides the literature review on OFDM, CE-OFDM, and MIMO systems in millimeter wave transmission for wireless communication.

2.1 Millimeter Wave Transmission Channel

With the rapid growth in demand for wireless communication services, high network capacity is required. However, the current network systems have faced increasing shortage in spectrum. The current research on 5G is expected to exploit the large amount of spectrum in the mmWave frequency bands of 30 – 300 GHz to increase the much needed communication capacity [22], [23]. The mmWave bands were once an afterthought for cellular because of the perceived increase in oxygen absorption and rain attenuation compared with today's cellular bands. However, researchers have indicated that the frequency band 28 GHz, 38 GHz, 60 GHz, and 73 GHz the E-band experience negligible effect of atmospheric attention when small cell technology is applied with maximum inter

site distance of 100 m. In addition, it has been shown that the effect of rain attenuation is small such that for heavy rainfall of 25 mm/hr, attenuation is only 1.4 dB at 28 GHz, 1.6 dB at 38 GHz, and 2 dB at 73 GHz at distances of 200 m [29], [34], [89]. Therefore, the application of small cells experiences negligible atmospheric attenuation compared with the current cellular cells. Since attenuation is determined per distance covered by cell in kilometer, then as the cell becomes smaller the atmospheric attenuation becomes negligible [29].

Various studies for the 28GHz band were done to assess coverage, large-scale path loss, and fading and multipath effects. Measurements by Elrefaie and Shakouri showed that better coverage was obtained for higher transmitter (TX) antenna heights than for lower heights due to less obstructions [30]. Violette et al. performed wideband non-line-of-sight (NLOS) studies for the 9.6, 28.8, and 57.6 GHz bands, and measurements indicated significant signal attenuation (as great as 100 dB) due to large building obstructions [23]. Penetration tests for glass with metalized layers showed that attenuation increased by 25 to 50 dB per layer [30]. The results also revealed that delay spreads were not more than 10 ns relative to the LOS component when transmitting over 500MHz of bandwidth while using narrow beam, linearly polarized antennas. Foliage attenuation measurements at the 35 GHz band resulted in a mean attenuation of 24.8 dB through approximately 15 m of red pine trees, and revealed a considerable loss in excess of free space [29-30].

The 60 GHz band has been one of the most studied mmWave bands as it is currently used for unlicensed Wireless HD and Wireless Gigabit Alliance (WiGig) WLAN devices [90], [91], that offer multiple gigabits per second data rates for short range indoor communications. A majority of measurements were conducted for indoor applications due

to the earliest intended use cases, WLAN, and high oxygen absorption centered around 60 GHz [34]. However, with the 2013 FCC part 15 rule change that greatly expanded the effective radiated power of WLAN devices in the 60 GHz band from 40 to 82 dBm [90], 60 GHz outdoor communication for unlicensed backhaul applications has just recently garnered great interest. Outdoor studies at 59 GHz were conducted in Oslo city streets, and showed that a majority of delay spreads were less than 20 ns over 7 different street scenarios for LOS and obstructed environments [92].

Wideband measurements with 200 MHz of bandwidth revealed that city streets do not cause much multipath, as the RMS delay spread was observed to be lower than 20 ns [93]. Measurements and models showed that path loss in LOS environments behaves almost identical to free space, with a path loss exponent (PLE) of 2 (i.e., power decays as the square of the distance). In regards to path loss between 1.7 GHz and 60 GHz, Smulders et al. showed that the most significant difference in path loss between these frequency bands is the initial close in free space path loss induced by the increase in carrier frequency due to Friis' free space equation [93], [94]. Other outdoor measurements in a city street environment at 55 GHz showed that power decreased much more rapidly with distance through narrower streets com- pared to a direct path or through wide city streets [95], and the coherence bandwidth range of 20–150 MHz closely matched the results by Violette et al. in [24].Additionally, recent outdoor studies at 60 GHz in a street canyon environment indicated that the LOS path is most dominant but that the ground reflected path is significant at larger distances where the LOS path may be blocked, resulting in an overall PLE of 2.13, very close to theoretical free space (PLE = 2) [96].

The 73 GHz was investigated in [31] which involved the E-band propagation measurements for both mobile and backhaul scenarios in [29-30] in a dense urban environment in New York city using a sliding correlator channel sounder. The outdoor measurement results showed that application of directional steerable antennas is advantageous, particular in achieving comparable path loss and channel statistics in previous work [29-30]. The investigation relating the 28 GHz and 73 GHz both with bandwidth of 500MHz in a small cell of 200m found that mmWave propagation in different bands experience comparable properties and viable for eLA access when directional and high gain antennas are used for receiving point and access points. Also, it was found that in every band experiences similar coverage, when large antenna array is used at high band to compensate for the path loss at high and low mmWave bands. The eLA system achieves peak data rate more than 10Gbps and more than 100 edge data rate due its ability to exploit large bandwidth in mmWave channel [32]. However, measurements showed that the 73 GHz channel experienced a high path loss that limits the capacity to half of that achieved with 28 GHz channel. Moreover, the use of a double antenna design alongside 73 GHz channel at the transmit side yields better results in comparison to the 28 GHz channel. This is because of its ability to exploit MIMO spatial diversity without changes in array size.

Authors in [33] highlighted that the measurement that was conducted at New York City for 28GHz and 73GHz provided the first real-world measurement. Thus, a comprehensive spatial statistical channel (SSC) model was derived for key channel parameters such as spatial clusters, outage, path loss and angular dispersion. The SSC model provide the realistic mmWave assessment for micro- and pico-cellular networks in a dense urban area.

According to [33], with the cell size being within 100-200 meters, the results indicated that strong signal can be detected in a highly non-line of sight environment.

Since small cell technology is expected to be implemented in 5G, mmWave MIMO is the best choice for future communication system technologies that provide affordable communication expenses. The mmWave MIMO was suggested by 3GPP standardization wireless solution for backhaul systems for LOS and NLOS in [35]. Research has shown that there is up to 5 GHz contiguous bandwidth in the E-band that can be used for both backhaul and mobile accesses for 5G communication [39]. Measurements conducted in [39] were performed to evaluate propagation characteristics in the mmWave channel. Key propagation parameters such as delay spread, path loss, and number of multipath components were determined at the frequency of 73 GHz. These were aimed at developing temporal and spatial channel models to be used in designing future generations of wireless systems such as 5G.

Regarding the above literatures, the real-world measurements for 73GHz for mmWave has been identified as the prototype for multipath channel for 5G communication. The increase in throughputs for 5G will be achieved by implementing MIMO system in which STSK MIMO system has been identified by different researchers as best MIMO scheme. [41], [48], [50], [51].

2.2 Orthogonal Frequency Division Multiplexing (OFDM)

The multi-carrier systems basically involve a splitting of a high-data-rate order into a number of lower-rate order that are transmitted simultaneously over a number of subcarriers. The fact that

the symbol duration for the low-rate parallel subcarriers increased, relative amount of dispersive time triggered by multipath delay spread reduces. The guard interval at each start of orthogonal frequency division multiplexing (OFDM) symbol is introduced so that to eliminate inter-symbol interference (ISI) [8].

Orthogonal Frequency-Division Multiplexing (OFDM) is a multicarrier modulation technique that uses the sub stream spectrum overlapping concept, where each sub stream is orthogonally transmitted through a sub channel, and they can be separated in a demodulator. The ability of OFDM to offer greater resistance over multipath fading and impulsive noise channels eradicates the need for complicated equalizers, because it is efficiently capable of transforming a frequency-selective fading channel into a flat fading channel. This process is achieved by subdividing the channel into smaller sub-bands, or subcarriers [64].

The OFDM was designed as a special case for Frequency Division Multiplexing (FDM) with a more efficient way of packing data on the spectrum than in the conventional FDM techniques. A comparison of FDM and OFDM can be observed in figure 2.2 in (a) and (b). The OFDM subcarrier are more overlapped and orthogonal which make it more advantageous in terms of spectral efficiency than FDM [73].

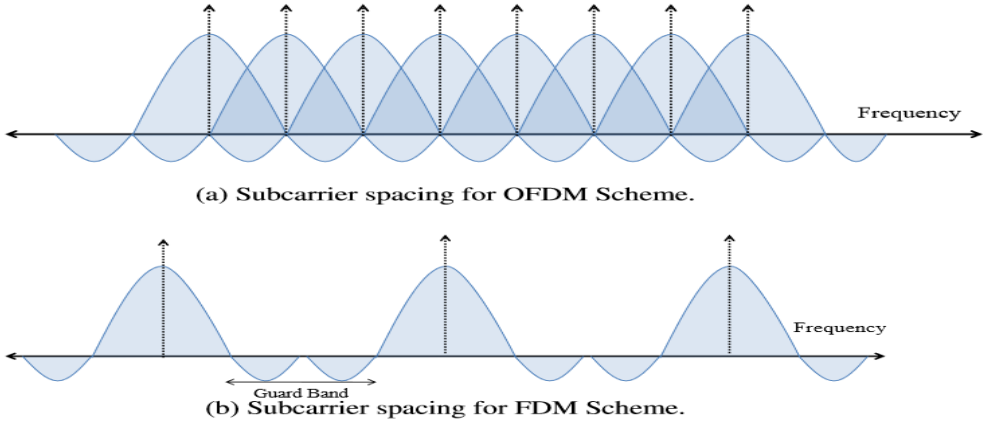

Figure 2.1: OFDM and FDM subcarrier spacing comparison

Furthermore, OFDM performance is limited by two major problems which are high waveform amplitude fluctuation which cause high Peak Average Power Ratio (PAPR) [73], and large power spectral side lobe and dedicated transmission processing before transmission.

For uplink communication, OFDM must be modified to acquire the above explained factors in order to enable efficient performance of mobile phone.

The OFDM system can be implemented based on the block diagram illustrated on figure 2.2. Firstly, at the transmitter the information bits are mapped to data symbols (I_k). The data symbol used can be from either one of the modulation schemes such as QPSK, QAM, etc. The sequence of data symbols is then arranged in M parallel stream spaced equally which are then mapped into the IDFT and then feed to cyclic prefix and then back to single stream from parallel stream.

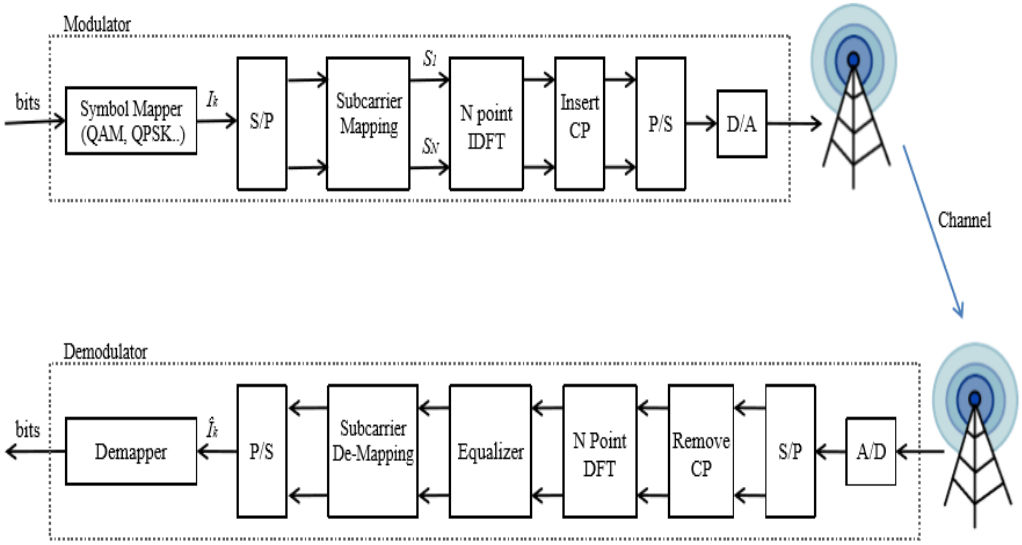

Figure 2.2: Block diagram for OFDM system

At the receiver, the CP interval is distorted due to ISI. Since CP does not carry new information, it is removed and the effect of channel is isolated from the signal carrying desired data. The effect of the channel is avoided by using cyclic prefix insertion, which is converted signal's linear convolutional to circular convolutional. The reverse process is done at the receiver with addition of power amplifier and is then transmitted across a wireless channel [21] [73].

OFDM has advantage and disadvantages over other multicarrier, which can be noticed down as follows; Resilience to fast fading; The nature of OFDM multicarrier Modulation involves the division of available bandwidth with multiple sub frequency with central frequency in which each sub frequency is modulated by data symbol. This process allows the OFDM to perform well in the presence of fast fading environment. Simple channel equalizer is used; The ability OFDM to be resilience to flat fading, the effect of channel become less or negligible. Thus cause the channel equalizer needed at the receiver to be

more simple or not used at all. Less Inter-Symbol Interference; this due to nature of OFDM modulation with orthogonal subcarrier, and Lastly is Spectrum efficiency this is due to overlapping style of OFDM subcarrier lead to increase of proper utilization of available spectrum [42].

Despite the advantages of OFDM, it suffers from two important disadvantages which are; Firstly, High Peak Average Power Ratio (PAPR); The OFDM signal experiences a noise-like amplitude fluctuation with a relatively large dynamic range which cause high PAPR. To combat this effects, the high efficient RF amplifier is required in order to accommodate large amplitude fluctuation. This shows that the presence of high PAPR requires the amplifier to perform with high efficiency level. These problem limits the application of OFDM to the uplink because mobile has limited power and the linear amplifier are more expensive which can lead to increase of the cost of communication services. In a single OFDM block the PAPR can be observed as shown in figure 2.3.

Sensitivity to frequency synchronization Carrier Frequency Offset (CFO) is one of the most common communication system impairment. When there is a mismatch of carrier frequencies used by the transmitter and the receiver the CFO occurs. The fact that the OFDM subcarrier spacing is very tight a slight mismatch in sampling can cause loss of orthogonality among the subcarriers. The loss of orthogonality causes the interference of energy from one subcarrier to the adjacent one which results in to poor bit error performance of the signal. CFO problem can be caused by relative motion between receiver and transmitter [8] [73].

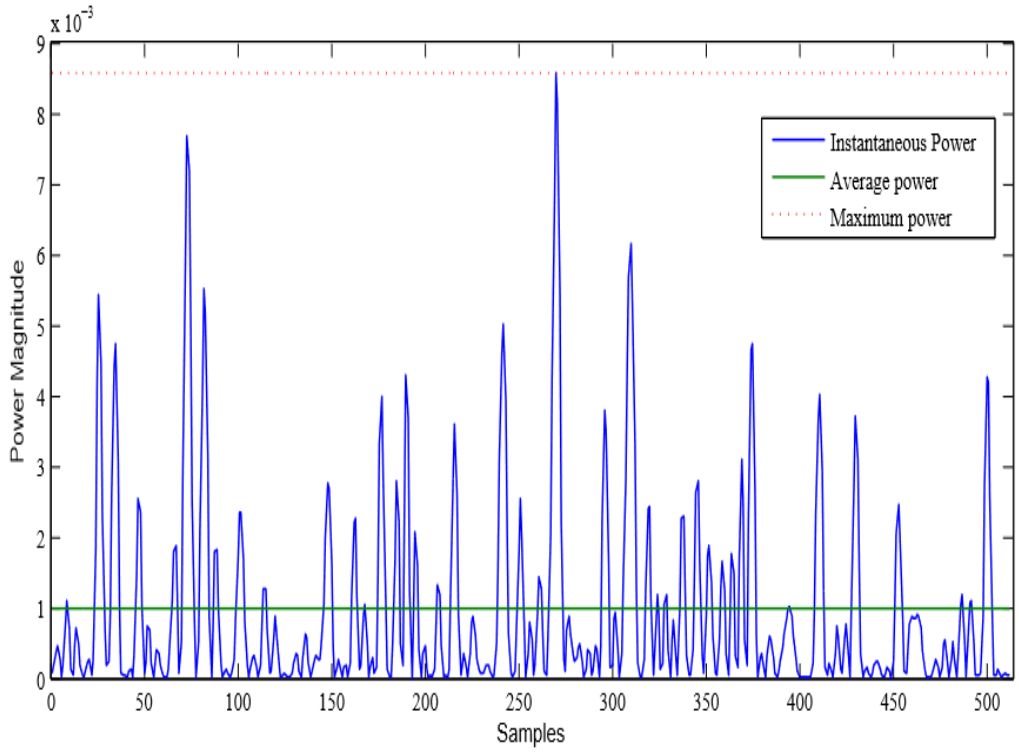

Figure 2.3: Peak-to-average power ratio of an OFDM signal (9.43 dB).

In addition, OFDM is not ideal for Uplink since it experiences larger power consumption unsuitable for mobile phone terminals. Therefore, to improve the performance of OFDM requires implementation of a single carrier (SC) multicarrier frequency domain equalizer (SC-FDE). The merits for SC-FDE against OFDM are [74]:

i. Low Peak Average Power Ratio (PAPR) due to SC modulation at the transmitter
ii. Lower sensitivity to carrier frequency offset
iii. Lower complexity at the transmitter, which is advantageous to mobile terminal in cellular uplink communications
iv. A well-confirmed technology in various prevailing wireless and wireline applications

2.2.1 Peak-to-Average Power Ratio Problem

When the signal flows in a communication system there is fluctuation of signal properties which affect the efficiency of the system. The nonlinearities are caused by high signal peak lead to intermodulation among subcarriers and lead to critical Out off Band radiation (OOB) [75]. This specifically occurs in OFDM, in which the peak value of the signal is substantially larger than the average value of the signal. The OFDM performance is limited by high PAP which reduces the efficiency and hence increases the cost of the RF power amplification stage at the receiver [76]. Assume transmitted OFDM signal is the band pass signal *s(t)* expressed as:

$$s(t) = \hat{s}(t)e^{j2\pi f_c t} \tag{2.1}$$

Where $\hat{s}(t)$ is the amplitude of the signal and f_c is the carrier frequency. Therefore, the PAPR of transmitted signal can be represented as;

$$PAPR = \frac{P_{peak}}{P_{average}} = \frac{\underset{0\leq k\leq k-1}{max}\{|s(t)|^2\}}{E[|s(t)|^2]} \tag{2.2}$$

Where

$$\mathrm{E}[|s(t)|^2] = \frac{1}{T}\int_0^T s(t)^2\, dt \tag{2.3}$$

E[.] represents the expected value and *K is* assumed to be the number of OFDM signal subcarrier. To determine how much the PAPR is reduced in the system the cumulative distribution function is used.

2.2.2 Cumulative Distribution Function (CDF) of PAPR

CDF is a technique used to measure PAPR reduction. However, the Complementary CDF(CCDF) is mostly used instead of CDF. CDF represents the probability of the PAPR exceeding the threshold value. The CCDF expression can be derived from a multicarrier signal with Nyquist sampling rate [8].

From central limit theorem for a large number of subcarriers *K*, the imaginary and real value of *s(t)* takes as Gaussian distribution. A CDF with amplitude of *x* for OFDM signal sample can be expressed as

$$F(x) = 1 - e^{-x} \tag{2.4}$$

Then, the CDF of a OFDM data block can be derived by assuming there are mutually independent and uncorrelated signal samples. Hence,

$$P(PAPR \leq x) = F(x)^2 = (1 - e^{-x})^K \tag{2.5}$$

However, the equation (2.13) is not valid for small number subcarrier (*K*) because the assumption taken does not apply for Gaussian distribution. The sampled signal with *K* subcarrier of PAPR is approximated by distribution of α*K*, in absence of oversampling where α is larger than 1. The oversampling effect is approximated by adding extra signal samples. The PAPR CDF of an oversampled signal is expressed as;

$$P(PAPR \leq x) \approx (1 - e^{-x})^{\alpha K} \tag{2.6}$$

It is suggested that $\alpha = 2.3$ is the preferable approximation for four times the oversampled OFDM. The probability for PAPR surpassing the threshold value ($PAPR_0$) can be expressed as;

$$P[PAPR \geq PAPR_0] = 1 - (1 - e^{-PAPR_0})^{\alpha K} \tag{2.7}$$

2.2.3 Effects of Nonlinear Power Amplifier

The effects of nonlinear power amplifier are observed when a signal is transmitted through a nonlinear device such as a High Power Amplifier (HPA) or digital to analogue converter that results into an out-of-band energy (spectral growth) and in band distortion. These effects limit the performance of the system severely.

There are various amplifier models that facilitate better efficiency of communication system such as Saleh Traveling-Wave Tube Amplifier (TWTA) model, Solid-State Power Amplifier (SSPA) model, and Rapp model commonly used due to its simplicity compared to the other models. However, TWTA and SSPA are more complicated, thus Rapp Model is suggested as the best model to be used in mobile communication systems [24].

Assuming $s_{in}(t)$ represent the input PA signal with amplitude A and input phase signal $\theta_i(t)$

$$s_{in}(t) = Aexp[j\theta_i(t)] \tag{2.8}$$

The output can be expressed as

$$s_{out}(t) = G * Aexp[j\{\theta_i(t) + \phi_a(t)\}] \tag{2.9}$$

In the Rapp model, the phase distortion is assumed to be small and neglected, only amplitude distortion is considered [63]. Thus, the amplitude conversion is expressed as:

$$G_{rapp}(A) = v_o \frac{A}{\left[1 + \left(\frac{A}{A_{sat}}\right)^{2i}\right]^{1/2i}} \tag{2.10}$$

Where v_o Amplitude gain, A input power, A_{sat} saturation input power, and i is the smoothness constant factor.

The undesired behaviour of nonlinear PA can be reduced by increasing the Input-Back-Off (IBO). The peak of OFDM signal is clipped by adjusting the average input power by applying an IBO to the signal before to amplification.

Thus equation (2.10) can be deduced into below expression.

$$g(A) = v_o \frac{A}{\left[1 + \left(\frac{A}{A_{sat}}\right)^{2i}\right]^{1/2i}} \quad x \quad \frac{\left[\left(\frac{A_{sat}}{A}\right)^{2i}\right]^{\frac{1}{2i}}}{\left[\left(\frac{A_{sat}}{A}\right)^{2i}\right]^{1/2i}}$$

$$g(A) = v_o \frac{A_{sat}}{\left[1 + \left(\frac{A_{sat}}{A}\right)^{2i}\right]^{1/2i}} \tag{2.11}$$

To reduce nonlinear distortion in the amplified OFDM IBO is given as in equation (2.12), alternatively:

$$IBO = \frac{A_{sat}^2}{P_{in}} \tag{2.12}$$

$$P_{in} = \left(\frac{A_{sat}^2}{IBO}\right)$$

Assuming the input PAPR in the peak power can be expressed as

$$P_{max} = PAPR_{in} * P_{in} \tag{2.13}$$

$$= PAPR_{in} * \frac{A_{sat}^2}{IBO}$$

$$= \frac{PAPR_{in}}{IBO} x\, A_{sat}^2 = \frac{A_{sat}^2}{K}$$

where

$$K = \frac{IBO}{PAPR_{in}}$$

From the above IBO directly relates to both the PAPR and the PA efficiency. Thus, as the PAPR high leads to increased IBO and reduced PA efficiency. In addition, IBO can be defined as the PAPR for a certain probability of clipping. In reference to class A power amplifier, the efficiency can be expressed as [8]:

$$\eta_{PA} = \frac{0.5}{PAPR} x100\% = \frac{0.5}{IBO} x100\%, \;\; IBO \geq 1 \tag{2.14}$$

The efficiency is inversely proportional to the IBO and the class A maximum efficiency, (50%) occurs at IBO = 1 (0 dB). This matter can be observed in the figure 2.4 [8].

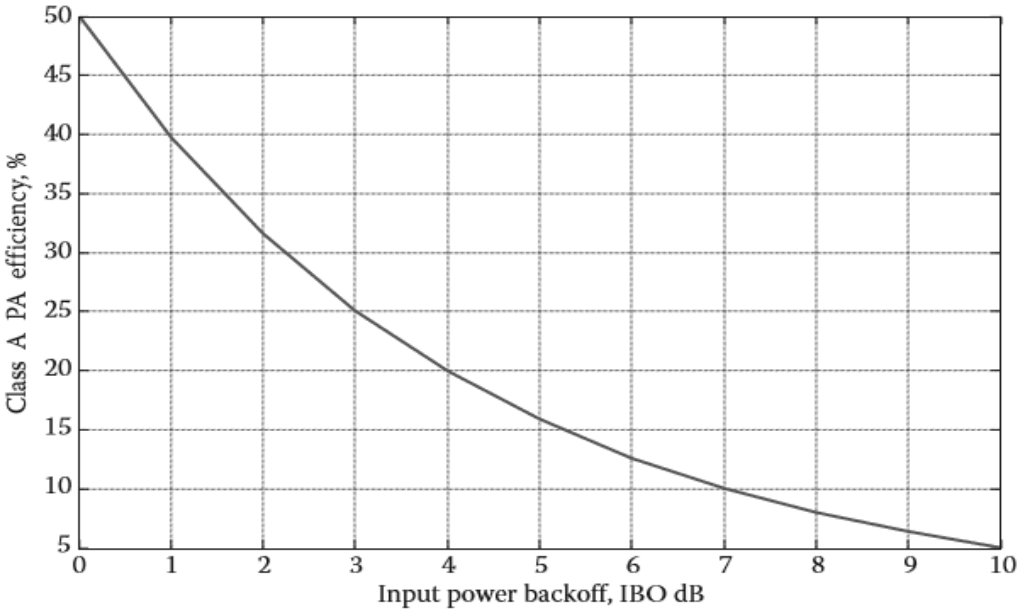

Figure 2.4: Class A power amplifier efficiency

Therefore, increasing the IBO is not a good solution for the PAPR problem. The variation of signal input and output can be explained in the diagram below in figure 2.5.

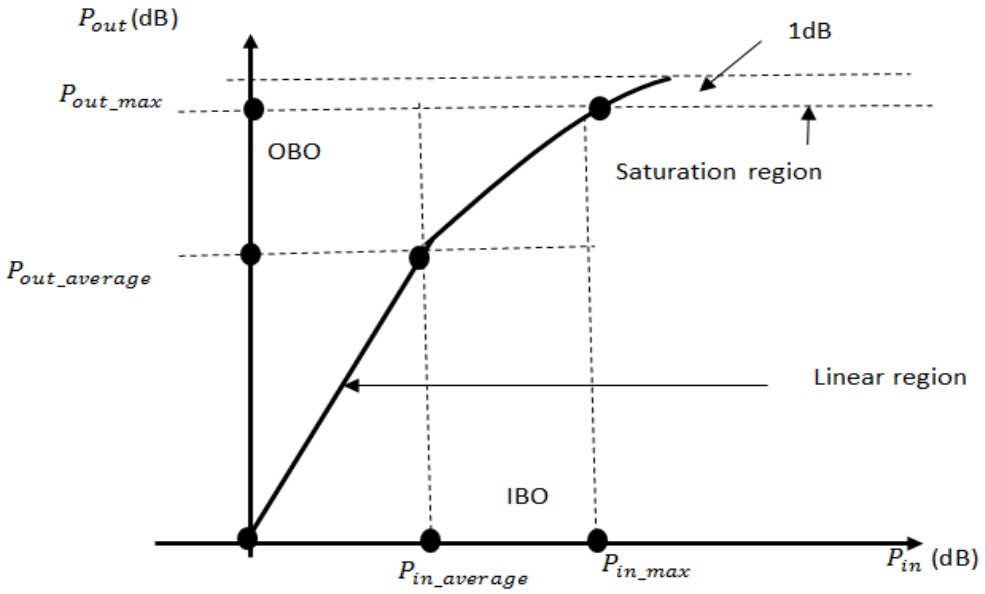

Figure 2.5: Power amplifier Input-Output characteristic

The signal with higher peak power must be transmitted via a linear region of power amplifier. That involves the input average power reduction which is known IBO which correspondingly affects the Output-Back-Off (OBO). As the back off increases, the efficiency of power amplifier reduces which results into limitation of battery life of mobile application and short range coverage [24], [62]. The nonlinearity property of PA leads to spectral leakage and performance reduction in the OFDM system. Unlike OFDM the constant envelope OFDM, having 0dB PAPR makes the spectrum to gain higher Out-Of-Band (OOB) power than conventional OFDM. Moreover, the OFDM has high PAPR that can be avoided by applying a nonlinear power amplifier PA. The large back off is needed

to avoid the impact of nonlinear distortion with a consequences reduced system efficiency [24]. In this research the IBO and OBO is estimated using the results for GaN power amplifier as shown in figure 2.6 [87].

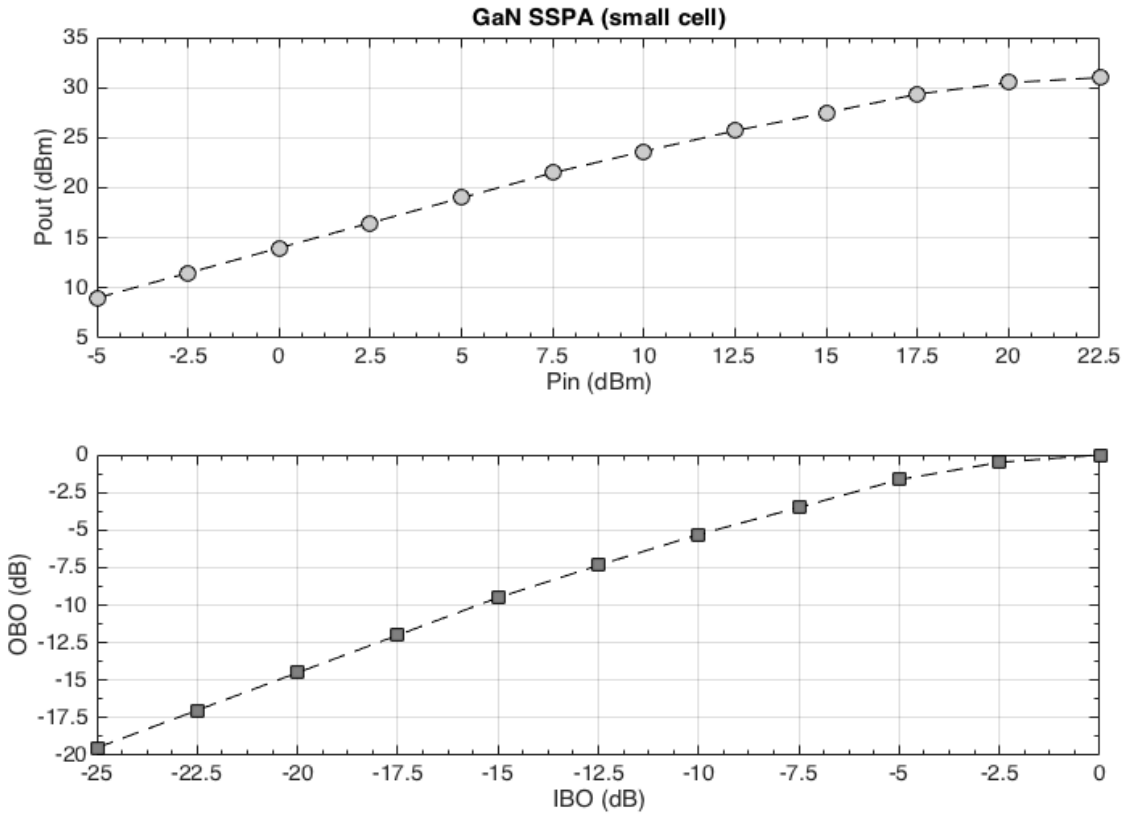

Figure 2.6: IBO and OBO relationship for GaN amplifier for small cell.

Figure 2.6 represents the relationship that is used to estimate the IBO for a required OBO of the PA used for small cell downlink.

2.2.4 PAPR Reduction Techniques

There are several approaches for solving the PAPR problem, and can be grouped into three categories [8].

i. Schemes causing distortion

ii. Distortionless schemes such as multiple signal representation schemes

iii. Signal transformation schemes

The first of category involves the supressing signal peak by modifying the transmitted OFDM signals. However, the modification can introduce in-band noise, which may reduce bit-error performance. The examples of this category are signal clipping method, and peak windowing.

The second schemes category involves the transmitter to generates multiple sequences and chooses one with the lowest PAPR to transmit with distortion free and the essential idea which is that for information symbol sequence. The example of this category are selective mapping (SLM) scheme and the partial transmit sequences (PTS) scheme. The PAPR statistics is improved for an OFDM signal significantly without any in-band distortion or out-of-band radiation at the expenses of increasing complexity of the transmitter. This category scheme requires side information (SI) to be transmitted to the receiver for receiver awareness of what happened at the transmitter side. The system performance degrades with errors detection of side information.

The third category is based on signal transformation before the Power Amplifier. The use of phase modulator (PM) at the transmitter side as a signal flows. PM is a new PAPR reduction scheme with capability of transforming high PAPR OFDM signal to a constant envelope signal with 0 dB PAPR. This process of using Phase modulator cause the multicarrier signal to observed as the single carrier multicarrier frequency domain equalizer (SC-FDE) [8].

The example of SC-FDE is constant envelope Orthogonal Frequency Division Multiplexing (CE-OFDM). The OFDM and CE-OFDM can be differentiated using bandpass diagram as shown in figure 2.4.

2.3 Constant Envelope OFDM System

A constant-envelope waveform is a waveform with constant amplitude. The baseband constant envelope signal form is expressed as [8][73]:

$$s(t) = Ae^{j\phi(t)} \tag{2.15}$$

Where *A* represents signal amplitude and ϕ(t) represents signal phase.

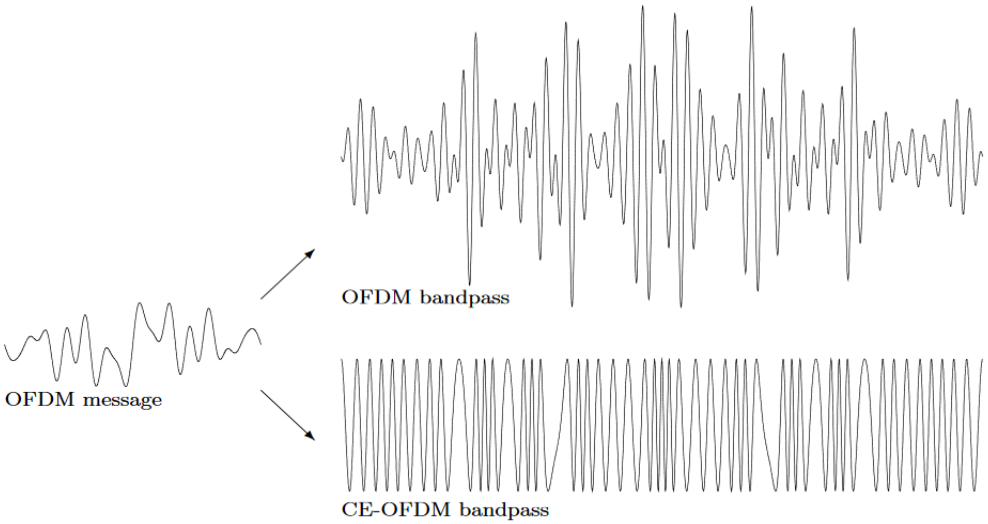

Figure 2.7: OFDM and CE-OFDM bandpass signal

The constant envelope signal form implies constant instantaneous power i.e. $|s(t)|^2 = A^2$. The discrepancy in peak power and average power applying a constant envelope to OFDM creates another modulation technique known as Constant Envelope OFDM (CE-OFDM). When CE is added to a multicarrier system, it results in a nonlinear phase system [24].

The OFDM signal is partitioned into real and imaginary signal and the signal is passed through phase modulator that results to CE-OFDM band pass signal. The phase modulator is normally added at the transmitter side and the phase demodulator is added at the receiver

side. The phase modulator normally causes the CE-OFDM bandpass signal to have a constant envelope bandpass signal. In figure 2.8 indicates the difference between the OFDM lowpass signal and CE-OFDM lowpass signal which shows the OFDM lowpass signal is mapped into unit circle CE-OFDM [24].

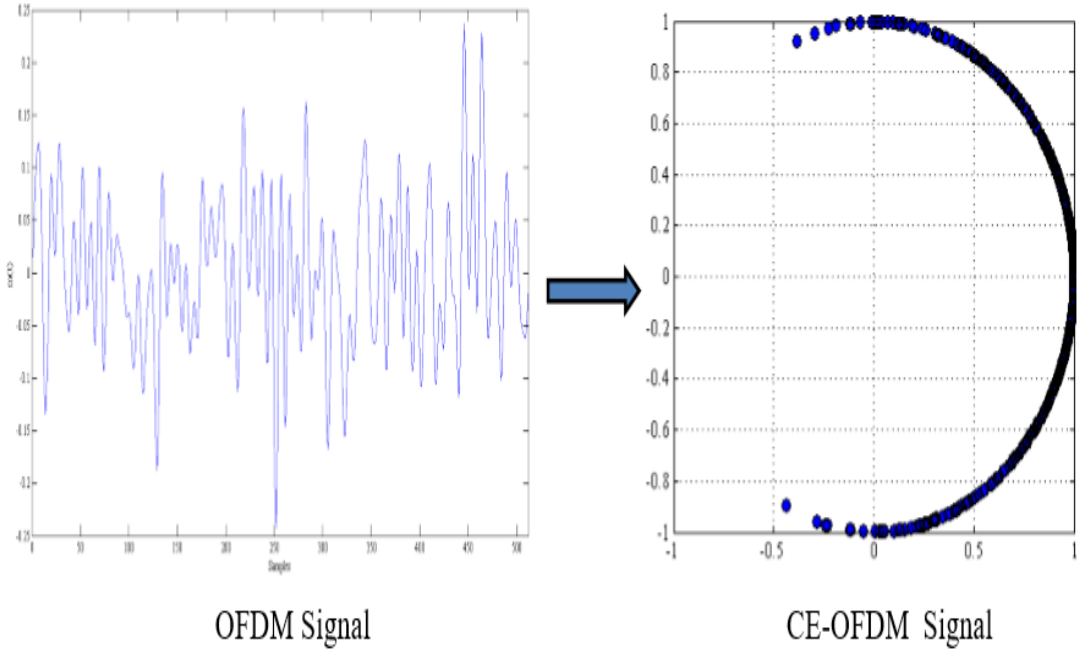

Figure 2.8: Wave map for OFDM and CE_OFDM

The CE-OFDM was originally proposed by Thompson et al. in [24]. The basic motive behind CE-OFDM is the application of a nonlinear phase modulation to a real-valued normalized OFDM signal that increases the power efficiency. The key features of such a waveform can be listed as follows:

i. Fixed lower PAPR of 0dB which mitigate the effect of in-band distortion and out-of-band radiation when the signal is subjected to pass through non-linear power amplifier. The in-band causes the growth of BER while the out-of-band radiation

results inter channel interferences. Thus, proper power consumption in CE-OFDM transmitter is efficiently achieved.

ii. CE-OFDM practically encapsulates OFDM into a transmitted single carrier signal. Therefore, the advantages of OFDM are still maintained, but with an improved diversity against multipath fading, yielded by the insertion of the cyclic prefix and the MMSE equalization in the frequency domain applied to the single-carrier signal [79]. The price to be paid is in terms of increased signal bandwidth, which is at least doubled with respect to the conventional OFDM.

However, spectral precoding of CE-OFDM shown in [26] can dramatically reduce spectral side-lobes as in OFDM the side lobe decays asymptotic as $\boldsymbol{f^{-2}}$ while the precoded CE-OFDM the side-lobes decays asymptotically as $\boldsymbol{f^{-2-2i}}$ where i depend on the design of the precoding. This, results to bandwidth equal to, and even lower than, that of conventional OFDM. It should be noted that spectral precoding involves a little performance degradation with respect to the CE-OFDM as proposed in [24].

One of the open issues of CE-OFDM is the multi-user management in the uplink. Indeed, the usual OFDMA strategy, based on the allocation of blocks of orthogonal subcarriers to the users, is possible only in the downlink, where the base station broadcast the multi-user CE-OFDMA signal to the hand terminals that demodulate the signal and access to the assigned orthogonal subcarrier blocks. In the uplink, even subcarrier set would be partitioned among several users; the asynchronous transmission of single CE-OFDM signals would not be orthogonal and would lead to cross-talk [79].

The recent design of CE-OFDM in 73GHz channel by Claudio et al. [28] has introduced good performance for small cell technology under millimetre wave transmission. However,

this has been implemented in Single Input Single Output (SISO) system only. Figure 2.5 shows the transmitter and receiver for the system in [28] where mm-Wave reception based on SISO trellis CE-OFDM is highlighted in Figure 2.9 and figure 2.10 [17].

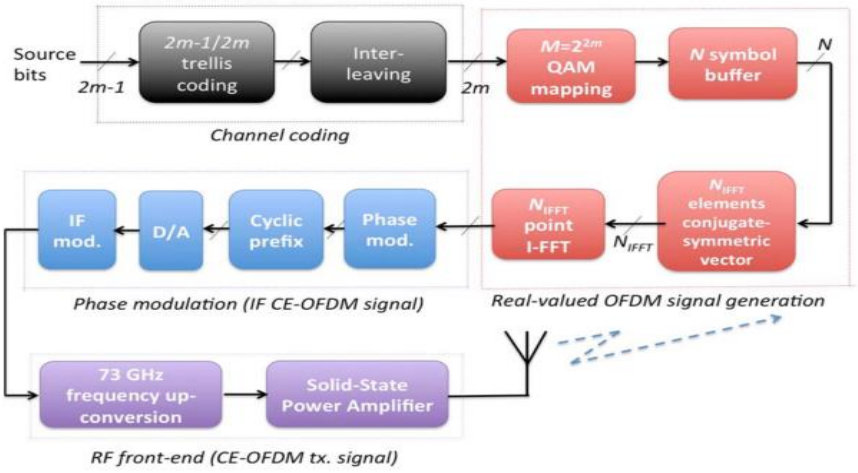

Figure 2.9: mmWave transmission system based on SISO trellis-coded CE- OFDM

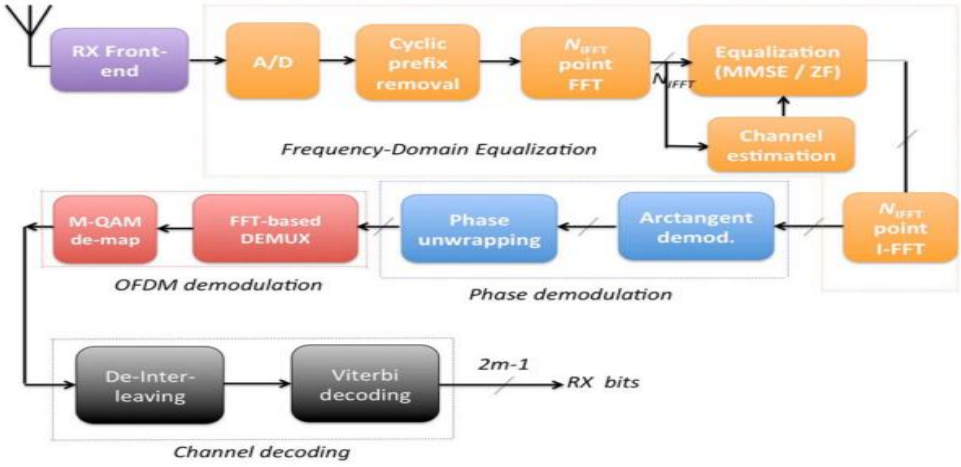

Figure 2.10: mm-Wave reception based on SISO trellis CE-OFDM

The effectiveness of CE-OFDM with respect to OFDM is shown in [28] and the transmission was performed over multipath LOS 73GHz channel. The performance

improvement of trellis-coded CE-OFDM against coded OFDM is very significant, in particular for higher-order modulation constellations. No spectral precoding has been considered for these simulations; therefore, spectral efficiency of CE-OFDM is still 50% less than that of OFDM. It is also worth noting that the performance of CE-OFDM is influenced by the modulation index of phase modulation. Increasing the constellation order, modulation index should be increased, but also bandwidth increases accordingly.

This gives room for novel multiple inputs and multiple outputs system for CE-OFDM based on mm-Wave transmission. The STSK scheme suggested in the previous section is a useful candidate for MIMO to be incorporated with CE-OFDM in mm-Wave transmission as shown in Figures 2.9 and 2.10, The process remain the same as SISO, except the end nodes with multiple antennas in which all signal streams are transmitted parallel as the same time. Since the PAPR of CE-OFDM signal is 0dB, the power amplifier can operate at saturation (optimum) levels which lead to the following advantages [8]:

i. An increase in the average transmitted power which encourages good coverage.
ii. An increase in the power amplifier efficiency that facilitates the battery life.
iii. Since linearity of power amplifier is not a must then a nonlinear power amplifier can be used in which case it is more efficient and cheap.

Despite of all these merits, a constant envelope system has two major problems namely; the application of phase modulation to the system increases the complexity of the receiver, and the growing of signal bandwidth with respect to modulation index of the phase modulator, which reduces the bandwidth efficiency.

2.4 MIMO System Developments

As stated in section 1.1.1, MIMO is a system containing multiple transmit antennas and multiple receive antennas. The main development objectives of MIMO system is to provide diversity and multiplexing gains [45]. These are three main types of MIMO system;

- ❖ The first type is capable of improving transmit power efficiency and maximizing spatial diversity such as Spatial Modulation /Space Shift Keying (SM/SSK),
- ❖ The second type is capable of providing high capacity where spatial multiplexing is used to have parallel data streams transmitted for increased data rates such as Bell Labs layered space–time (BLAST)
- ❖ The third type provides Diversity and Multiplexing Tradeoff (DMT)

The Bell Labs layered space–time (BLAST) is one the MIMO technique that uses a layered space–time approach to increase capacity by transmitting multiple independent data streams over the antennas. This type of MIMO is known to be rich in multiplexing gain due to its ability to reach capacities near the Shannon limit [48-49]. There are different types of BLAST such as Vertical-BLAST(V-BLAST), and Diagonal-BLAST(D-BLAST) in which each tries to overcome the limitations of the previous one with expense of losing the diversity [41]. These aforementioned schemes suffer from a number of problems such as;

i. The multiplexing transmission scheme experiences high inter-channel interference (ICI) at the receiver due to concurrent transmission on the same frequency with multiple antennas.

ii. The scheme requires a complex receiver algorithm to overcome high ICI.

iii. Experiences poor diversity since there is high ICI in the system.

iv. To acquire maximum performance, the transmit antenna should be less than or equal to receiver antenna.

There are major contributions into MIMO development that motivated the development of STSK concepts. These are combination of benefits of previous MIMO techniques to acquire the better MIMO system capable of providing the trade-off between the diversity and multiplexing. Figure 2.11 indicate the MIMO family which paved the way for STSK technique [15].

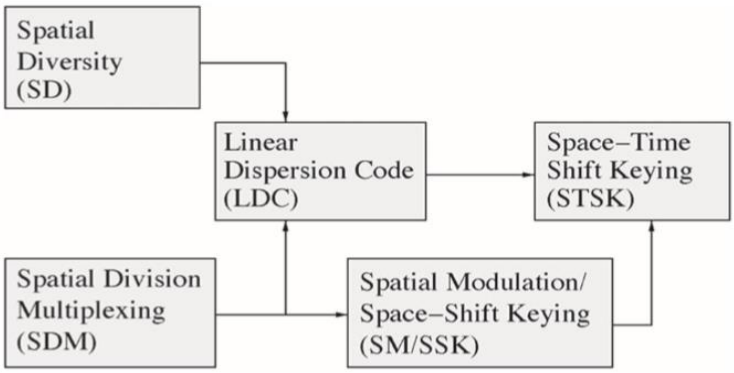

Figure 2.11: Development of the STSK concept for striking a flexible DMT

In addition, the MIMO system is not expected to be able to provide entirely diversity nor total multiplexing gain instead is expected to provide the flexible diversity and multiplexing trade-off [16]. In [17] Hassibi *et .al* introduced Linear Dispersion Codes (LDC) technique for striking DMT that focused mostly on high data rate multiplexing or diversity for high link reliability which was based on frame theory. This technique was introduced for dispersive channel to provide the bridge between multiplexing and diversity gap and produces codes that normally perform better in terms of Bit-Error-Rate (BER) and ergodic capacity. This technique was advantageous at the expenses of involving high decoding complexity. These problems could be resolved by applying Spatial Modulation

or Space Shift Keying [19]. SM and SSK provided low complexity solution that is rich in diversity.

The SM is the MIMO techniques that was primary introduced by Mesleh *et al* [19] that uses multiple antennas to map a bits information block carrying two information units; i.e. a symbol chosen from a constellation diagram and unique transmit antenna number chosen from a set of transmit antennas. The use of the transmit number of antenna as an information bearing unit increases the overall spectral efficiency due its rich in diversity. During transmission, the SM activates one transmit antenna to transmit one symbol while the other antenna elements are inactive; this reduces the inter-channel interferences (ICI), and does not require synchronization between the transmitting antennas. This increases the diversity gain and reduces receiver complexity. The use of SM provides another advantage of power conservation due to use of single Radio frequency chain when one antenna element is active that reduces power usage and minimize the complicity of power amplifier circuit [36 - 39]. This development of SM was followed by another improvement of SM that was initially introduced by Jeganathan *et al*. [43] who transmitted information in the presence or absence of energy without using signal constellation and that called Space Shift Keying (SSK). Despite SM/SSK having high spectral efficiency it could not meet the major objectives of MIMO system of achieving high diversity and multiplexing gain simultaneous. These MIMO techniques all uses modulation schemes such as PSK and QAM.

The solution of these two major problem between the SM and LDC was overcame by introduction of Space Time Shift Keying (STSK).

2.4.1 Space Time Shift Keying

The Space Time Shift Keying (STSK) was first introduced by Sugiura et al. [14] as an improvement to the existing MIMO multiplexing techniques.

The STSK modulation scheme for MIMO communication systems is the extension of the concept of spatial Modulation to include both space and time dimensions so as to provide an overall shift-keying framework. The shift keying process involves the limitation of the carrier according to the discrete information being transmitted in digital communication. In STSK scheme, each transmitted block involves activation of only one out of Q dispersion matrices which achieve a flexible diversity and multiplexing tradeoff. This is achieved by optimizing both the space-time block duration as well as the number of the dispersion matrices in addition to the number of transmit and receive antennas [59]. The STSK has been developed as combination of SM and SMUX by Claudio et al in [36] implemented with mmWave channel. A typical structure of a coherent STSK is given in Figure 2.12 [14].

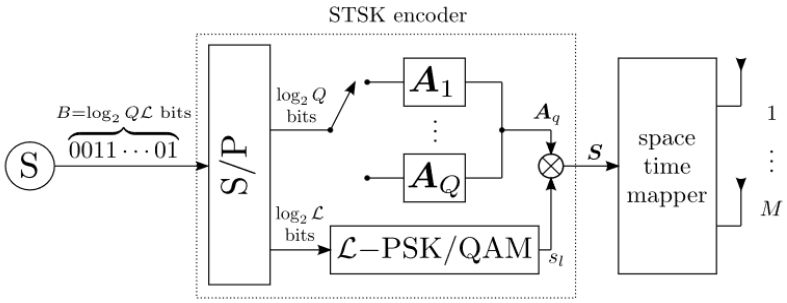

Figure 2.12: Transmitter structure for coherent STSK

Assuming, the number of transmitter antennas is represented by *N* and receiver antennas *M*, the MIMO system is represented as $N \times M$ antenna configuration. The ability of STSK to view information in two dimension (i.e. Temporal dimension (TD) and spatial dimension

(SD)) enables it to handle errors uniquely. It also provides equal error protection, making it preferable in MIMO communication [39]. However, in narrowband channel, the STSK scheme performance deteriorates in multipath. The system rate for STSK depends on the number of dispersion matrices *Q*, the number of symbols *L* for PSK/QAM with symbol duration interval of *T* as given in equation 2.19 [14], [62-65].

The STSK borrow the SM/SSK idea of activating a single AE during each symbol durations. In STSK, transmitter activates one out of Q LDC-like dispersion matrices (DMs) $Aq \in C^{M\times T}(q = 1, 2, \ldots, Q)$, which are pre-assigned before transmission. The DM was introduced in LDC technique and used in STSK which are element matrices of complex numbers with size of (M × *T*) generated using the Objective Function optimization (OF) under power constraints criterion capable of dispersing the source information in both the spatial and time domain [44], [45], [54]. The combination of dispersion matrix (DMs) weighted by the L-PSK/QAM symbols $S_1[i]S_2[i] \ldots \ldots S_Q[i]$, produces the codeword with form of $X[i] \in C^{MXT}$ for every symbol interval T , the only one symbol is mapped corresponding to the DM active at that index which can be expressed in equation (2.16) [69];

$$A_1 = \begin{bmatrix} a_{1,1}^1 \ldots a_{1,T}^1 \\ a_{2,1}^1 \cdots a_{2,T}^1 \\ \vdots \quad \ddots \quad \vdots \\ a_{M,1}^1 \cdots a_{M,T}^1 \end{bmatrix}, A_2 = \begin{bmatrix} a_{1,1}^2 \ldots a_{1,T}^2 \\ a_{2,1}^2 \cdots a_{2,T}^2 \\ \vdots \quad \ddots \quad \vdots \\ a_{M,1}^2 \cdots a_{M,T}^1 \end{bmatrix} \ldots\ldots\ldots A_Q = \begin{bmatrix} a_{1,1}^Q \ldots a_{1,T}^Q \\ a_{2,1}^Q \cdots a_{2,T}^Q \\ \vdots \quad \ddots \quad \vdots \\ a_{M,1}^Q \cdots a_{M,T}^Q \end{bmatrix} \tag{2.16}$$

Thus the STSK codeword can be expressed as equation (2.17)

$$X^{STSK}[i] = S_1[i] \times \mathbf{0}_{M\times T} \dots \dots + S_q[i] \begin{bmatrix} a_{1,1}^q \dots a_{1,T}^q \\ a_{2,1}^q \cdots a_{2,T}^q \\ \vdots \ddots \vdots \\ a_{M,1}^q \cdots a_{M,T}^q \end{bmatrix} \tag{2.17}$$

Where the $\mathbf{0}_{M\times T}$ is the deactivated dispersion matrix and $\begin{bmatrix} a_{1,1}^q \dots a_{1,T}^q \\ a_{2,1}^q \cdots a_{2,T}^q \\ \vdots \ddots \vdots \\ a_{M,1}^q \cdots a_{M,T}^q \end{bmatrix}$ is the activated dispersion matrix. Additionally, to maintain a unity average transmission power the DMs is optimized by using power constraints expressed as [69];

$$t_r\left(A_q A_q^H\right) = T \tag{2.18}$$

Where by $t_r(.)$ is the trace matrix of (.) and $(.)^H$ is the Hermitian operation of matrix (.).

The following are the benefits for STSK over other MIMO systems.

i. The STSK provide flexible DMT with low complexity compare to LDC
ii. It is capable of achieving both transmit and receive diversity gain unlike SM/SSK which provide only receive diversity gain.
iii. The STSK is capable of mitigating the impact of ICI since only one DM is activated at every symbol interval that makes it to behave as a single stream based on which maximum likelihood (ML) can be simply implemented.
iv. STSK has ability to support an arbitrary number of transmit and receive AEs.

The STSK's normalized throughput for every symbol duration can be expressed as [15]

$$R_{STSK} = \frac{\log_2 LQ}{T} \quad [\frac{bits}{channel\ use}] \tag{2.19}$$

The STSK scheme is uniquely configured using specific parameters (M, N, T, Q) in combination with the classic modulation (i.e. $\mathcal{L}$-PSK/QAM).

The selection of DMs determine the performance of STSK which depends on specific OF used, and DM optimization procedures. Thus, the optimization set of DM is mostly important in facilitating the STSK performances which can be summarized as:

a. DM optimization based on Random searching; The DM selection A_q $(q=1 \ldots. Q)$ which is pre-assigned at the transmitter is generated by performing exhaustive searching through a large random set generated matrices in which the best one is selected using the criterion explained in [45].
b. DM optimization based on Genetic Algorithms (GA); To reduce the computational burden of random searching as explained above the GA is applied and the best one is the one with high probability [46]. The flowchart of GA is shown in figure 2.13 which was introduced in [47].

The GA is based on adaptive heuristic search algorithm where individual population follows the evolutionary concepts of natural selection and genetic operators of crossover and mutation optimization OF or fitness function. In DM optimization process, DMs set defines an individual matrix that will be used for creating the STSK scheme under the power constraint as expressed in equation 2.18. The initial population of DMs is selected randomly from Gaussian distribution which is a complex-value with zero average and unity variance. In addition, the algorithm is repeatedly processed such that each repeated stage is known as a generation and the process proceed until pre-specified number of generations is obtained [47].

2.4.2 Multicarrier STSK

The single carrier STSK is categorised both in narrowband and wideband environments. It experiences better performance in narrowband scenario but suffer error floor in wideband

channels. Therefore, the performance degradation of single carrier STSK in dispersive channel is avoided when combined with multicarrier (MC) such as OFDM and SC-OFDM. The most preferable MC that is capable of minimizing the error floor and ISI when combined with MIMO is called OFDM, which has attracted great attention due to ability of OFDM to convert realistic wideband channels into a multiple low-rate, non-dispersive sub channels [55-57]. OFDM enables the application of single-tap frequency domain equalizer at the receiver, which provides additional advantage to MIMO system in terms of simple receiver.

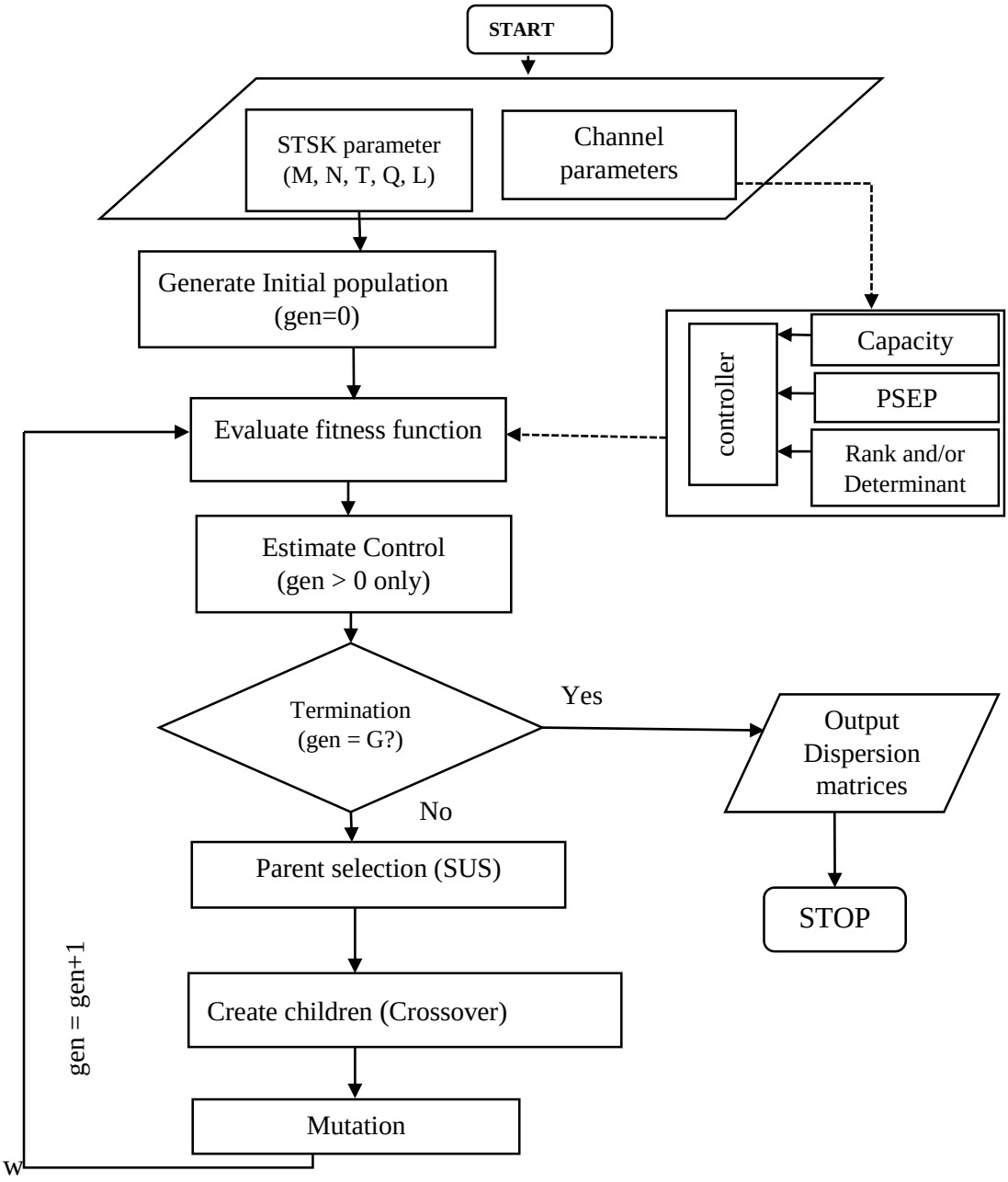

Figure 2.13: Generation of the GA-optimized dispersion matrix set to be used in STSK.

2.5 Space Time Shift Keying OFDM

OFDM-aided STSK [58] was introduced to avoid the performance degradation of STSK schemes operating in wideband channels. The STSK OFDM system was motivated by behavior of OFDM in multipath where it creates a number of orthogonal parallel frequency domain sub-channels which are less affected by dispersive channel.

The application of STSK OFDM in downlink communication is given in [62] and comparison of its performance that of Single Carrier Frequency Division Multiple Access aided (SC-FDMA) with STSK in a multipath environment is given in [63]. The combination of STSK with OFDM or SC-FDMA increase the STSK performance in multipath fading channel. In addition, the STSK with OFDM attains a appreciably good diversity-multiplexing trade-off in multipath channel with performance similar to STSK in narrowband channel [65]. Transmission model of the OFDM-aided STSK scheme with S source bits and D received data as illustrated in Figure 2.14 [15].

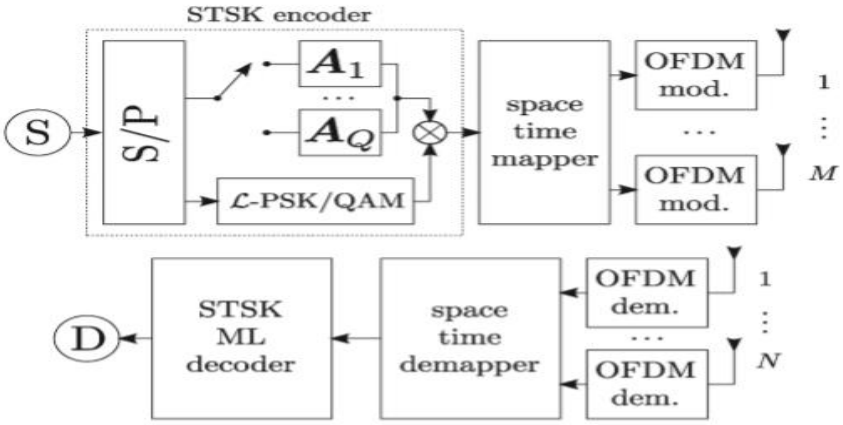

Figure 2.14: Transmission model of the OFDM-aided STSK scheme

The mmWave transmission provide enough bandwidth that facilitate multi-gigabyte capacity [66]. The integration of mmWave in MIMO system provide additional advantage in terms of design and capacity. The mmWave provide small wavelength which facilitate the application of large number of antenna. In addition, the capacity is achieved at the expenses of signal processing complexity [67], and the optimal power consumption is achieved [68]. The STSK Multicarrier in mmWave transmission was developed from

mmWave-MIMO and Massive MIMO concepts. In [36] and [69] the mmWave was introduced in STSK system with OFDM and SC-FDMA respectively. The STSK in mmWave dispersive channel provide the enough capacity that could be useful for 5G communication. In [36] STSK indicated better performance in terms of STKS throughputs when applied in small cell under backhaul communication system over other type of MIMO (spatial modulation and spatial multiplexing). The fact that 5G communication requires the high bandwidth, capacity and coverage. In [69], the STSK indicated strong capability of exploiting transmit and receive diversity. Therefore, communication of mmWave in multiuser fashion, STSK is required to enhance performance which is better than other MIMO systems.

2.6 Performance Analysis.

The performance of constant envelope OFDM and OFDM and that of [24], and [28], were compared in terms of Bit-Error-Rate (BER) against Signal-to-Noise-Ratio (SNR) depending on the modulation index, and channel error estimation. Channel error estimation plays important role in ability to extract error so as to improve the performance of the system.

Channel error estimation can be achieved in MIMO system using any of the following three techniques; Maximum Likelihood (ML), Minimum Mean Square (MMSE) or Zero Forcing (ZF) method [70-71]. However, ML is preferred due its ability to minimize errors though it has complex implementation. In this study only ML and MMSE will be considered. The MIMO signal transmitted through a dispersive channel to the receiver can be expressed as [70];

$$Y(i) = H(i)S(i) + V(i) \tag{2.20}$$

$$Y(i) = H_1S_1 + H_2S_2 + \cdots H_NS_N + V \tag{2.21}$$

Where

$$V = [V_1, V_2, V_3 \ldots \ldots V_N]^T$$

Where *Y(i)* is the received signal, *V(i)* is the noise and *S(i)* is the transmitted signal and the operator $V = [.]^T$ represent the transpose of matrix [.];

The transmitted MIMO signal when passes via wireless experiences the error, and this error can be detected by two major type of detectors which are Maximum likelihood detection and linear signal detection. The linear signal detection consists of two techniques which are zero forcing (ZF) and minimum mean square error (MMSE).

2.6.1 Linear Signal Detection

This method assumes that all signals are transmitted as interferences except for the preferred stream from the target transmit antenna. Therefore, the interference to signals for transmit antennas are reduced or nullified in the course of detecting the desired signal from the target transmit antenna. To enable the detection of preferred signals from each antenna, the effect of the channel is inverted by a weight matrix *W* as expressed in equation (2.22) [70].

$$\mathrm{s} = [s_1 s_2 \ldots . s_N]^T = W_y \tag{2.22}$$

2.6.1.1 Zero Forcing (ZF) Signal Detection

ZF is the linear signal detection technique which involves the least square method to detect the error by inverting the frequency channel response. However, it is capable of removing

the interference between the transmitted streams but the noise power increase which lead to poor performance [72]. The Zero forcing uses the weight matrix W_{ZF} to cancel out the interference which is expressed as:

$$W_{ZF} = (H^H H)^{-1} H^H \tag{2.23}$$

The error performance is directly related to noise power, and the estimated power is denoted as V_{ZF} , thus the post-detection error is given as;

$$\left|\left|V_{ZF}\right|\right|^2 = ||(H^H H)^{-1} H^H||^2 \tag{2.24}$$

The drawback of ZF signal detector is inability to extract the useful signal in the interference since it rejects any desired signal energy contained in the interference subspace [71] [72].

2.6.1.2 Minimum Mean Square Error Signal Detection

MMSE is linear signal detection techniques which address the drawback of ZF by considering the noise power to reduce the overall expected error [72]. To maximize the post-detection Signal-to-Interference and Noise Ratio (SINR), the MMSE weight matrix is given as;

$$W_{MMSE} = (H^H H + \delta_s^2 I)^{-1} H^H \tag{2.25}$$

Where δ_s^2 is the statistical channel noise ratio and the *I* is the identity matrix with same dimension to transmitted signal. The SNR increases as the mean square error (MSE) is minimized, therefore MMSE signal detector achieves higher SNR in comparison to ZF signal detector.

2.6.2 Maximum Likelihood Signal Detection

The ML signal detection computes the Euclidean distance between the received signal vector and the product of all possible transmitted signal vectors with the given channel H, and finds the one with the minimum distance. From equation (2.20), ML detection can estimate the transmitted signal *s*.

$$s_{ML} = \arg\min\left||Y - Hs|\right|^2 \tag{2.26}$$

Where s_{ML} is the estimated error, the optimum ML signal detector performs by reducing the probability of error. Thus, it is capable of minimizing the error than linear signal detection methods at the expense of increased complexity [70].

2.6.3 Bit-Error-Rate (BER) and Noise-to-Signal Ratio (SNR)

The bit error rate (BER) is defined as the ratio of bit errors that occur in a transmission to the received bits during a studied time interval. It is a unit-less quantity which expresses the degree or percentage of error in a received signal [71]. BER can be simply expressed as;

$$BER = \frac{Numbr\ of\ errors}{Total\ number\ of\ bits\ sent} \tag{2.27}$$

The SNR is the measure that express how much the desired signal is found in the system during transmission. The SNR is given as the ratio of the received signal power to the noise power in the frequency range of the process. The SNR is measured in terms of decibel (dB), in which is inverse proportional to BER [71]. The SNR simply can be expressed in terms of power as;

$$SNR = \frac{P_{signal}}{P_{noise}} \tag{2.28}$$

The BER can be expressed in terms of SNR as shown in equation (2.28) as;

$$BER = \frac{1}{SNR} \tag{2.29}$$

2.7 Research Gaps

Based on the literature reviewed, there are gaps identified that gives the research area of the study. The following are the research area identified from the literature above:

i) There has been research on CE-OFDM and SC-FDMA, but only for single user system in downlinks, this gives room for researching the performance of multi-user constant envelope OFDM for uplink purposes.

ii) No work has been done for Space Time Shift keying (STSK) with a constant envelope multicarrier. There is another room of using STSK MIMO to achieve the multiuser constant envelope OFDM.

iii) Linear detection has only been used in STSK SC-OFDM but not in STSK OFDM. However, it is useful when comparison of CE-OFDM with OFDM in STSK MIMO system is investigated for uplink scenario.

2.6 Summary of Literature Review

The constant envelope OFDM achieved better performance in mmWave transmission in [81] for single input single output (SISO) system. CE-OFDM in SISO challenged OFDM in its performance. However, CE-OFDM in mmWave has not been implemented for multiuser. The STSK MIMO system was found performing better when it was investigated along other MIMO system [14], [36] [59], [84] due its ability to provide spatial diversity and spatial multiplexing at the same time. Therefore, there is research gap to be

investigated for the CE-OFDM for multiuser system using STSK MIMO system in mmWave transmission in backhaul environment for uplink communication.

CHAPTER THREE

METHODOLOGY

This work involves the combination of two main previous research work [28] and [36]. In [28] a new design of CE-OFDM in mm-wave transmission is articulated, whilst a new method of STSK MIMO system aided with OFDM under mmWave transmission is provided in [36]. The combination results into a new STSK CE-OFDM designed system which is the multiuser fashion of CE-OFDM in [28]. This chapter highlight the steps used to investigate the performance of STSK OFDM with different detection scheme (ML, MMSE, and ZF). It also provides the step used to achieve a novel design of STSK CE-OFDM under mmWave Transmission. Finally, the analysis of the performance of the new design STSK CE-OFDM under mmWave Transmission is presented.

3.1 Performance Investigation of STSK OFDM Under mmWave Transmission

The performance of STSK OFDM in mmWave channel in [36] has been investigated with respect to signal detectors such as MMSE, ZF linear detection to check the performance difference with linear detection mechanism. There are a number of steps adopted in this investigation which involve the configuration of STSK, and combination of STSK with OFDM, transmission process in dispersive mmWave channel and type of signal detection at the receiver in backhaul environment it assumed that $T \leq N$ and $M = N$ where M is the number of transmit antenna and N is the number of receive antenna. The Figure 3.1 shows the block diagram of STSK OFDM in mm-Wave transmission with different detection schemes.

Figure 3.1 indicates that the signal detection mechanism is being applied one after another. Therefore, the dotted arrow indicates that performance is first analyzed using ML and then MMSE detection, and lastly the ZF is used. The application involved in each block has been explained in detail below.

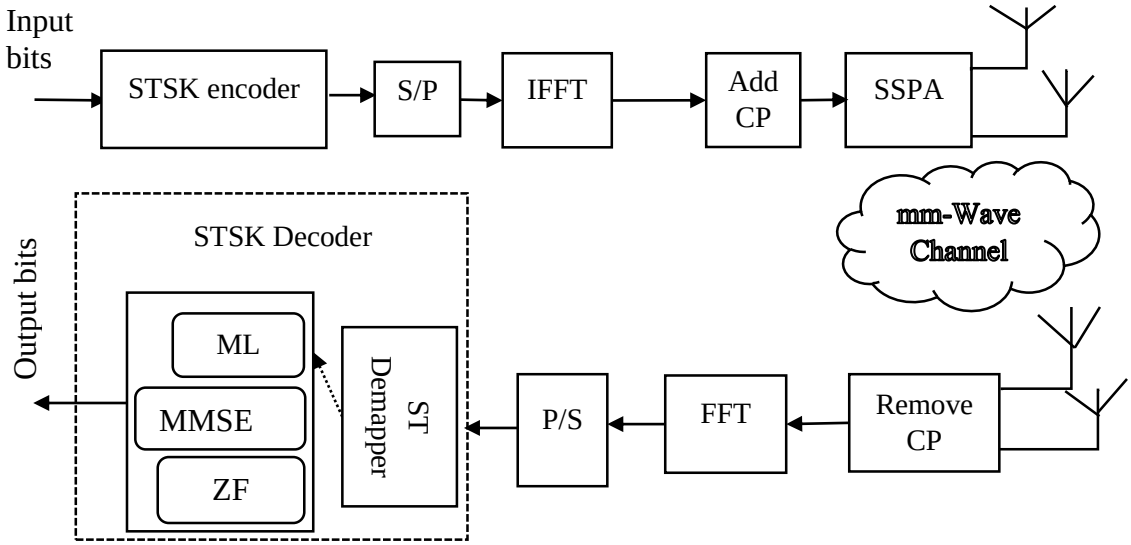

Figure 3. 1: STSK OFDM system under mmWave Transmission.

3.1.1 Space Time Shift Keying (STSK)

The STSK is uniquely identified by four parameters which are arranged as (M, N, T, Q) where M represent a number transmit antennas, N is the number of receive antennas, dispersion matrix number is represented as *Q*, and the symbol duration interval is represented as T. The input bits is given as $\log_2(Q.L)$ bits where only $\log_2(Q)$ bits is used to activate one dispersion matrix $A_{q(q=1,\dots Q)}$ and then $\log_2(L)$ bits are used for mapping one symbol *S[i]* (*i=1,..Q*) with symbol duration of *T* [59]. The activated dispersion matrix ($A_q \in C^{M\times T}$) is selected by using DMs optimization procedure as explained in section 2.4.1

depending on GA process which was done separately and are being used in this research under the power constraints as given in equation (2.18).

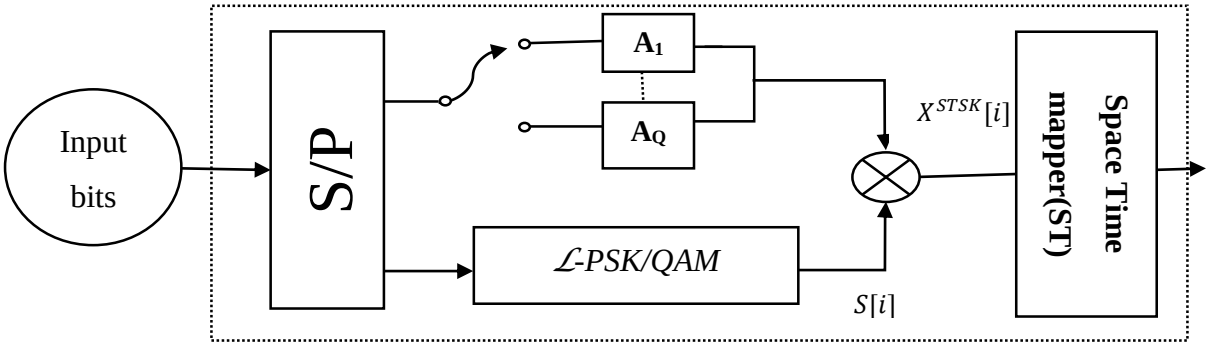

Figure 3.2: STSK encoder

Assuming the symbol mapped at index *i* corresponds to the dispersion matrix A_q at same index *i* and since only one index is used per symbol, then the STSK codeword can be formed as $X^{STSK}[i]$. When one dispersion matrix is active and only one symbol at index *i*, then other DMs are assumed to be zero or nullified and the active codeword to be mapped can be expressed as [81].

$$X^{STSK}[\mathrm{i}] = S_k[i]A_q[\mathrm{i}] \tag{3.1}$$

Thus; the nullification process for inactive DM elements can be included in $X^{STSK}[i]$ and expressed as

$$X^{STSK}[\mathrm{i}] = S_k[i] \times \mathbf{0}_{M\times T} \ \ldots\ldots + S_k[\mathrm{i}] \times A_q[\mathrm{i}] \ldots\ldots S_Q[\mathrm{i}] \ \times \mathbf{0}_{M\times T} \tag{3.2}$$

Where the first term and last term of equation 3.2 above indicate the nullified term of STSK codeword when the DM elements are inactive. Finally, it arrives at the space time matrix as $S_{k,l} = X^{STSK}[\mathrm{i}] \in \mathbb{C}^{MxT}$ that is transmitted from each of the transmit antenna

elements for every T symbol duration. The N receive antenna elements receive the signal as expressed below;

$$\mathrm{Y} = \mathrm{H}S_{k.l} + V \tag{3.3}$$

Where $\mathrm{H} \in \mathbb{C}^{N\times M}$ represents the channel matrix which is complex-valued Gaussian distribution modeled as $CN(0,1)$whilst $V \in \mathbb{C}^{N\times T}$ represents the complex-valued Gaussian noise distribution of $CN(0, N_O)$ where the $N_O$represent the noise variance. It should note that the dispersion matrix Q is pre-assigned. Therefore, to achieve the flexible tradeoff the STSK relies on selection of Q and T. Since the only 4-QAM modulation is used and suitable number of DM (Q) is 4 this was explained as an example in table 1 of [59].

In this research the dispersion matrix used for each specific index for Q=4 which was off-line computed by using the genetic algorithm used in [19], [85]. Therefore, the dispersion matrix is expressed in complex matrix as $A_{q(q=1,\dots Q)\in\mathbb{C}^{M\times T}\equiv\mathbb{C}^{2\times 2}}$.

$$\left.\begin{aligned} A_1 &= \begin{bmatrix} -0.408494 + 0.751684i & 0.306275 - 0.417491i \\ -0.340328 - 0.390231i & -0.470312 - 0.714635i \end{bmatrix} \\ A_2 &= \begin{bmatrix} -0.249687 + 0.462124i & 0.0119701 + 0.850855i \\ 0.744645 + 0.411826i & -0.52526 + 0.00223415i \end{bmatrix} \\ A_3 &= \begin{bmatrix} -0.899663 + 0.16027i & 0.334726 + 0.229954i \\ 0.0451734 + 0.403584i & -0.565158 + 0.718106i \end{bmatrix} \\ A_4 &= \begin{bmatrix} -0.479234 + 0.351821i & -0.526223 - 0.607986i \\ 0.583274 - 0.553488i & -0.442447 - 0.397093i \end{bmatrix} \end{aligned}\right\} \tag{3.4}$$

Thus, the corresponding symbol mapped for every activated dispersion matrix representing 4 QAM used in this work can be expressed below as $s(i)$. Each symbol is mapped independently for every duration symbol of T.

$$s(i) = \begin{bmatrix} 0.707107 + 0.707107i \\ -0.707107 + 0.707107i \\ 0.707107 - 0.707107i \\ -0.707107 - 0.707107i \end{bmatrix} \quad (3.5)$$

Therefore, STSK codeword is obtained as the multiplication of mapped symbol and single selected dispersion matrix in which only one is active for every mapped symbol as represented in equation 3.1 above.

Since the STSK codeword is given as $X_{STSK}[i] = s[i]A_q$ then we can deduce the first term codeword when $i = 1$ as

$$X^{STSK}[1] = (0.707107 + 0707107i)A_1 \quad (3.6)$$

Thus, the STSK codeword is computed as shown in (3.6) and continues in the same manner from $i = 1$ ... ... 4 because $Q = 4$.

The codeword is transmitted as the Space Time Block code set (STBC_Set) which can be demonstrated in terms of an example as shown in Table 3.1 below.

Assuming the transmitted message at the input such that: **0 0 0 1 0 1 1 0 1 0 1 0 0 1 0 1 1 0 1 1**. Then, the transmitted code-word (S) bits. will be grouped in form of four bits and the transmitted as $\underbrace{0001}, \underbrace{0110}\ \underbrace{1010}\ \underbrace{0101}\ \underbrace{1011}$

Table 3.1: The example of 4 bit distribution in STSK transmission system

$log_2(Q.L)$=4bits	2bits to DM(A_q)	2bits to symbols(s_l)	Code-word($S(i)$)
0000	00	00	STBC_Set(:, :, 1)
0001	00	01	STBC_Set(:, :, 2)
0010	00	10	STBC_Set(:, :, 3)
0011	00	11	STBC_Set(:, :, 4)

0100	01	00	STBC_Set(:, :, 5)
0101	01	01	STBC_Set(:, :, 6)
0110	01	10	STBC_Set(:, :, 7)
⋮	⋮		⋮
1111	11	11	STBC_Set(:, :, 16)

Therefore, for the above example the transmitted codeword will take the form STBC_Set (:,:, 2) STBC_Set(:, :, 7)STBC_Set(:, :, 11) STBC_Set(:, :, 6) STBC_Set(:, :, 12).

3.1.2 Space Time Shift Keying OFDM

OFDM contains a number of parallel subcarrier frequency domain sub-channels which are orthogonal for mitigating the channel dispersion effect. The STSK OFDM transmission system is organized as follows; Firstly, the Space Time (ST) mapper collects *J* codeword which is given as $J = \frac{N_C}{T}$, where N_c is the number of OFDM subcarriers which is multiples of *T* and with *T* being the symbol duration interval. The collected J forms a frame which is expressed as;

$$\mathcal{F}_T = [\boldsymbol{X}(1)\boldsymbol{X}(2) \dots \dots \dots \dots \boldsymbol{X}(J)] \in \mathbb{C}^{M \times N_C} \tag{3.7}$$

Where $\boldsymbol{X}(J)$ is the ST-codeword in the frame. The frame can be expressed in terms of OFDM subcarrier per user as; $x^u[n_C]$ and equation (3.7) can be re-written as[14-15].

$$\mathcal{F}_T = \left[\widetilde{\boldsymbol{X}}[0]\widetilde{\boldsymbol{X}}[1] \dots \dots \dots \widetilde{\boldsymbol{X}}[N_c - 1\right] \in \mathbb{C}^{M \times N_C} \tag{3.8}$$

Each transmitted frame $\mathcal{F}_T$ consist N_C subcarriers, where $\widetilde{\boldsymbol{X}}[\boldsymbol{n_c}] \in \mathbb{C}^{\boldsymbol{M \times 1}}$ for every subcarrier (sub-channel) with $n_c = 0 \dots \dots \dots \dots N_C - 1$. The transmitted frame per user *u* can be expressed in matrix form as

$$\bar{X}^u = \begin{bmatrix} \bar{X}^u_{0,0} & \bar{X}^u_{0,1} & \cdots & \bar{X}^u_{0,(N_C-1)} \\ \vdots & \vdots & \cdots & \vdots \\ \vdots & \vdots & \ddots & \vdots \\ \bar{X}^u_{(M-1),0} & \bar{X}^u_{(M-1),1} & \cdots & \bar{X}^u_{(M-1),(N_C-1)} \end{bmatrix} \in \mathbb{C}^{M \times N_C} \tag{3.9}$$

This process can be demonstrated as shown in Figure 3.3 which shows the mapping process of STSK code-word into OFDM subcarriers [15].

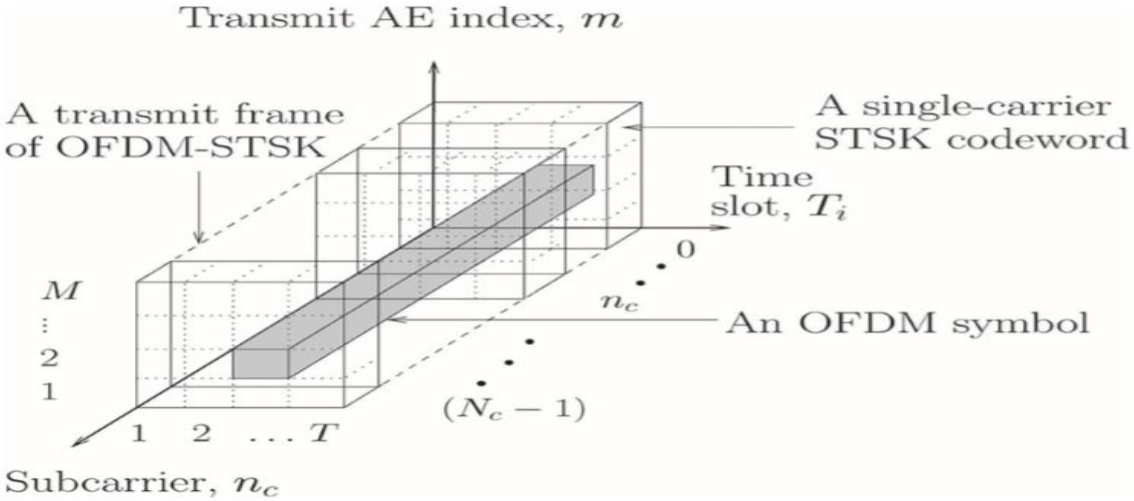

Figure 3.3: The mapping process of STSK code-word in to OFDM subcarriers

The OFDM signal that is transmitted from *m*-th transmit antenna element(s) at the time slot of T may be expressed as [15];

$$x_{m,T_i}(t) = \frac{1}{\sqrt{N_C}} \sum_{n_c=0}^{N_C-1} \boldsymbol{X}_{m,Ti}[n_c] e^{j2\pi f_{n_c} t} \qquad 0 \le t \le N_C\tau \tag{3.10}$$

Where $X_{m,T_i}[n_c]$ is the *m*-th data symbol and τ is the duration for one OFDM symbol whilst $N_C\tau$ is the OFDM symbol length. During the mapping process the subcarrier frequency are equally spaced in order to maintain the orthogonality property in which $f_{n_c} = \frac{n_c}{N_C\tau}$. The OFDM time domain sampling can be expressed as [15];

$$x_{m,T_i}(n_s\tau) = \frac{1}{\sqrt{N_C}} \sum_{n_c=0}^{N_C-1} X_{m,Ti}[n_c] e^{j2\pi \frac{n_s n_c}{N_C}} \qquad 0 \le n_s \le (N_C - 1) \tag{3.11}$$

which is expressed as N_C- point symbol streams $\boldsymbol{X}_{m,Ti} = \{X_{m,Ti}[n_c]\}_{n_c=0}^{N_c-1}$ and

$$\boldsymbol{x}_{m,Ti} = IFFT_{N_C}\{\boldsymbol{X}_{m,Ti}\} \tag{3.12}$$

where m=1, 2...M and T_i=1,2……. T. Therefore, for every time domain OFDM signal the CP is added so that to eliminate the Inter-Symbol interference(ISI).

3.1.3 Millimeter Wave Transmission Channel

In this work the mmWave frequencies of 73GHz band has been used. The real-world measurement data as explained in section 2.1, obtained in New York City [31] was used in this work. The complex data that was collected in that experiment was for line of Sight (LOS) setup and Not line sight (NLOS). The LOS data was used to represent this mmWave channel in study. In additional, it was outdoor experiment that was conducted by New York University which included more than 30 transmitter-to-receivers at different location within a distance of 200 metres. The measurement was about channel characteristics and expressing the importance of using directional antenna. There were different parameters was measured such as path loss, angle of arrival effects and delay spread. These measurements gave the general characteristics of the channel.

The mmWave channel as modelled in [31] for LOS and NLOS outdoor experiment was achieved through Statistical Spatial Correlation Channel Model (SSCM) which is based on temporal and spatial lobes. The SSC model provides the realistic mmWave assessment for micro- and picocellular networks in a dense urban area. Temporal clusters are made up of numerous intra-cluster sub-paths with different random delays [36], [69]. Using a double-

directional time invariant, the channel impulse response for MIMO can be modelled as [36];

$$h\left(t,\vec{\theta},\overrightarrow{\Phi}\right)=\sum_{s=1}^{S}\rho_s e^{(j\varphi_s)}\delta(t-\tau_s)\delta\left(\vec{\theta}-\overrightarrow{\theta_s}\right)\delta\left(\overrightarrow{\Phi}-\overrightarrow{\Phi_s}\right) \tag{3.13}$$

Where, *s* is the total number of multipath components, *t* is the propagation time, ρ_s is the amplitude of s-th multipath components, φ_s and τ_s are phase propagation and time delay of s-th components respectively, $\vec{\theta},\overrightarrow{\theta_s}$ is the vector containing azimuth/elevation *AoD* and *AoA* for *s*-th multipath components. The multipath components of non-parametric omnidirectional MIMO channel can be expressed as [70];

$$H_s=R_r^{\frac{1}{2}}H_w R_t^{\frac{1}{2}} \tag{3.14}$$

H_s is $M\times N$ MIMO channel matrix, R_r *and* R_t represent the receive and transmit spatial correlation matrix respectively and H_w represent matrix of small scale spatial path amplitudes and phases which is Rician fading channel for LOS and Rayleigh fading channel for NLOS.

The results indicated improved cellular network performance in terms of data rate, coverage and high strength of signal, even for moving vehicles.

A similar experiment for NLOS was carried out in the same condition at the same mmWave frequency of 73GHz and the results indicated that a strong signal can be detected even in a highly non-line sight environment.

At the receiver the process continues in reverse of the transmitter process. The cyclic prefix (CP) is removed and then the signal is passed through FFT with N_c- points to each antenna

element. The Frequency Domain channel matrix is expressed as diagonal matrix as shown in (3.11) then, FFT output is fed to signal detector before the STSK decoder [80].

$$\bar{H}_{n,m} = \quad diag\{ \quad \bar{h}_{n,m}[0], \bar{h}_{n,m}[1], \ldots\ldots \bar{h}_{n,m}[N_C - 1] \} \in \mathbb{C}^{N_C \times N_C} \tag{3.15}$$

At the receiver the frequency domain channel output matrix $\boldsymbol{Y}$ can be expressed as

$$\boldsymbol{Y} = H\boldsymbol{X} + \boldsymbol{Z} \tag{3.16}$$

Where, $\boldsymbol{Y} \in \mathbb{C}^{\boldsymbol{N \times T}}$ is the received signal , $\boldsymbol{H} \in \mathbb{C}^{\boldsymbol{N \times M}}$ is the channel matrix , $\boldsymbol{X} \in \mathbb{C}^{\boldsymbol{M \times T}}$ is the transmitted signal, and $\boldsymbol{Z} \in \mathbb{C}^{\boldsymbol{N \times T}}$.represent the noise .

3.1.4 Signal Detection

Signal detection in STSK OFDM system is illustrated in fig 3.1 where one signal detection is used at a time.

i. The received symbol $\boldsymbol{Y}$ in (3.14) is passed over the single-stream optimum maximum-likelihood detector (ML). The ML estimates the index of dispersion matrix *q*, and the index of mapped symbol *l*, in which estimates the source information under the assumption that the channel is known. The maximum likelihood for one stream for indexes *q* and *l* can be estimated as minimum Euclidean distance (d^2_{min})[15];

$$d^2_{min} = (q, l) = arg \ min_{q,l} \left\{ \left| |Y_p - H_p \chi K_{q,l}| \right|^2 \right\} \tag{3.17}$$

Where $Y_p = \text{vec}(\mathbf{Y}) \epsilon C^{MTX1}$ is the vectorial stacking of MIM0-STSK of received signal over p[th] subcarriers$H_p \triangleq I \otimes H(i) \in C^{MTXNT}$. is the channel matrix related to the p[th] subcarrier $\chi \triangleq \left[vec(A_1). vec\left(A_Q\right) \right] \in C^{NTxQ}$ is the channel matrix related to p[th], subcarrier. $K_{q,l} \triangleq [0 \ldots.0, S[i], 0 \ldots.0]^T \in C^{Qx1}$

[s(i)] is the one of the mapped symbol.

ii. Then after ML detector the demodulated STSK OFDM is passed through MMSE detector in which is expressed in terms of weight complex matrix as shown in (3.16) below;

$$W_{MMSE} = (H^H H + \delta_N^2 I)^{-1} H^H \in \mathbb{C}^{N_C M \times N_C N} \tag{3.18}$$

Where $(.)^H$ represents the Hermitian operation and δ_N^2 represents variance of the additive noise. Then the equalized STSK OFDM signal can be expressed as

$$V_{eq} = W_{MMSE}\, \boldsymbol{Y} = \overline{\boldsymbol{X}} + \overline{\boldsymbol{Z}} \in \mathbb{C}^{N_C M \times T} \tag{3.19}$$

Where **Y** is from equation (3.12) and $\overline{\boldsymbol{X}}$ is the equalized signal and $\overline{\boldsymbol{Z}}$ is the zero mean i.i.d Gaussian noise matrix with variance elements $\|W_{MMSE}\|^2 \delta_N^2$.

For computation simplification the vectorial stacking is applied to STSK OFDM received signal , obtained by the parallel-to-serial (P/S) conversion of V_{eq} and expressed as $\widetilde{\Psi}_{STSK} = vec(\mathbf{V}_{eq}) \in \mathbb{C}^{MT \times 1}$ hence the estimated active dispersion matrix index q and the symbol mapped l for $\mathcal{L}$-QAM/PSK is given as [69]

$$(q, l) = arg\ \ min_{q,l} \left\{ \left\| \widehat{\Psi}_{STSK} - \mathcal{L}_{q,l} \right\|^2 \right\} \tag{3.20}$$

Where, estimates value is equivalent to d_{min}^2 for ML, and

$$\widehat{\Psi}_{STSK} = \frac{1}{T} A^H \widetilde{\Psi}_{STSK} = [v_1 \dots \dots \dots . v_Q] \in \mathbb{C}^{Qx1} \tag{3.21}$$

$$\mathcal{L}_{q,l} = A \chi_{q,l}$$

Thus, A represent the dispersion matrix set and $\chi_{q,l}$ is the *l*-th symbol from *L-QAM/PSK* signal set position at *q*-th in vector in (3.20)

$$A = [vec(A_1), vec(A_2) \dots \dots vec(A_{Q)}] \tag{3.22}$$

$$\chi_{q,l} = \underbrace{0, \dots .0}_{q-1}, S_k, \underbrace{0, \dots \dots 0}_{Q-q} \tag{3.23}$$

iii. Lastly is the Zero Forcing (ZF) is used in which it operates in the same way as MMSE, but its weight matrix is given as [69], [80].

$$W_{ZF} = (H^H H)^{-1} H^H \ \in \mathbb{C}^{N_C N \times N_C M} \tag{3.304}$$

$$V_{eq} = W_{ZF}\, \boldsymbol{Y} \in \mathbb{C}^{N_C M \times T} \tag{3.25}$$

Where the computation process and error estimation is performed in the same way as MMSE.

3.2 Design of CE-OFDM STSK Based On mmWave Transmission.

In designing constant envelope systems amplitude and phase are the two major factor to be considered. Moreover, the amplitude of the signal is a unity and therefore only phase effect is considered in the constant envelope systems

The CE-OFDM STSK system has been designed and implemented as shown in figure 3.4. The designed system is modularized in block form with realization and functional of each block discussed below.

Referring to section 3.1.1 and figure 3.2, the STSK encoder output is mapped by ST mapper and then mapped into parallel stream from single stream. The STSK encoder output is transmitted in form of frame for every *T* duration symbol, is $x_{m,Ti}[n]$ and number of Inverse Fast Fourier Transform (N_{IFFT}) points calculates a block of time samples $\{x_{m,Ti}[n]\}$. The sample rate is expressed as;

$$\boldsymbol{S_R} = \frac{N_{IFFT}}{T} \tag{3.26}$$

The STSK frame is oversampled and then fed to Hermitian IFFT as the input which are in a zero padded conjugate symmetric data manner as expressed as[24]:

$$\mathbf{X} = \left[0 \;\; \boldsymbol{X}_{m,Ti}[\mathrm{k}] \;\; Z_p \; 0 \;\; flip\left(\boldsymbol{X}^*_{m,Ti}[k]\right)\right] \tag{3.27}$$

Where Z_p is the number of padded zeros and $\boldsymbol{X}^*_{m,Ti}[n]$ is the conjugate symmetry of $\boldsymbol{X}_{m,Ti}[n]$, in which $\{\boldsymbol{X}_{m,Ti}[n]\}_{k=1}^{N_C}$ where N_C is the number of STSK frames mapped. Therefore, the number of IFFT can be expressed as;

$$N_{IFFT} = 2N_C + \; L_{Zp} \; + 2 \tag{3.28}$$

Where, L_{Zp} is the length of padded zero sequences. The zeros from $k = 0$ to $k = N_C + L_{Zp} + 1$ are used to maintain the conjugate symmetric and the remaining zeros cater for effect of oversampling. The oversampling factor can be defined as;

$$S_{ov} \equiv \frac{N_{IFFT}}{N_{IFFT} - L_{Zp}} \tag{3.29}$$

From the above convention, the output of Hermitian IFFT which expressed as [24], [82]:

$$x[n] = \sum_{k=0}^{N_{IFFT}} \frac{\boldsymbol{X}[k] \exp(j2\pi nk)}{N_{IFFT}} \tag{3.30}$$

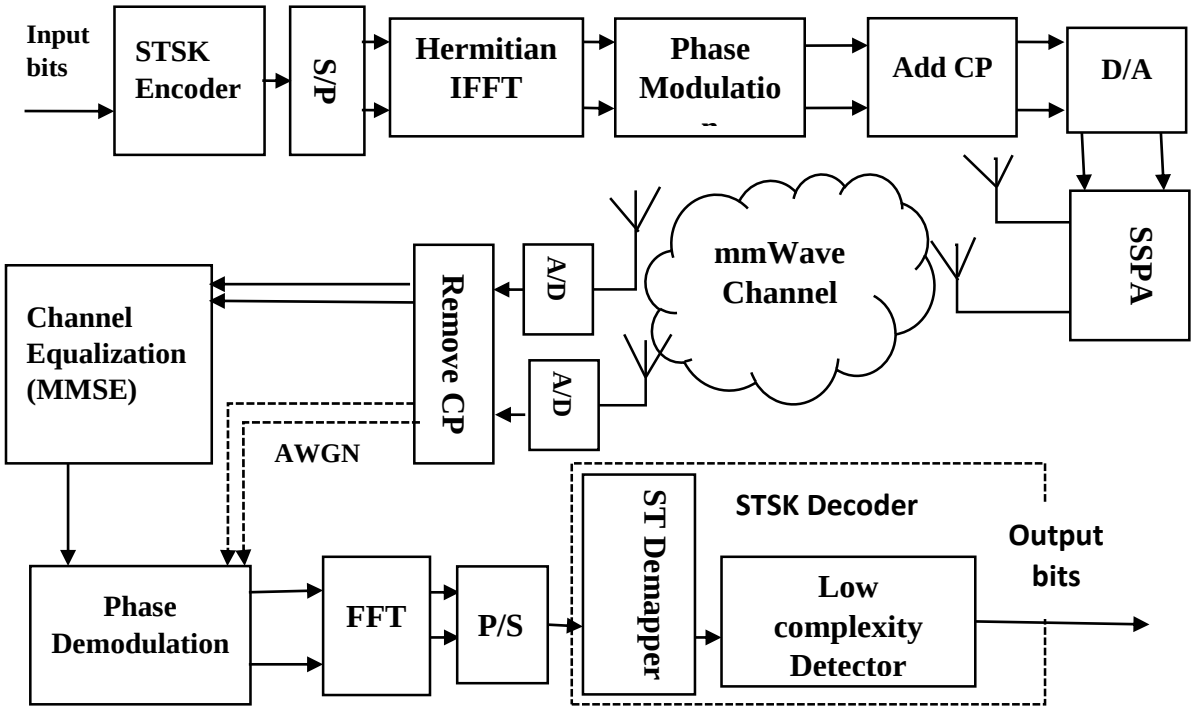

Figure 3.4: Block diagram for Transceiver system of STSK MIMO CE-OFDM

The $x[n]$ is then normalized before is fed to phase modulator, assumed to be $x_{norm}[n]$. There are two major factors which are considered in constant envelope systems, which are amplitude and phase. Thus the amplitude of the signal is a unity and therefore only phase effect is considered in the constant envelope systems. The phase modulation is obtained by multiplying with radian modulation index $2\pi h$ with normalized output of IFFT [87]. This because to enable to fix the angle spread of the unit circle, where changing h on the constellation of CE-OFDM signal lead to phase spread of constellation broadens as shown in Figure 3.5 [86].

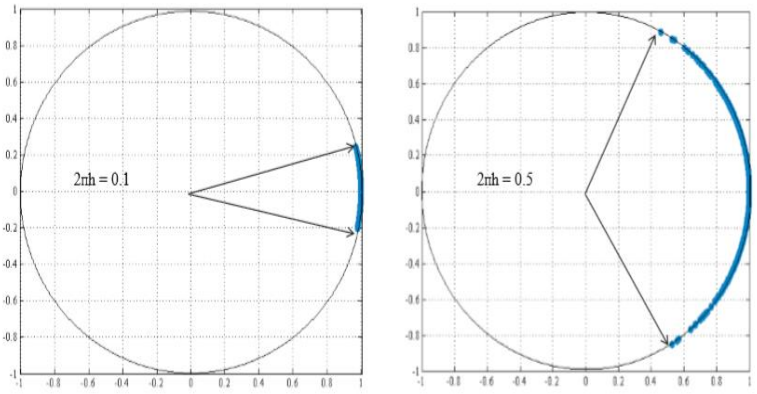

Figure 3.5: Variation of CE-OFDM signal variation due to variation in h

The output of phase modulator can be expressed as:

$$s[n] = \frac{A_s}{\sqrt{M}} exp(j2\pi h x_{norm}[n]) \tag{3.31}$$

Since the amplitude is a unity and effect is observed only at phase then at any time T the sum of total transmitted energy should be equal to a unity. For M transmit antenna element every antenna element will be consisted $\frac{A_s}{\sqrt{M}}$ where $A_s = 1$. Therefore, for M transmit antenna the total phase modulation will be given as;

$$s[n] = \sum_{m=1}^{M} \left(\frac{A_s}{\sqrt{M}} exp(j2\pi h x_{norm}[n]) \right) \tag{3.32}$$

The phase modulator output is then fed to cyclic prefix for ISI mitigation. Therefore, the N_{CP} cyclic prefix samples is attached to $s[n]$ to obtain;

$$\{s[n]\}_{n=-N_{CP}}^{N_{IFFT}-1} \tag{3.33}$$

Where $s[n] = s[N_{IFFT} + n]$ and $n = -N_{CP} \ldots . -2 \ldots -1 \ldots$

The discrete time sample are then passed through Analog-to-Digital convertor and the results are amplified by SSPA power amplifier and transmitted to the 73GHz mmWave channel. The lowpass equivalent representation RF modulated CE-OFDM signal is expressed as [25], [78]:

$$S(t) = \sum_{m=1}^{M} \frac{A_s}{\sqrt{M}} \{\exp(j2\pi hq(t) + \theta)\}, \quad -T_{CP} \leq t \leq T \tag{3.34}$$

Where $\frac{A_s}{\sqrt{M}}$ is the signal amplitude, and θ is the phase offset which may be used for phase continuous modulation, the cyclic prefix duration T_{CP} is obtained as $T_{CP} = \frac{N_{CP}}{J_0}$ and block duration $T = \frac{N_{IFFT}}{J_0}$ and the signal caring information is $q(t)$ is real valued OFDM wave form derived from (2.15), which is in the form of

$$q(t) = B \sum_{k=1}^{N_C} \Re\{X[k]\} \cos\left(\frac{2\pi kt}{T}\right) - \Im\{X[k]\} \sin\left(\frac{2\pi kt}{T}\right), \tag{3.35}$$

$-T_{CP} \leq t \leq T,$ where B is the constant. In this research the PA used is, the Gallium Nitride (GaN) power amplifier as in [88]. However, the CE-OFDM system experiences free effect from power amplifier since operate at saturation therefore the IBO=0dB. Only the effect will be observed in OFDM system so that can operate at linear region.

At the receiver after removing the cyclic prefix, the received signal $r[n]$ is fed to Frequency Domain Equalizer (FDE) for case of multipath channel otherwise it is skipped to phase demodulation. The FDE is purposely for mitigating the effect of multipath in the channel. Thus includes the FFT, equalizer and IFFT block which can be expressed in equation as

$$s[n] = \{FFT(r[n])\}_{k=0}^{N_{FFT}} \tag{3.36}$$

Then from equation (3.32) $s[n]$ is equalized by weight matrix as shown in equation 3.16 thus, $s[n] = s[n] * W_{eq}$ and then fed to IFFT which can be expressed as

$$\hat{s}[n] = \{IFFT(s[n])\}_{k=0}^{N_{IFFT}} \tag{3.37}$$

The output of IFFT is fed to phase demodulation to obtain the $\hat{x}[n]$ which can be expressed as;

$$\hat{x}[n] = unwrap\{\arctan(\hat{s}[n])\} \tag{3.38}$$

Then the reverse of IFFT which was done on the transmitter is done after phase demodulation process expressed as;

$$\hat{X}[n] = \{FFT(\hat{x}[n])\}_{k=0}^{N_{IFFT}} \tag{3.39}$$

The output of FFT ($\hat{X}[n]$) is converted into single stream from parallel stream before ST demapper. The output of ST demapper is decode space time codeword with some error. To eliminate error low complex detector is used to estimate error in which MMSE error estimator is used for mmWave channel and ML error estimator is used for an Additive White Gaussian Noise (AWGN) channel since it does not require equalization. Therefore, in Figure 3.4, the indicates that when the AWGN is considered the dotted arrow to the phase demodulation is used otherwise it is mmWave channel considered.

3.3 Performance Analysis of the Designed System

The analysis of performance of $2x2$ space time shift keying uncoded constant envelope OFDM has been done in MATLAB environment with exhaustive Monte-Carlo simulations. In this work only 4QAM modulation order was used this implies the

unwrapping process at the phase demodulator is not used since it is more useful in higher modulation order.

The uncoded STSK CE-OFDM system has been compared to uncoded STSK OFDM system. The performance has been analyzed in terms of BER for mm-wave channel scenario versus the Signal- to-Noise Ratio while taking into consideration the effect of amplifier (OBO). In addition, only two channel states are considered; Additive White Gaussian Noise (AWGN) and mmWave channel with line of sight (LOS).

The configuration of 2224 STSK OFDM is used with MMSE linear detection and per-subcarrier ML optimum detection used. While 2224 STSK CE-OFDM is using MMSE frequency-domain signal detection. The performance is investigated using both detections for STSK OFDM. The effect of modulation indexes 1.0, 1.3 and 1.5 rad has been investigated. The experimented data for millimeter wave channel, 73GHz multipath channel transmission has been considered in simulation (LOS propagation) and non-linear amplification has been used as well.

A 30dBm saturation power, SSPA working at 73GHz has been used, with the IBO and OBO being estimated using Figure 2.6. The IBO required to resort to linear amplification is -15 dB and the corresponding OBO is -9.5 dB [88].

The configuration of STSK CE-OFDM system is expected to outperform STSK OFDM at higher modulation indices but only when the STSK OFDM is using non-linear amplifier. When the linear power amplifier is used with ML detection the STSK OFDM will outperform the new design STSK CE-OFDM. Despite Linear amplifier applied on STSK OFDM giving better performance than the new design it is expensive implementation used in Uplink communication system.

3.4 Bit-Error Rate Performance and Signal-to-Noise Ratio

The Figure 3.4, indicates the low complex detector which detects the error contained in the received information. The amount of error is expressed in terms of ratio or probability of error explained in previous chapter. Then probability of error per bit can be expressed as [70]:

$$P_b = Q\left(\sqrt{\frac{d_{min}^2 E_b}{N_0}}.\right) \tag{3.40}$$

Where the E_b/N_0 is the signal-to-noise ratio (SNR) per bit and d_{min}^2 is minimum Euclidean distance between all possible pair signal in Viterbi algorithm [70];

CHAPTER FOUR

RESULTS AND DISCUSSION

This chapter gives the results of the study including their discussion. The results for the investigation of the STSK OFDM under different detection mechanism for mmWave channel are first discussed, then, the results observed for the novel CE-OFDM STSK designed system in section 3.2 with different modulation indices are given. Lastly, the performance of the novel designed system is analyzed and compared to that of STSK OFDM under mmWave transmission.

4.1 Performance Investigation of STSK OFDM Under mmWave Transmission

In this study the performance of STSK OFDM using linear power amplifier was investigated when ML signal detection is applied [36] and compared to when linear signal detection (i.e. MMSE and ZF) is used. The performance results for the 2224 STSK OFDM with different signal detection mechanism for mmWave Channel with LOS are shown in Figure 4.1.

The results show that STSK OFDM with ML detector performs better than linear signal detection mechanism (i.e. MMSE and ZF) in such a way that as the SNR increases the BER reduces. The STSK OFDM with MMSE detection outperforms that of ZF signal detection though both show poor performance as compared to that of STK OFDM with ML detection. This is because of ML detection is capable of minimizing probability of error than other detection such as MMSE and ZF.

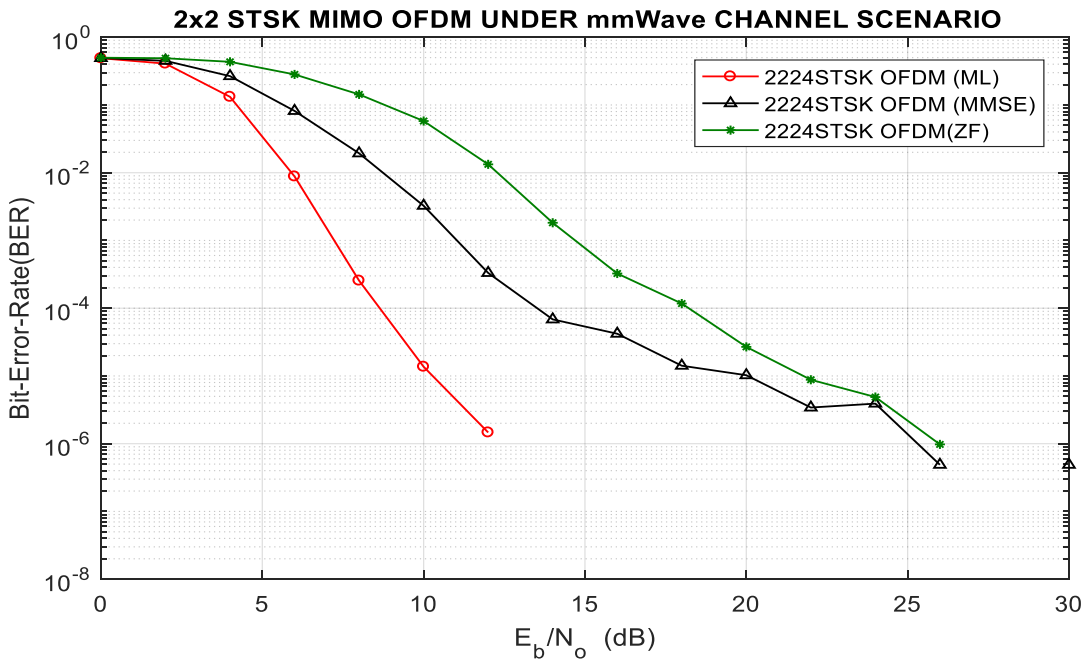

Figure 4. 1: The 2224 STSK OFDM performance with different signal detection for mmWave (LOS)

This scheme uses conventional OFDM which experiences high PAPR which cause high power consumption and is presumed to be costly and therefore, not preferable for uplink communication. However, the use of non-linier amplifier is limited by the nature of OFDM which consist high PAPR that reduces the performance of non-linear power amplifier.

4.2 Performance Analysis of CE-OFDM STSK Based on mmWave Transmission.

The analysis of the performance of the new design explained in section 3.3 was performed without coding of input bits. This section provides the analysis of the simulated results under MATLAB environment using Monte Carlo Simulation. The parameters which were considered in this analysis are modulation order of 4QAM, SSPA characteristics with IBO = -15dB and OBO = -9.5dB which were estimated in section 2.2.3. The values have been chosen so as to provide optimal performance. In addition, the analysis was conducted based on the modulation index which was done through exhaustive trials.

The analysis involved two channel scenarios which were analyzed and compared to STSK OFDM which are;

i) Additive White Gaussian Noise (AWGN) Channel

This is an ideal scenario where it is assumed to have a direct connection between a transmitter and receiver. The attenuation of the signal in this channel is negligible and the effect of multipath is neglected. This scheme is the foundation for mmWave Channel multipath channel.

ii) Dispersive mmWave Channel

This is channel where the radio signal arrives at the receiver antenna from transmitter through two or more paths. The multipath cause interferences which results into multipath fading. This is categorized into two scenarios which are Rayleigh channel fading (NLOS) and Rician fading (LOS). In this study only the LOS scenario was considered.

4.2.1 Selection of Modulation Index

Selection of modulation index involved the analysis of modulation index versus Bit-Error-Rate in order to observe the best Modulation index which can provide the better performance. The modulation index used for both AWGN and mmWave was varied between 0.1 to 2.0.

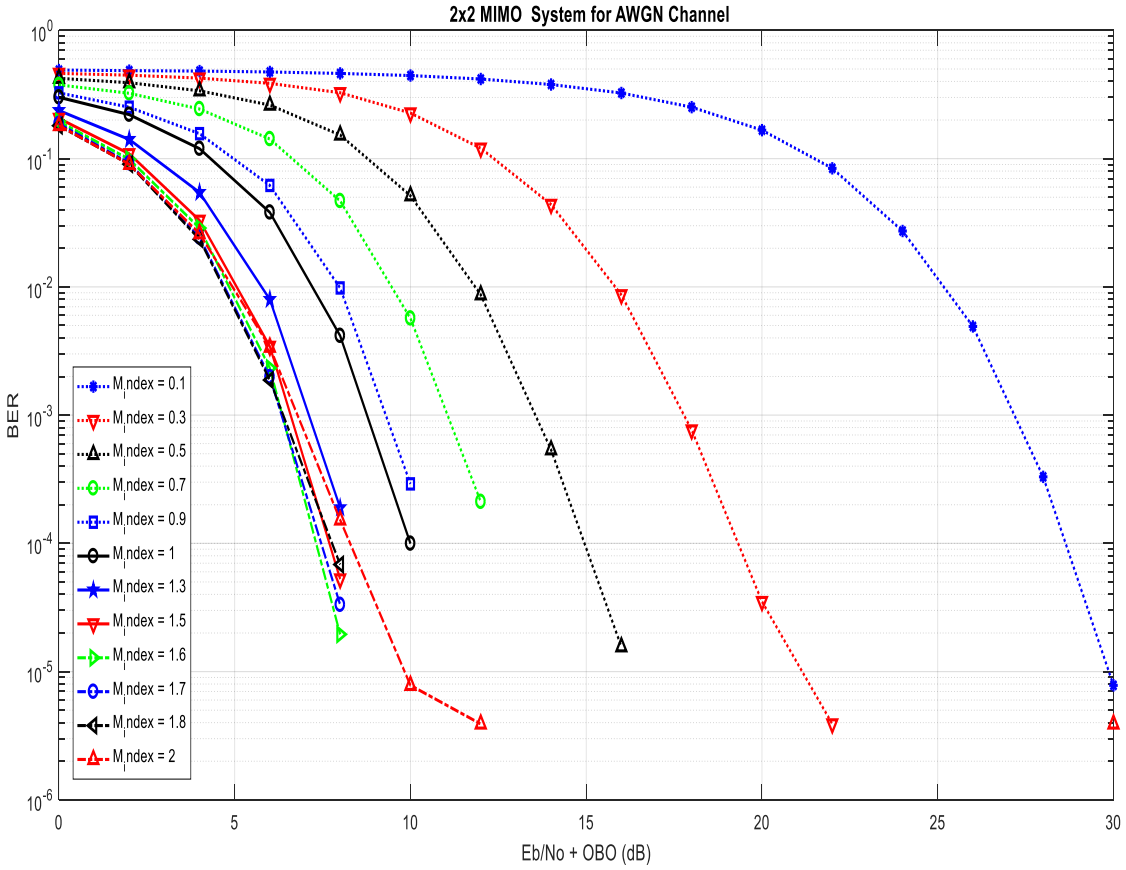

Figure 4.2: Performance Variation with Modulation index in AWGN Channel

The Figure 4.2 indicate that as the modulation index increases the BER decreases to extent when there is no more increase in performance and system misbehave. From Figure 4.2 it can be seen that if the BER is higher example at $BER = 10^{-4}$ the modulation index which can provide optimal performance is between 1, and 1.5.

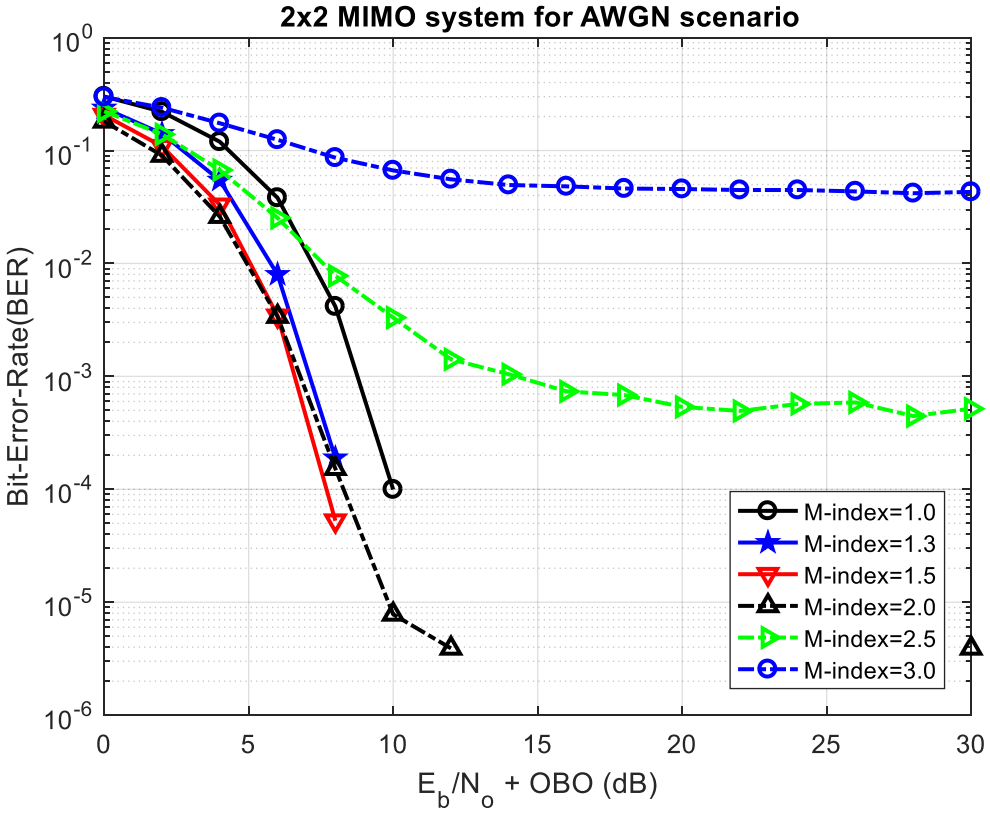

Figure 4.3: Variation of modulation index beyond 1.0 (**MI ≥ 1.0**) in AWGN Channel

The Figure 4.3 indicates that the performance increases as modulation index increases up to 1.5, beyond 1.5 the performance degrades as shown from the above figure from modulation index 2.0 to 3.0.

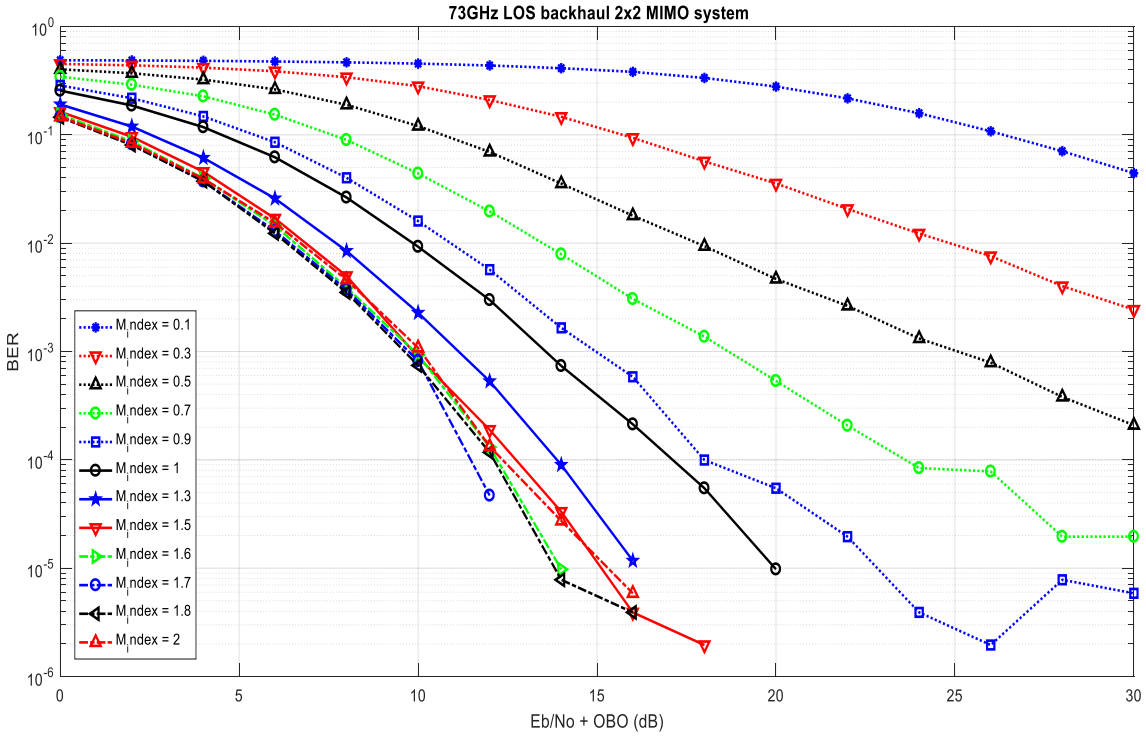

Figure 4.4: Performance Variation with Modulation index in mmWave Channel

The variation of the BER as the function of SNR in multipath channel when the modulation index is varied as shown in Figure 4.4.

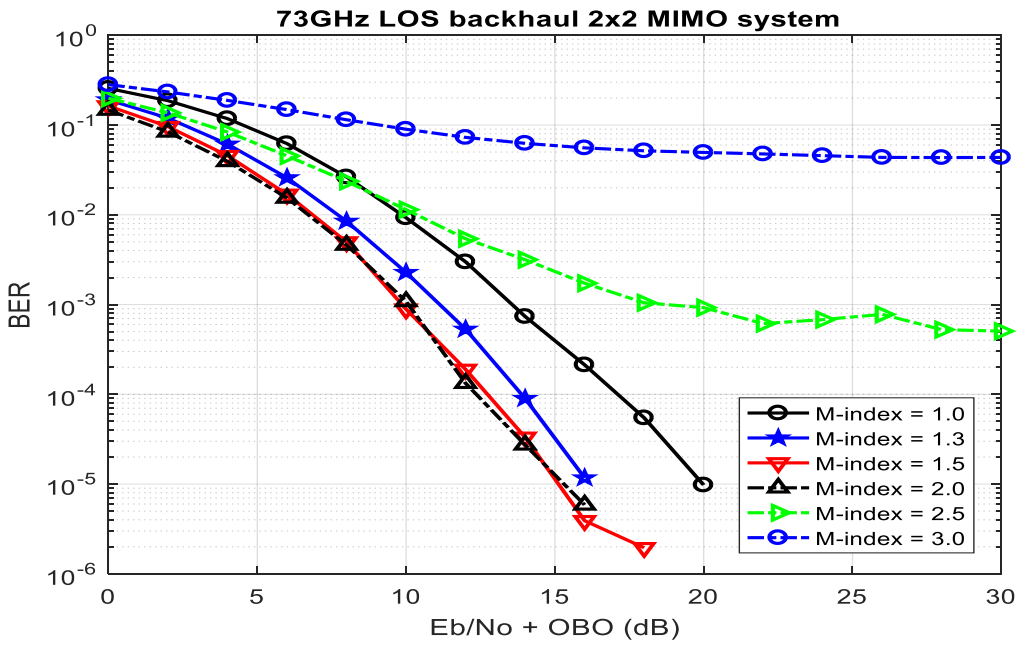

Figure 4.5: Variation of MI beyond 1.0 (**MI $\geq$ 1.0**) mmWave Channel

It can also be seen in Figures 4.3 and 4.5 that there is diminishing performance improvement as the modulation index increased beyond 1.5. to 2.0 and beyond 2.0 the performance degrades. The increase of angular modulation index ($\boldsymbol{2\pi h}$) causes an increases in the phase of the CE-OFDM signal spread across a greater part of the unit circle as shown in Figure 3.5. However, beyond the modulation index the BER performance degrade. This is due to the fact that at high value of modulation index, the signal can have phase beyond $\boldsymbol{2\pi}$. Therefore, this makes it to be difficult for phase modulator to decode such phase correctly hence probability of error increases [86].

Table 4.1: Distribution of BER vs Modulation index in Multipath channel and AWGN at SNR =8 dB.

Indices	0	0.1	0.3	0.5	0.7	0.9	1.0
SNR (dB)	8	8	8	8	8	8	8
AWGN BER	0.5004	0.4619	0.3265	0.1529	0.04679	0.009811	0.004156
mmWave BER	0.4948	0.4665	0.3402	0.1894	0.08972	0.04012	0.0264

Indices	1.3	1.5	1.6	1.7	1.8	2.0
SNR	8	8	8	8	8	8
AWGN BER	0.0001895	5.273e-05	1.953e-05	3.32e-05	6.836e-05	7.813e-06
mmWave BER	0.008477	0.004979	0.003895	0.003721	0.003506	0.004602

Table 4.1 gives a sample of the results showing the variation of BER in both AWG and mmWave Channel as the modulation index is increased at constant SNR of 8 dB. This results are also plotted in Figure 4.5.

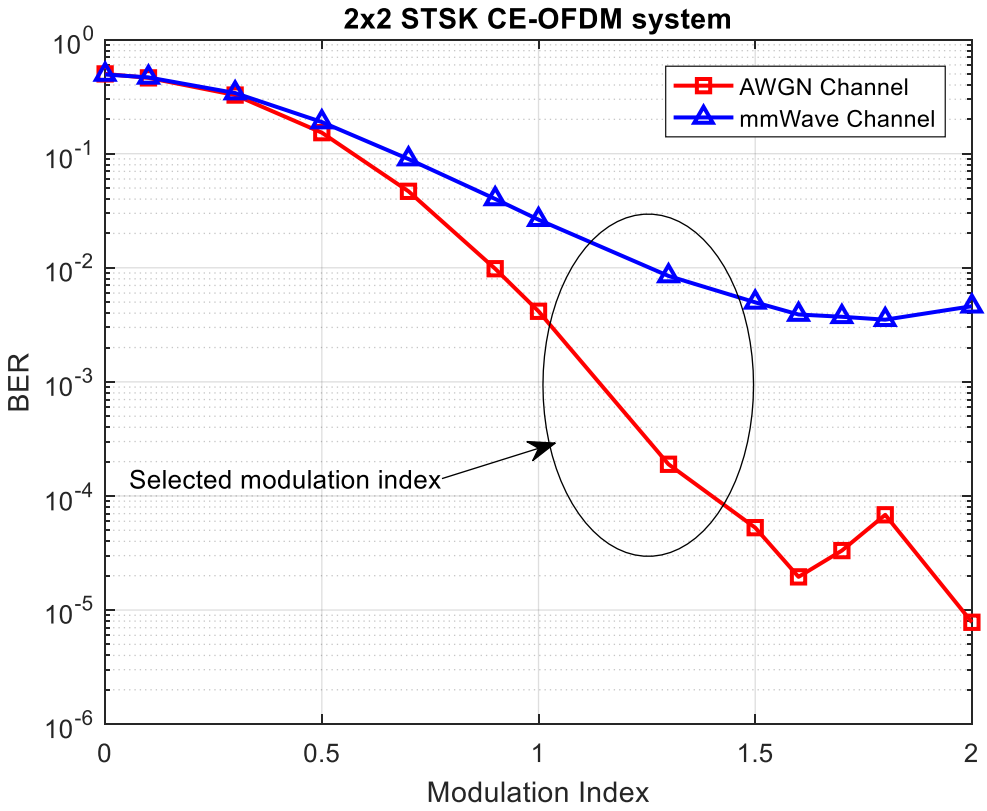

Figure 4.6: Performance comparison of BER vs Modulation index at SNSR = 8 dB

It can be observed from Figure 4.6 that the BER decreases as the modulation index is increased in the two channels. However, average the BER remain relatively constant for the modulation indices from 1.5 to 2.0 but BER increases beyond 2.0. The reduction of BER with respect to modulation index is higher in AWGN channel as compared to that of mmWave Channel. This is because the AWGN channel exhibits minimal signal distortion The performance analysis of the designed STSK CE-OFDM system was investigated for the modulation indices between 1.0 and 1.5.

4.2.2 AWGN Channel

The design in Figure 3.4 show that equalization is not required for an AWGN channel and signal error detection used is maximum likelihood as explained in section 3.1.4. The results

given in Figure 4.7 show that the performance of the CE-OFDM STSK in AWGN channel at modulation indices 1.0, 1.3 and 1.5 improves with every increase of the modulation index where BER decreases as the modulation index increases. Moreover, the CE-OFDM STSK system performs better than STSK OFDM for both linear amplifiers and non-linear amplifiers. This because, both schemes use ML detectors. Also, since CE-OFDM is the improved version of OFDM it leads to a decrease in BER as the SNR increases. In additional, the CE-OFDM STSK operates at saturation point of non-linear power amplifier when IBO = 0 dB. Unlike CE-OFDM STSK, the OFDM STSK is not considered when IBO = 0 dB, because its BER against SNR is very high and undesired.

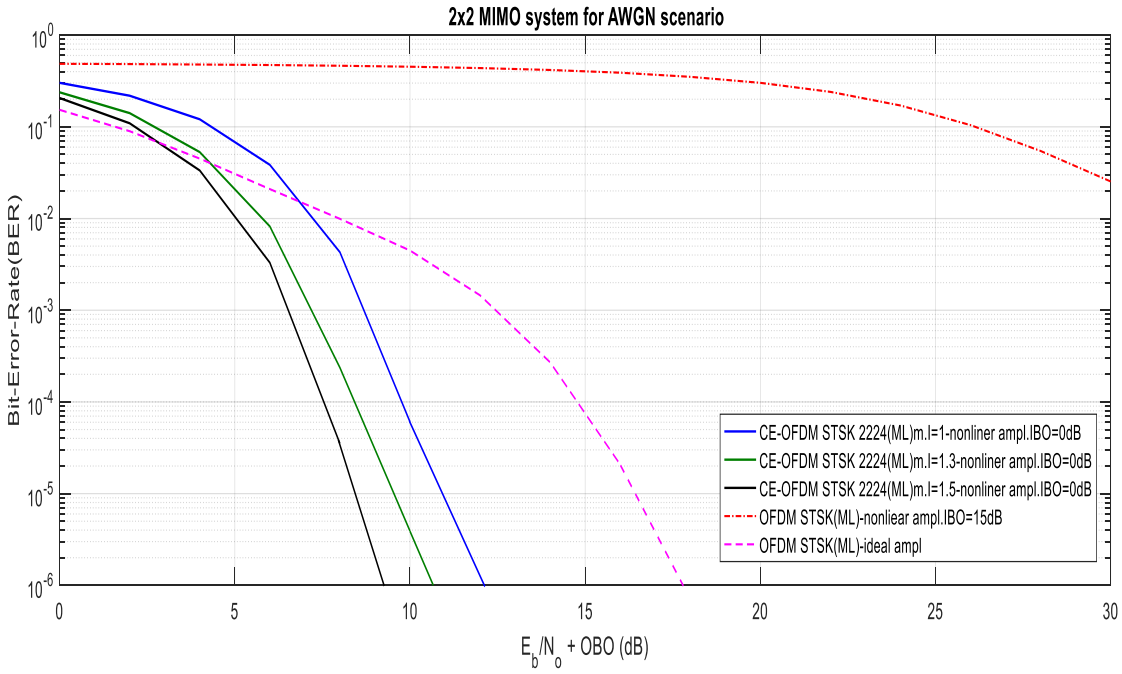

Figure 4.7: BER Performance Comparison of CE-OFDDM STSK (solid line) and OFDM STSK (dotted lines) in AWGN channel for 2x2 antenna in a small cell backhaul environment.

4.2.3 Millimeter Wave Channel (Dispersive Channel)

The Figure 4.8 indicates the performance analysis of CE-OFDM STSK as compared to that of OFDM STSK under millimeter wave transmission channel. Modulation indices from 1.0 to 1.5 were used to observe the performances. Furthermore, the OFDM STSK performance was verified by considering the effect of both linear amplifier and nonlinear amplifiers along with two signal detections, ML and MMSE.

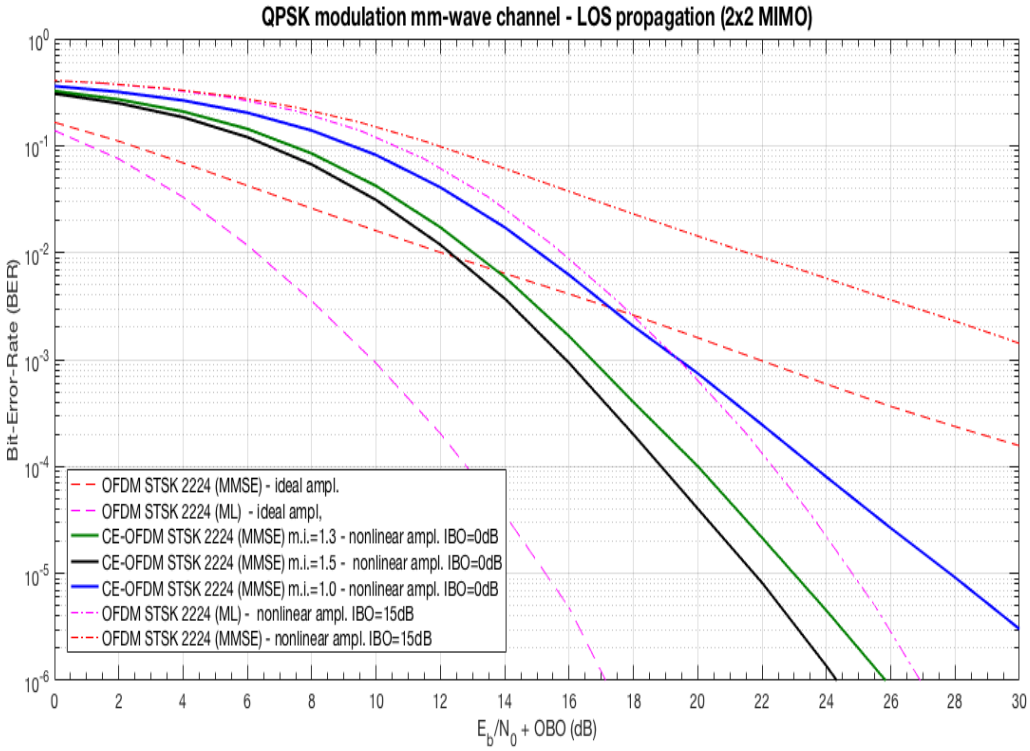

Figure 4.8: BER Performance Comparison of CE-OFDDM STSK (solid line) and OFDM STSK (dotted lines) in 73GHz mmWave channel: small cell backhaul environment.

The CE-OFDM STSK results show that the Bit-Error-Rate decreases with the increase in modulation indices. The results for STSK OFDM using MMSE detection show that when the linear power amplifier is used the performance is better than when the nonlinear amplifier is used. Likewise, for STSK OFDM using ML detection, results indicate that the

STSK OFDM system with linear power amplifiers perform better than the STSK OFDM system with nonlinear power amplifier. This is because the OFDM experience high peak average power ratio which degrade the performance of nonlinear power amplifier. Despite that, the use of linear power amplifier in STSK OFDM which uses ML signal detector outperforms the novel design STSK CE-OFDM, but that scheme experience high power consumption which make the system expensive due to the use of linear amplifier and is only useful for downlink communication.

The results also show that, the STSK OFDM with ML detector for both linear power amplifier and nonlinear power amplifier outperform STSK OFDM system when MMSE detection is applied. This is because of the better error estimation in the ML detector. The STSK CE-OFDM system which uses MMSE detector with nonlinear power amplifier outperforms the STSK OFDM with nonlinear power amplifier using ML detection. This is because the STSK CE-OFDM experience low PAPR of 0dB and the performance of STSK OFDM with nonlinear power amplifier is degraded by the high PAPR in the OFDM. This STSK CE-OFDM is therefore useful for uplink communication because of the minimal power consumption requirements.

The designed STSK CE-OFDM is the improvement of the design in [28] by extending it to Multi-user system for uplink communication. The STSK OFDM in [36] performs better than this new design CE-OFDM STSK but the former is not useful for uplink communication because of the low power consumption required for mobile phone to increase the battery life. The [36] system experience high PAPR which the uplink communication system cannot withstand.

CHAPTER FIVE

CONCLUSION AND RECOMMENDATION

5.1 Conclusions

The performance of STSK OFDM under mmWave transmission has been investigated under linear amplifiers with different signal detection mechanism in this study. The performance of STSK OFDM system was better when ML detector with linear amplifier was used as compared to the case when MMSE and ZF signal detector were used. This because the ML is capable of extracting the error better in a complex system where linear detection mechanism cannot.

The design of a novel multiuser constant envelope orthogonal Frequency multiplexing (CE-OFDM) has been achieved using Space Time Shift Keying Multiple Input Multiple Output system. The design has been implemented in a millimeter wave transmission channel. The results showed that this design is a good multicarrier candidate for uplink for next communication generation. Despite the fact that the STSK OFDM under linear amplifier perform better than CE-OFDM for nonlinear amplifiers, but it is not preferable for mobile phone application for uplink communication, since OFDM experience high PAPR which consumes more power and is more expensive. The use of STSK OFDM with linear amplifier in uplink can result in an increase in cost of communication to the end user.

It was also observed that the desired STSK with CE-OFDM system had better performance as compared to STSK OFDM system, when nonlinear amplification is adopted. When both systems using MMSE linear detection are compared, CE-OFDM is superior. In the case of nonlinear amplification, CE-OFDM with MMSE-FDE outperforms STSK OFDM with

optimum ML detection. From the results it was found that performance of STSK CE-OFDM performance increased with an increase in modulation index. Generally, this work has achieved intended all intended objectives as described in section 1.3 in chapter one.

The STSK CE-OFDM scheme is beneficial especially in respect to the power amplifier of the transmitter since it has low PAPR (0 dB) which degrade the performance of PA. Therefore, STSK CE-OFDM does not affect the performance of non-linear PA as OFDM in addition, this scheme is more helpful for uplink channels, especially due to the fact that mobile handsets cannot withstand the adverse effects of the high PAPR.

5.2 Recommendation and Future Work

The novel design of STSK CE-OFDM scheme is recommended for uplink communication because it experiences low power consumption since it has 0 dB PAPR. It is useful for mobile phones (user equipment) application to enable longer battery life.

The STSK CE-OFDM scheme designed in this research can be used as the basis for future work such as:

- The investigation of the effect of phase noise since this work only focused on transmission of STSK CE-OFDM.
- Higher modulation order investigation such as 16 QAM and 64 QAM.
- Application of larger number of antenna elements such as 4×4 , and 8×8 .since this research only considered 2×2 configuration.
- An investigation of constant envelope Single Carrier Frequency Division Multiple Access scheme specifically using Space Time shift Keying (STSK CE-SC-FDMA).

REFERENCES

[1] P. Sharma, “Evolution of Mobile Wireless Communication Networks-1G to 5G as well as Future Prospective of Next Generation Communication Network,” *International Journal for Computer Science and Mobile Computing,* vol. 2, no. 8, pp. 47–53, 2013.

[2] M. L. J. Vora, “Evolution of Mobile Generation TechnologY : 1G to 5G and Review of Upcoming Wireless Technology 5G,”*International Journal of Modern Trend in Engineering and Research,* Vol. 2, no. 10, pp. 281–291, 2015.

[3] Z. Pi and F. Khan, “An Introduction to Millimeter-Wave Mobile Broadband Systems,” *IEEE Communication Magazine,* vol. 4, no, 7, pp. 101–107, 2011.

[4] S. Schindler “Introduction to MIMO Application Note Products ,”International Journal on Communications Antenna and Propagation, vol. 1, no. 3, pp. 1–22, 2009.

[5] J. R. Hampton, “*Introduction to MIMO Communications,*” cambridge University Press, vol. 1, pp. 1–260, 2014.

[6] N. Giri, A. Sahoo, J. . Swain, P. Kumar, A. Nayak, and P. Debogoswami, “*Capacity & Performance Comparison of SISO and MIMO System for Next Generation Network (NGN),*” *International journal of Advanced Research in Computer Engineering & Technology (IJARCET)* , vol. 3, no. 9, pp. 3031–3035, 2014.

[7] E. G. Larsson, O. Edfors, F. Tufvesson, and T. L. Marzetta, “Massive MIMO for Next Generation Wireless Systems,” *IEEE Communication Magazine,* vol. 3, no. 1, pp. 1–20, 2014.

[8] E. S. Hassan, "*Multicarrier communication system with example in MATLAB*".

New York: CRC Press Taylor & Francis Group, 2016, pp 18-43,

[9] S. Verdú, “Multiuser Detection”. Cambridge, UK: Cambridge University Press, 1998.

[10] N. Jindal and A. Goldsmith, “Dirty-paper coding vs. TDMA for MIMO broad- cast channels”, *IEEE Transactions on Information Theory*, vol. 51, no. 5, pp. 1783 1794, 2005.

[11] C. Suh, M. Ho, and D. N. C. Tse, “Downlink interference alignment”, I*EEE Transactions on Communication*, vol. 59, no. 9, pp. 2616 2626, Sep. 2011.

[12] B. T. Scholar, “Capacity & Performance Comparison of SISO and MIMO System for Next Generation Network (NGN),” *International Journal of Advanced Research in Computer Engineering and Technology*, vol. 3, no. 9, pp. 3031–3035, 2014.

[13] P. Sharma and S. Gawande, “A review on Bell Labs Layered Space Time Architecture(V-BLAST),” *International Journal of Advanced Research in Engineering and Technology.*, vol. 1, no. 4, pp. 96–100, 2013.

[14] S. Sugiura, S. Chen, and L. Hanzo, “Space-time shift keying: A unified MIMO architecture,” GLOBECOM - *IEEE Global Telecommunion Conference,* pp. 1–5, 2010.

[15] M. I. Kadir, S. Sugiura, S. Chen, and L. Hanzo, “Unified MIMO-Multicarrier Designs: A Space–Time Shift Keying Approach,” *IEEE Communication Surveys and Tutorials*, Vol. 17, no. 2 pp. 550 - 579, 2015.

[16] L. Zheng and D. N. C. Tse, “Diversity and multiplexing: A fundamental tradeoff in multiple-antenna channels,” *IEEE Transaction on Information Theory,* vol. 49, no.

5, pp. 1073–1096,2003.

[17] B. Hassibi and B. M. Hochwald, “High-rate codes that are linear in space and time,” *IEEE Transaction on Information Theory*, vol. 48, no. 7, pp. 1804–1824,2002.

[18] R. Mesleh, H. Haas, S. Sinanovic, C. W. Ahn, and S. Yun, “Spatial modulation,” *IEEE Transaction on Vehicle Technology*, vol. 57, no. 4, pp. 2228–2241, 2008.

[19] R. W. Heath, Jr. and A. J. Paulraj, “Linear dispersion codes for MIMO systems based on frame theory,” *IEEE Transaction on Signal Processing*, vol. 50, no. 10, pp. 2429–2441, 2002.

[20] I. S. T. He and W. M. Esh, “key elements to enable millimeter wave communication for 5G wireless system,” *IEEE Wireless Communication*, vol. 14, pp. 104–111, 2010.

[21] M. H. Qutqut, “Mobile Small cells in Cellular Heterogeneous Networks,”PhD Thesis,Electrical & Computer Engineering, Queen’s University, Ontario, 2014.

[22] E. Dahlman, G. Mildh, S. Parkvall, J. Peisa, J. Sachs, Y. Selén, and J. Sköld, “5G Wireless Access :,” *IEEE Communication Magazine*, vol. 6, no. 2, pp. 42–47, 2014.

[23] E. Violette, R. Espeland, R. DeBolt, and F. Schweri*ng, “Millimeter-wave propagation at street level in an urban environment,” IEEE Transaction on Geoscience Remote Sensing*, vol. 26, no. 5, pp. 368–380, May 1988.

[24] S. C. Thompson, A.U. Ahmed, J.G. Proakis, J.R. Zedler,M.J. Geile “Constant Envelope OFDM,” *IEEE Journal Selected Areas in Communications, vol. 56, no. 8, pp. 1300–1312, 2008.*

[25] R. Mulinde, T. F. Rahman, and C. Sacchi, “Constant-envelope SC-FDMA for nonlinear satellite channels,” GLOBECOM - *IEEE Global Telecommunication*

Conference, pp. 2939–2944, 2013.

[26] C. Chung, "Spectral Precoding for Constant-Envelope OFDM," *IEEE Transactions on Communication*, vol. 58, no. 2, pp. 555–567, 2010.

[27] H. Ming Chen, W.-C. Chen, and C. Dir Chung, "An Improved Spectral Precoding Technique for constant envelope OFDM," *IEEE Transaction on Vehicle Technology*, vol. 37, no. 3, pp. 385–390, 2011.

[28] C. Sacchi, T. F. Rahman, N. Bartolomei, S. Morosi, and F. Ciabini, "Design and Assessment of a CE-OFDM-based mm- Wave 5G Communication System," *GLOBECOM - IEEE Global Telecommunication Conference*, pp. 0–6, 2016.

[29] Y. Azar, G. N. Wong, K. Wang, R. Mayzus, J. K. Schulz, H. Zhao, F. Gutierrez, D. Hwang, T. S. Rappaport, ''28 GHz propagation measurements for outdoor cellular communications steerable beam antennas in New York City," *IEEE International Conference on Communications (ICC)*, pp. 5143 - 5147, 2013.

[30] A. Elrefaie and M. Shakouri, "Propagation measurements at 28 GHz for coverage evaluation of local multipoint distribution service," *IEEE Proceeding Wireless Communication Conference*, pp. 12–17, Aug. 1997.

[31] G. R. M. Jr and T. S. Rappaport, "73 GHz Millimeter Wave Propagation Measurements for Outdoor Urban Mobile and Backhaul Communications in New York City," *IEEE International Conference Communication*, pp. 4862–4867, 2014.

[32] A. Ghosh, T. A. Thomas, M. C. Cudak, R. Ratasuk, P. Moorut, F.W. Vook, T. S. Rappaport, G. R. MacCartney, S. Sun, and S. Nie, "Millimeter Wave Enhanced Local Area Systems: A High Data Rate Approach for Future Wireless Networks," *IEEE Journal on Selected Areas Communications*, vol.32, no. 6, pp. 1152–1163,

2014.

[33] M. R. Akdeniz, Y. Liu, M. K. Samimi, S. Sun, S. Rangan, T. S. Rappaport, E. Erkip,, "Millimeter wave channel modeling and cellular capacity evaluation," *IEEE Journal on Selected Areas in Communications*, vol. 32, no. 6, pp. 1164–1179, 2014.

[34] T. S. Rappaport, G. R. McCartney, M. K. Samimi, S. Sun, "Millimeter wave mobile communications for 5G cellular: It will work," *IEEE Access*, vol. 1, no. 6, pp. 335–349, 2013.

[35] R. W. Heath, "Comparing massive MIMO and mmWave MIMO," *IEEE Communication Theory Work,* Vol. 4, no. 7, pp. 511-519, 2014.

[36] C. Sacchi, T. F.Rahman, I. A. Hemadeh, and M. El-Hajjar, "Millimeter-Wave Transmission for Small-Cell Backhaul in Dense Urban Environment : a Solution based on MIMO-OFDM and Space-Time Shift Keying," *IEEE Transactins on Wireless Communications,* vol. 5, no. 20, pp. 4000–4017, 2017.

[37] M. K. Samimi and T. S. Rappaport, "3-D Statistical Channel Model for Millimeter-Wave Outdoor Mobile Broadband Communications," *IEEE International Conference Communication,(ICC),* pp. 8–12, 2015.

[38] T. S. Rappaport, G.R. McCartney, M. K. Samimi, S. Sun, "Wideband Millimeter-Wave Propagation Measurements and Channel Models for Future Wireless Communication System Design," *IEEE Transactions on Communications*, vol. 63, no. 9, pp. 3029–3056, 2015

[39] Z. Gao, L. Dai, D. Mi, Z. Wang, M. A. Imran, and M. Z. Shakir, "MmWave massive-MIMO-based wireless backhaul for the 5G ultra-dense network," I*EEE Wireless Communication,* vol. 22, no. 5, pp. 13–21, 2015.

[40] E. Torkildson, H. Zhang, and U. Madhow, "Channel Modeling for Millimeter Wave MIMO," I*EEE Iformation Theory and Apllications Workshop (ITA) Conference,* pp. 1-18, 2010.

[41] S. Haykin and M. Moher, Modern Wireless Communications. Englewood Cliffs, NJ: Prentice-Hall, 2003.

[42] M. Bhardwaj, A. Gangwar, D. Soni, "A Review on OFDM: Concept, Scope & its Applications" *IOSR Journal of Mechanical and Civil Engineering (IOSRJMCE),* Vol. 1, no. 1, pp. 7-11, 2012

[43] J. Jeganathan, A. Ghrayeb, L. Szczecinski, and A. Ceron, "Space shift keying modulation for MIMO channels," *IEEE Transaction on Wireless Communication,* vol. 8, no. 7, pp. 3692–3703, 2009.

[44] B. Hassibi and B. M. Hochwald, "High-rate codes that are linear in space and time," *IEEE Transaction on Information Theory*, vol. 48, no. 7, pp. 1804–1824, 2002.

[45] R. W. Heath, Jr. and A. J. Paulraj, "Linear dispersion codes for MIMO systems based on frame theory," *IEEE Transaction on Signal Process,* vol. 50, no. 10, pp. 2429–2441, 2002.

[46] F. Babich, A. Crismani, M. Driusso, and L. Hanzo, "Design criteria and genetic algorithm aided optimization of three-stage-concatenated space–time shift keying systems," *IEEE Signal Processing Letter*, vol. 19, no. 8, pp. 543–546, Aug. 2012.

[47] K. A. D. Jong, Evolutionary Computation—A Unified Approach. Cambridge, MA, USA: MIT Press, 2006.

[48] R. W. Heath, S. Sandhu, A. Paulraj, "Antenna Selection for Spatial Multiplexing Systems with Linear Receivers", *IEEE Communications Letters,* Vo. 5, no. 4, 2001

[49] G. J. Foschini, “Layered space-time architecture for wireless communication in a fading environment when using multi-element antennas, “*Bell Labs Technologies Jaipur,* vol. 1, no. 2, pp. 41–59, Sep. 1996.

[50] R. Mesleh, H. Haas, C. Ahn, and S. Yun, “Spatial modulation—a new low complexity spectral efficiency enhancing technique," *Procceding First International Conference for Communication. Network in Beijing, China,* pp. 1-5, 2006.

[51] R. Mesleh, H. Haas, S. Sinanovic, C. Ahn, and S. Yun, “Spatial modulation," *IEEE Transaction on Vehicle Technology,* vol. 57, no. 4, pp. 2228-2242, 2008.

[52] J. Jeganathan, A. Ghrayeb, and L. Szczecinski, “Spatial modulation: optimal detection and performance analysis," *IEEE Communication Letter,* vol. 12, no. 8, pp. 545-547, 2008.

[53] J. Jeganathan, A. Ghrayeb, L. Szczecinski, and A. Ceron, “Space shift keying modulation for MIMO channels," *IEEE Transaction on Wireless Communication*, vol. 8, no. 7, pp. 3692-3703, 2009.

[54] S. Sugiura, S. Chen, and L. Hanzo, “Coherent and Differential Space-Time Shift Keying: A Dispersion Matrix Approach,” *IEEE Transactions on Communications*, vol. 58, no. 11 pp. 3219– 3230, 2010.

[55] G. L. Stuber, J. Barry, S. W. McLaughlin, Y. Li, M. A. Ingram, T. Pratt, “Broadband MIMO-OFDM wireless communications,” *Proceedings of IEEE*, vol. 92, no. 2, pp. 271–294, Feb. 2004.

[56] H. Sampath, S. Talwar, J. Tellado, V. Erceg, and A. Paulraj, “A fourth generation MIMO-OFDM broadband wireless system: Design, performance, field trial

results," *IEEE Communication Magazine*, vol. 40, no. 9, pp. 143– 149, 2002.

[57] H. Bolcskei, "MIMO-OFDM wireless systems: Basics, perspectives, challenges," *IEEE Wireless Communication*, vol. 13, no. 4, pp. 31–37, 2006.

[58] M. Driusso, F. Babich, M. I. Kadir, and L. Hanzo, "OFDM aided space–time shift keying for dispersive downlink channels," *IEEE Vehicular Technology Conference (VTC Fall)*, pp. 1–5, 2012.

[59] S. Sugiura, S. Chen, and L. Hanzo, "Generalized space-time shift keying designed for flexible diversity-, multiplexing- and complexity-tradeoffs," *IEEE Transaction on Wireless Communication,* vol. 10, no. 4, pp. 1144–1153, 2011.

[60] G. Leus, W. Zhao, and G. B. Giannakis, "Space – Time Frequency-Shift Keying," *IEEE Transactions on Communications*, vol. 52, no. 3, pp. 346–349, 2004.

[61] C. Dehos, J. González, A. Domenico, D. Kténas, and L. Dussopt, "Millimeter-wave access and backhauling: The solution to the exponential data traffic increase in 5G mobile communications systems," *IEEE Communications Magazine*, vol. 52, no. 9. pp. 88–95, 2014.

[62] M. Driusso, F. Babich, M. I. Kadir, and L. Hanzo, "OFDM aided space-time shift keying for dispersive downlink channels," *IEEE Vehicle Technology Conference*, vol. 2, 2012.

[63] M. I. Kadir, S. Sugiura, and S. Member, "OFDMA / SC-FDMA Aided Space – Time Shift Keying for Dispersive Multiuser Scenarios," *IEEE Transactions on Vehicular Technolog* vol. 62, no. 1, pp. 408–414, 2013.

[64] H. J. Taha and M. F. M. Salleh, "Multi-carrier Transmission Techniques for Wireless Communication Systems : A Survey," *WSEAS Transaction on*

Communication., vol. 8, no. 5, pp. 457–472, 2009.

[65] M. I. Kadir, S. Chen, K. V. S. Hari, K. Giridhar, and L. Hanzo, "OFDM-aided differential space-time shift keying using iterative soft multiple-symbol differential sphere decoding," *IEEE Transactions on Vehicular Technology*, Vol. 63, no. 8, 2014

[66] O. El Ayach, S. Rajagopal, S. Abu-Surra Z. Pi, and R. W. Heath, "Spatially Sparse Precoding in Millimeter Wave MIMO Systems," *IEEE Transaction on Wireless Communication*, vol. 13, no. 3, pp. 1499–1513, 2014,

[67] A. Alkhateeb, J. Mo, N. Gonzalez-Prelcic, R. W. Heath, "MIMO Precoding and Combining Solutions for Millimeter-Wave Systems" *IEEE Communications Magazine*, Vol. 52, no. 12, pp. 122-131, 2014

[68] S. Buzzi, C. D'Andrea, T. Foggi A. Ugolini, and G. Colavolpe, "Single-Carrier Modulation versus OFDM for Millimeter-Wave Wireless MIMO", *IEEE Transactions on Communications* , Vol. 66, no. 3, pp. 1335 – 1348, 2018.

[69] T. F. Rahman, A. Habib, C. Sacchi, and M. El-Hajjar, "Mm-Wave STSK-aided Single Carrier Block Transmission for Broadband Networking", IE*EE Symposium on Computers and Communications (ISCC),* pp. 507 – 514, 2017.

[70] E. Larsson, and P. Stoica, "Space time block coding for wireless communications" Cambridge University Press, New York, USA, 2008

[71] R. J. Upadhyay, A. B. Makwana and A. Durvesh, "BER Comparison of Linear and Nonlinear MIMO Detectors in AWGN, Rician Fading and Rayleigh Fading channel" *International Journal of Emerging Trends in Electrical and Electronics (IJETEE)*, Vol. 2, no. 2, pp. 78- 83, 2013.

[72] Y. L. Oo, S. S. Y. Mon, and H. M. Tun, “BER Analysis of IEEE802.11n MIMO System Using MMSE and ZF Detectors”, I*nternational Journal of Scientific & Technology Research,* Vol. 4, no. 6, pp. 401-404, 2015.

[73] T. Nistha, “Constant-Envelope Modulation Schemes with Turbo Coding,” Ms Thesis, Electrical and Computer Engineering, University of California, Irvine, 2015.

[74] B. F.Boroujeny and H. Moradi, “OFDM Inspired Waveforms for 5G,” *IEEE Communication Survey Tutorials,* vol. 18, no. 4, pp. 2474–2492, 2016.

[75] A. Gangwar and M. Bhardwaj, “An Overview: Peak to Average Power Ratio in OFDM system & its Effect,” *International Journal of Communication and Computer Technologies,* vol. 1, no. 2, pp. 22–25, 2012.

[76] N. Varghese, J. Chunkath, and V.S sheeba, “Peak-to-Average Power Ratio Reduction in OFDM Systems using Huffman Coding,” *WASET International Journal of Electronics and Communication Engineering,* vol. 2, no. 7, pp. 266–270, 2008.

[77] S. C. Thompson, A. U. Ahmedt, J. G. Proakis, and R. James, “Constant envelope ofdm phase modulation: spectral containment, signal space properties and performance,” *IEEE MILCOM 2004. Military Communications Conference,* Vol. 2, pp. 1129 – 1135, 2004.

[78] S. C. Thompson, “Constant Envelope OFDM Phase Modulation,” PhD Thesis, Electrical Engineering, University of California San Diego, 2005.

[79] Z. Wang, X. Ma, and G. B. Giannakis, “OFDM or single-carrier block transmissions,” *IEEE Transactions on Communication,* vol. 52, no. 3, pp. 380–394,

2004.

[80] T. F. Rahman, “Broadband radio interfaces for 4G and beyond cellular systems in smart urban environments,” PhD Thesis, Information Egnineering & Computer Science, University of Trento, Trento, 2015.

[81] C. Sacchi, T. F. Rahman, N. Bartolomei, S. Morosi, and F. Ciabini, “Design and Assessment of a CE-OFDM-based mm- Wave 5G Communication System,” *IEEE Globecom Workshops (GC Wkshps)*, pp. 1–7, 2016.

[82] S. Nath and D. Ghosh, “Channel Capacity and BER Performance Analysis of MIMO System with Linear Receiver in Nakagami Channel,” *International Journal for Wireless and Microwave Technology*, vol. 1, no. 3, pp. 26–36, 2013.

[83] V. Jungnickel and L. Grobe, “Localized SC-FDMA with Constant Envelope," *IEEE 24th Annual International Symposium on Personal, Indoor, and Mobile Radio Communications (PIMRC)*, pp. 24–29, 2013.

[84] S. Sugiura, S. Chen, and L. Hanzo, “Coherent and Differential Space-Time Shift Keying ,”*IEEE Transactions on Communication,* vol. 58, no. 11, pp. 3219–3230, 2010

[85] M. Driusso, F. Babich, and I. Industriale, “OFDM Aided Space-Time Shift Keying for Dispersive Downlink Channels,” *IEEE Vehicular Technology Conference (VTC Fall)*, pp. 1 - 5, 2012

[86] E. Uludag, “Constant-Envelope Modulation Schemes with Turbo Coding,” MS Thesis Electrical Engineering, University of California, Irvine, 2016.

[87] K. Joshin, K. Makiyama, S. Ozaki, T. Ohki, N. Okamoto, Y. Niida, M. Sato, S. Masuda, K. Watanabe, "Millimeter-Wave GaN HEMT for Power Amplifier

Applications", IEICE Transactions on Electronics, vol. E97.C, no. 10, 2014.

[88] A. Brown, K. Brown, J. Chen, D. Gritters, and K. C. Hwang, “High Power , High Efficiency E-Band GaN Amplifier MMICs,” *IEEE International Conference on Wireless and Information Technology System*, pp. 1–4, 2012.

[89] S. Nie, G. R. MacCartney, S. Sun, and T. S. Rappaport, “72 GHz millimeter wave indoor measurements for wireless and backhaul communications,” *in Personal Indoor and Mobile Radio Communications (PIMRC), 2013 IEEE 24th International Symposium on*, pp. 2429–2433, Sept 2013,

[90] T. S. Rappaport, R. W. Heath, Jr., R. C. Daniels, and J. N. Murdock, Millimeter Wave Wireless Communications. Englewood Cliffs, NJ, USA: Prentice Hall, 2015.

[91] C. Hansen, “WiGiG: Multi-gigabit wireless communications in the 60 GHz band,” *IEEE Wireless Communication.*, vol. 18, no. 6, pp. 6–7, Dec. 2011.

[92] G. Lovnes, J. Reis, and R. Raekken, “Channel sounding measurements at 59 GHz in city streets*,” IEEE International symposium on Pers., Indoor Mobile Radio Communication on Wireless Network —Catching Mobile Future*, Sep. 1994, vol. 2, pp. 496–500.

[93] P. F. M. Smulders and L. M. Correia, “Characterisation of propagation in 60 GHz radio channels,” *IEEE Electronics and Communication Engineering Journal*., vol. 9, no. 2, pp. 73–80, Apr. 1997.

[94] T. S. Rappaport, Wireless Communications: Principles and Practice, 2nd ed. Upper Saddle River, NJ, USA: Prentice-Hall, 2002.

[95] H. Thomas, R. Cole, and G. Siqueira, “An experimental study of the propagation of 55 GHz millimeter waves in an urban mobile radio environment,” *IEEE*

Transaction on Vehicle Technology., vol. 43, no. 1, pp. 140–146, Feb. 1994.

[96] W. Keusgen, R. Weiler, M. Peter, M.Wisotzki, and B. Goktepe, "Propa- gation measurements and simulations for millimeter-wave mobile access in a busy urban environment," *in Proceeding on 39th IRMMW-THz,* Sep. 2014, pp. 1–3.

APPENDICES

I. OFDM aided STSK Matlab Programing Code

```
%close all
%clear all
%clc
% This code is prepared by Chrianus Kyaruzi Kajuna
%Department of Electrical Engineering
%Pan Africa University
%December 2017
%Simulation for OFDM STSK with ML, MMSE, and ZF detection
%% ------------------------Configuration of the system-------------------------------------
Nt=2;
% Nr=2;
Q=4;
M = 4;
T=2;
Nifft = 512;    % IFFT size
BW = 500e6; % bandwidth
coding='OFF';
PowAmp='ON';

if strcmp(PowAmp, 'ON')
   IBO= -15;
   OBO = 9.5;
else
   IBO= 0;
   OBO = 0;
end
phaseNoise='OFF';
CHAN='MMW';%MMW or NO
snr= 0:2:30;
env_condition='LOS';%LOS or NLOS
detector='linear';%ML or linear
niter = 100;% no_iterations
phn_psd=[0 0];
off_vect= [0 0];

%% Selecting configuration

if Nt == 8
   Nr = 8;
elseif Nt == 4
   Nr = 4;
else
   Nr = 2;
end
%% Modulation and coding parameters
snr1 = snr - OBO ;
```

```
if strcmp(coding, 'ON')
   if M == 4
 coderate = 1/2;
 str2 = 483991; % For random interleaver
 trellis=poly2trellis(7, [171 133]);
 block_size = coderate*(log2(Q) + log2(M));
modConst = 2; % modulation constant
tbl = 36; % traceback length
hModulator =  comm.RectangularQAMModulator(M,'BitInput',true);
hDemod = comm.RectangularQAMDemodulator('ModulationOrder', M, 'BitOutput', true);

elseif M == 8
coderate = 2/3;
str2 = 483991; % For random interleaver
trellis = poly2trellis([5 4],[23 35 0; 0 5 13]);
block_size = log2(Q) + coderate*log2(M);
tbl = 34; % traceback length
%        punc_vec = [1;1;0;1]; % 1/2 to 2/3
hModulator = comm.PSKTCMModulator(trellis,'ModulationOrder',M);
hDemod = comm.PSKTCMDemodulator(trellis,'ModulationOrder',M, 'TracebackDepth', tbl);
end
else
M = 4; % 4 for QPSK; 2 for BPSK
modConst = 2; % modulation constant
block_size = log2(Q) + log2(M);
hModulator =  comm.RectangularQAMModulator(M,'BitInput',true);
hDemod = comm.RectangularQAMDemodulator('ModulationOrder', M, 'BitOutput', true);
end
BW = 500e6; % bandwidth
%% Channel and hardware impairments

PN1=abs(phn_psd(1));
PN2=abs(phn_psd(2));
%% Simulation runs and space-time matrix formation
chaniter = 20; % Channel changes every niter iterations

%% load dispersion matrix Q
if strcmp (coding, 'ON')
disp('This is coded OFDM STSK system')
if M == 4
load(strcat('Q',num2str(Nt),num2str(Nr),num2str(T),num2str(Q), 'qpsk', '.mat'))
for q = 1:Q
A_q{q} = DM(1:Nt, (q-1)*T+1:q*T);
end
elseif M == 8
load(strcat('Q',num2str(Nt),num2str(Nr),num2str(T),num2str(Q), '8psk', '.mat'))
for q = 1:Q
A_q{q} = DM(1:Nt, (q-1)*T+1:q*T);
end
%    elseif M==64
%         load(strcat('Q',num2str(Nt),num2str(Nr),num2str(T),num2str(Q), '16psk', '.mat'))
%        for q = 1:Q
%           A_q{q} = DM(1:Nt, (q-1)*T+1:q*T);
end
```

```
else
disp('This is OFDM STSK system')
load(strcat('Q',num2str(Nt),num2str(Nr),num2str(T),num2str(Q), 'qpsk', '.mat'))
if Nt == 8
for q = 1:Q
A_q{q} = Q8888(1:Nt, (q-1)*T+1:q*T);
end
elseif Nt == 4
for q = 1:Q
A_q{q} = DM(1:Nt, (q-1)*T+1:q*T);
end
else
for q = 1:Q
A_q{q} = DM(1:Nt, (q-1)*T+1:q*T);
end
end
end

error_snr = zeros(length(snr),1);

for cc = 1:chaniter
%% Channel Channel
if strcmp(CHAN, 'MMW')

if strcmp(env_condition, 'NLOS');

addpath('C:\Users\ADMIN\Desktop\Papers\OFDM_Chrianus_working_STSK 2\ChannelFolder_NLOS');
chanMat = strcat('Sampled_delaySpread_73_GHz_Outdoor_ ', num2str(Nt), 'x', num2str(Nr), '_',
num2str(cc), '_CIRs', '.mat');
load(chanMat);
else
addpath('C:\Users\ADMIN\Desktop\Papers\OFDM_Chrianus_working_STSK 2\ChannelFolder_LOS');
chanMat = strcat('Sampled_delaySpread_73_GHz_Outdoor_ ', num2str(Nt), 'x', num2str(Nr), '_',
num2str(cc), '_CIRs', '.mat');
load(chanMat);
end

Hvec = sampled_delaySpread;
% %       Hvec = mmWaveChanFunc(Nt, Nr, BW);
CP_len = length(Hvec)+20; % Cyclic prefix

idx_woCP = CP_len+1:Nifft+CP_len;
if strcmp(phaseNoise, 'ON')
hPhNoise = comm.PhaseNoise('Level', phn_psd, 'FrequencyOffset', off_vect, 'SampleRate', BW);

end
elseif strcmp(CHAN, 'IID')
CP_len = 150; % Cyclic prefix
idx_woCP = CP_len+1:Nifft+CP_len;

chanseed = randi([1,100], 1,1);
       fd = 0;
Ts = 1/1e6; % Sampling time
impulse_samples = [0 1 2 3 5]; % impulse samples
%        impulse_samples = 0;
Tau = impulse_samples*Ts;
```

```
pdB = [0 -2 -5 -9 -10]; % in dB
%       pdB = 0; % in dB

hMIMOChan = comm.MIMOChannel(...
'SampleRate',               1/Ts,...
'PathDelays',               Tau,...
'AveragePathGains',         pdB,...
'MaximumDopplerShift',      fd,...
'TransmitCorrelationMatrix', eye(Nt),...
'ReceiveCorrelationMatrix',  eye(Nr),...
'RandomStream',             'mt19937ar with seed',...
'Seed',                     chanseed,...
'NormalizePathGains',       true,...
'PathGainsOutputPort',      true);
elseif strcmp(CHAN, 'NO')
Hvec = 1;
CP_len = 0; % Cyclic prefix
idx_woCP = CP_len+1:Nifft+CP_len;
end
%% Monte Carlo simulation starts here

for jj = 1:length(snr)
error_niter_zf = zeros(niter , 1);
error_niter_mmse = zeros(niter , 1);
snr_lin = block_size/T*10.^(snr1(jj)/10);
for ii = 1:niter
%% Generation and modulation
if strcmp(coding, 'ON')
intial_bits = (randi([0 1], block_size*Nifft, 1));

coded_data = convenc(intial_bits,trellis);
inter = randintrlv(coded_data,str2); % Interleave

QnM = reshape(inter, Nifft, block_size/coderate);
Q_no = QnM(:, 1:log2(Q));
M_stream = QnM(:, log2(Q)+1:end);

mappedSymbol = 1/sqrt(modConst)*step(hModulator, M_stream(:));
else
intial_bits = (randi([0 1], block_size*Nifft, 1));
QnM = reshape(intial_bits, Nifft, block_size);
Q_no = (QnM(:, 1:log2(Q)));
M_stream = (QnM(:, log2(Q)+1:end));

mappedSymbol = 1/sqrt(modConst)*step(hModulator, M_stream(:));
end
st_block = complex(zeros(Nt*Nifft, T)); % ST block initialized
ofdmTxIn = [];
%% STSK mapping and OFDM symbol making
for jj_ifft = 1:Nifft
take_one_col = Q_no(jj_ifft, :);
convert_decimal = bi2de(take_one_col, 'left-msb') + 1; % +1 is to remove 0
st_block(((jj_ifft-1)*Nt+1):(Nt*jj_ifft), :) = mappedSymbol(jj_ifft)*A_q{convert_decimal};
end
ofdmTx = complex(zeros(Nifft+CP_len, Nt, T));
for jj_tx = 1:Nt
```

```
st_block1 = st_block(jj_tx:Nt:end, :);
ifft_ant = sqrt(Nifft)*(ifft(st_block1, [], 1)) ;% size is NifftxT

ofdmTxIn = [ifft_ant(Nifft-CP_len+1:Nifft, :);   ifft_ant] ;% CP is added

%% Phase noise and power amplifier
for t = 1:T
ofdmTxIdeal = ofdmTxIn(:, t);
papr_t(1, t) = (max(abs(ofdmTxIdeal).^2)/mean(abs(ofdmTxIdeal).^2));
if strcmp(PowAmp, 'ON')
[ofdmTx(:, jj_tx, t),  cons, clip_noise(jj_tx, t)] = rappModel(ofdmTxIdeal, IBO, Nt, T);
elseif strcmp(PowAmp, 'OFF')
ofdmTx(:, jj_tx, t) = ofdmTxIdeal ;
cons = 1;
end
end % Nt
end

var_sig = Nt;
%% MIMO channel modeling & AWGN
faded_noisy_signal = complex(zeros(Nifft+CP_len, Nr, T));       % Pre-allocations
chan_FR = complex(zeros(Nifft, Nt*Nr));                         % Pre-allocations

if strcmp(CHAN, 'IID')
for t = 1:T

[faded_signal(:, :, t), chanPGs] = step(hMIMOChan, ofdmTx(:,:, t));

y_awgn = 1/sqrt(2)*(randn(length(faded_signal),Nr)+1i*randn(length(faded_signal),Nr));
resultant_signal_variace = var_sig;
faded_noisy_signal(:, :, t) = faded_signal(:, :, t) + sqrt(resultant_signal_variace/snr_lin)*y_awgn;
kk = 0;
for jj_tx = 1:Nt
for jj_rx = 1:Nr
kk = kk+1;
chan_sampled(kk, impulse_samples+1) = mean(chanPGs(:,:,jj_tx,jj_rx));
chan_FR(:, kk, t) = (fft(chan_sampled(kk, :), Nifft)); % Frequency response of Tx1 to Rx1
end
end
end
elseif strcmp(CHAN, 'MMW')
% Millimeter wave channel MIMO Channel is added here
for t = 1:T
kk = 0;
faded_signal_PN    = complex(zeros(Nifft+CP_len, Nr));       % Pre-allocations
for jj_tx = 1:Nt
for jj_rx = 1:Nr
kk = kk +1;
Hvec(kk, :) = Hvec(kk, :)./sqrt(sum(abs(Hvec(kk, :)).^2));
faded_signal =  filter(transpose(Hvec(kk, :)), 1, ofdmTx(:, jj_tx, t));
if strcmp (phaseNoise, 'ON')
faded_signal_PN(:, jj_rx) = faded_signal_PN(:, jj_rx) + step(hPhNoise, faded_signal);
elseif strcmp (phaseNoise, 'OFF')
faded_signal_PN(:, jj_rx) = faded_signal_PN(:, jj_rx) + faded_signal;
end
```

```
chan_FR(:, kk) = (fft(Hvec(kk, :), Nifft, 2)); % Frequency response of Tx1 to Rx1
end
end
y_awgn = 1/sqrt(2)*(randn(length(faded_signal), Nr)+1i*randn(length(faded_signal), Nr));
resultant_signal_variace = var_sig;
faded_noisy_signal(:, :, t) = faded_signal_PN + sqrt(resultant_signal_variace/snr_lin)*y_awgn;
end
elseif strcmp(CHAN, 'NO')
% MIMO Channel is added here
faded_signal_PN    = complex(zeros(Nifft+CP_len, Nr,T));
chan_FR = ones(Nifft, Nt*Nr, T); % Frequency response of Tx1 to Rx1
for t = 1:T
for jj_tx = 1:Nt
for jj_rx = 1:Nr
faded_signal =  filter(1, 1, ofdmTx(:, jj_tx, t));
faded_signal_PN(:, jj_rx, t) = faded_signal_PN(:, jj_rx, t) + faded_signal;
end
end
% Adding noise
y_awgn = 1/sqrt(2)*(randn(length(faded_signal_PN), Nr)+1i*randn(length(faded_signal_PN), Nr));
resultant_signal_variace = var_sig;
faded_noisy_signal(:, :, t) = (faded_signal_PN(:, :, t)) + sqrt(resultant_signal_variace/snr_lin)*y_awgn;
end
end
%% CP removal and OFDM demodulation

ofdmRx_fft  = complex(zeros(Nifft, Nr, T)); % Preallocating
ofdmRx = complex(zeros(Nr, Nifft, T));
for t = 1:T
for jj_rx = 1:Nr
ofdmRx_noCP = faded_noisy_signal(idx_woCP, jj_rx, t);
ofdmRx_fft(:, jj_rx, t) = 1/sqrt(Nifft)*(fft(ofdmRx_noCP, Nifft, 1)); % FFT operation
end
ofdmRx(:, :, t) = (transpose(ofdmRx_fft(:, :, t)));
end

%% Detection
if strcmp(detector, 'ML')
[Q_error_ml, Est_bit_ml] = ...
MLdetectr( chan_FR, Nt, Nr, ofdmRx, Nifft, A_q, Q, Q_no, T, cons, M);
Dispersion_error_ml= length(find(Q_error_ml' - Q_no));

if strcmp(coding, 'ON')
if M == 4
Q_error_ml1 = Q_error_ml';

reshaped_Q_error_ml = reshape(Q_error_ml1, log2(Q)*Nifft, 1);

Demod_ML = step(hDemod, Est_bit_ml);

concentenated_codedML_bits = [reshaped_Q_error_ml; Demod_ML];

Est_bit_ml_deInterleave =  randdeintrlv(concentenated_codedML_bits, str2); % Deinterleave.

decodedData_ml = vitdec(Est_bit_ml_deInterleave, trellis, tbl,'trunc','hard');
```

```
error_niter_ml(ii, 1) = length(find(decodedData_ml - intial_bits)) ;
elseif M == 8
Demod_ML = step(hDemod, Est_bit_ml);
decodedData_ml = Demod_ML((2*tbl+1):end);
Bit_error_ml = length(find((decodedData_ml - bits_tx(1:end-(2*tbl)))));
error_niter_ml(ii, 1)  = Bit_error_ml + Dispersion_error_ml;   % Error calculated
end
else % Coding
Demod_ML = step(hDemod, Est_bit_ml);
Bit_error_ml = length(find((Demod_ML - M_stream(:))));
error_niter_ml(ii, 1)  = Bit_error_ml + Dispersion_error_ml;   % Error calculated
end

elseif strcmp(detector, 'linear')
        [ Q_error_zf,  Q_error_mmse, Est_bit_zf, Est_bit_mmse] = ...
                            ismatProposedDetector(chan_FR, Nt, Nr, ofdmRx, Nifft, A_q, Q, Q_no, T,
resultant_signal_variace, snr_lin, M, cons);

%         Dispersion_error_zf = length(find(Q_error_zf(:) - Q_no(:)));
%         Dispersion_error_mmse = length(find(Q_error_mmse(:) - Q_no(:)));

if strcmp(coding, 'ON')
reshaped_Q_error_mmse = reshape(Q_error_mmse, log2(Q)*Nifft, 1);
reshaped_Q_error_zf = reshape(Q_error_zf, log2(Q)*Nifft, 1);

Demod_zf = step(hDemod, Est_bit_zf);
Demod_mmse = step(hDemod, Est_bit_mmse);

concentenated_codedMMSE_bits =  [reshaped_Q_error_mmse; Demod_mmse];
concentenated_codedZF_bits =  [reshaped_Q_error_zf; Demod_zf] ;

Est_bit_mmse_deInterleave =  randdeintrlv(concentenated_codedMMSE_bits ,str2); % Deinterleave.
Est_bit_zf_deInterleave =  randdeintrlv(concentenated_codedZF_bits, str2); % Deinterleave.

decodedData_zf = vitdec(Est_bit_zf_deInterleave, trellis, tbl,'trunc','hard');
decodedData_mmse = vitdec(Est_bit_mmse_deInterleave, trellis, tbl,'trunc','hard');

%             error_niter_mmse(ii, 1)  = length(find(decodedData_mmse - M_stream)) +
Dispersion_error_mmse;   % Error calculated
%             error_niter_zf(ii, 1)  = length(find(decodedData_zf - M_stream)) + Dispersion_error_zf;   %
Error calculated
error_niter_mmse(ii, 1)  = length(find(decodedData_mmse - intial_bits));   % Error calculated
error_niter_zf(ii, 1)  = length(find(decodedData_zf - intial_bits));   % Error calculated

else
Demod_zf = step(hDemod, Est_bit_zf);
Demod_mmse = step(hDemod, Est_bit_mmse);

Bit_error_zf = length(find(Demod_zf - M_stream(:))); % Constellation error
Bit_error_mmse = length(find(Demod_mmse - M_stream(:)));

Dispersion_error_zf = length(find(Q_error_zf(:) - Q_no(:)));
Dispersion_error_mmse = length(find(Q_error_mmse(:) - Q_no(:)));

error_niter_zf(ii, 1)  = Bit_error_zf +  Dispersion_error_zf;  % Error calculated
error_niter_mmse(ii, 1)  = Bit_error_mmse + Dispersion_error_mmse;   % Error calculated
```

```
end
elseif strcmp(detector, 'all')
[ Q_error_ml, Est_bit_ml ] = ...
MLdetectr( chan_FR, Nt, Nr, ofdmRx, Nifft, A_q, Q, Q_no, T, cons, M);
[ Q_error_zf,  Q_error_mmse, Est_bit_zf, Est_bit_mmse] = ...
ismatProposedDetector(chan_FR, Nt, Nr, ofdmRx, Nifft, A_q, Q, Q_no, T, resultant_signal_variace,
snr_lin, M, cons);
Dispersion_error_zf = length(find(Q_error_zf ~= 0));
Dispersion_error_mmse = length(find(Q_error_mmse ~= 0));
Dispersion_error_ml= length(find(Q_error_ml ~= 0));

if strcmp(coding, 'ON')
Demod_zf = step(hDemod, Est_bit_mmse);
Demod_mmse = step(hDemod, Est_bit_zf);
Demod_ML = step(hDemod, Est_bit_ml);

Est_bit_mmse_deInterleave =  randdeintrlv(Demod_mmse ,st2); % Deinterleave.
Est_bit_zf_deInterleave =  randdeintrlv(Demod_zf, st2); % Deinterleave.
Est_bit_ml_deInterleave =  randdeintrlv(Demod_ML ,st2); % Deinterleave.

decodedData_zf = vitdec(Est_bit_zf_deInterleave,trellis,tbl,'trunc','hard');
decodedData_mmse = vitdec(Est_bit_mmse_deInterleave,trellis,tbl,'trunc','hard');
decodedData_ml = vitdec(Est_bit_ml_deInterleave,trellis,tbl,'trunc','hard');

Bit_error_zf = length(find(decodedData_zf - bits_tx));
Bit_error_mmse = length(find(decodedData_mmse - bits_tx));
Bit_error_ml = length(find(decodedData_ml - bits_tx));

error_niter_mmse(ii, 1)  = Bit_error_mmse + Dispersion_error_mmse;   % Error calculated
error_niter_zf(ii, 1)  = Bit_error_zf + Dispersion_error_zf;   % Error calculated
error_niter_ml(ii, 1)  = Bit_error_ml + Dispersion_error_ml;   % Error calculated
else

Bit_error_ml = length(find(round(Est_bit_ml - mappedSymbol)~=0));
Bit_error_zf = length(find(round(Est_bit_zf - mappedSymbol) ~= 0)); % Constellation error
Bit_error_mmse = length(find(round(Est_bit_mmse - mappedSymbol)~=0));

error_niter_ml(ii, 1)  = Bit_error_ml + Dispersion_error_ml;   % Error calculated
error_niter_zf(ii, 1)  = Bit_error_zf +  Dispersion_error_zf;  % Error calculated
error_niter_mmse(ii, 1)  = Bit_error_mmse + Dispersion_error_mmse;   % Error calculated
end
end

end % niter
if strcmp(detector, 'ML')

BER_ml(jj, cc) = sum(error_niter_ml)/(block_size*Nifft*niter)

elseif strcmp(detector, 'linear')
BER_zf(jj, cc) = sum(error_niter_zf)/(block_size*Nifft*niter);
BER_mmse(jj, cc) = sum(error_niter_mmse)/(block_size*Nifft*niter)
elseif strcmp(detector, 'all')
BER_zf(jj, cc) = sum(error_niter_zf)/(block_size*Nifft*niter)
```

```
BER_mmse(jj, cc) = sum(error_niter_mmse)/(block_size*Nifft*niter)
BER_ml(jj, cc) = sum(error_niter_ml)/(block_size*Nifft*niter)
end
end % snr loop
end % chan loop

%% Saving MAT file
if strcmp(detector, 'ML')
BERml_chaniter = [(snr)' sum(BER_ml, 2)/chaniter]
semilogy(BERml_chaniter(:,1), BERml_chaniter(:,2))

filename = strcat('BERml_chan_CodedAWGN', num2str(Nt), num2str(Nr), num2str(T), num2str(Q), '_',
num2str(IBO), 'dB', '_', num2str(PN1), num2str(PN2), '_', 'coded', env_condition);
save(filename, 'BERml_chaniter')

elseif strcmp(detector, 'linear')
BERzf_chaniter = [snr' sum(BER_zf, 2)/chaniter];
BERmmse_chaniter = [(snr)' sum(BER_mmse, 2)/chaniter];

semilogy(BERmmse_chaniter(:,1), BERmmse_chaniter(:,2))
filename = strcat('BERmmse_chan_UNcodedmmWave', num2str(Nt), num2str(Nr), num2str(T),
num2str(Q), '_', num2str(IBO), 'dB', '_', num2str(PN1), num2str(PN2), '_', 'coded',env_condition);
save(filename, 'BERmmse_chaniter')
elseif strcmp(detector, 'all')
BERzf_chaniter = [snr' sum(BER_zf, 2)/chaniter];
BERmmse_chaniter = [snr' sum(BER_mmse, 2)/chaniter];
BERml_chaniter = [snr' sum(BER_ml, 2)/chaniter];

filename1 = strcat('BERmmse_chan', num2str(Nt), num2str(Nr), num2str(T), num2str(Q), '_',
num2str(IBO), 'dB', '_', num2str(PN1), num2str(PN2), '_', 'coded', env_condition);
filename2 = strcat('BERmzf_chan', num2str(Nt), num2str(Nr), num2str(T), num2str(Q), '_', num2str(IBO),
'dB', '_', num2str(PN1), num2str(PN2), '_', 'coded', env_condition);
filename3 = strcat('BERml_chan', num2str(Nt), num2str(Nr), num2str(T), num2str(Q), '_', num2str(IBO),
'dB', '_', num2str(PN1), num2str(PN2), '_', 'coded', env_condition);

save(filename1, 'BERmmse_chaniter')
save(filename2, 'BERzf_chaniter')
save(filename3, 'BERml_chaniter')

end

disp('Files are saved !!!!')
disp('This is OFDM STSK system')
disp(env_condition)

disp(strcat('Nt :', num2str(Nt), ' Nr : ', num2str(Nr)))
if strcmp(PowAmp, 'ON')
disp(strcat('Power Amplifier :', PowAmp, ' Input BACKOFF : ', num2str(IBO), 'dB'))
end
if strcmp(coding, 'ON')
disp('***Coding is ON***')
end
if strcmp(phaseNoise, 'ON')
disp(strcat('Phase noise is ON', num2str(PN1), num2str(PN2)))
end
%}
```

II. CE-OFDM STSK Matlab Programing Code

```
%close all
%clear all
%clc
% This code is prepared by Chrianus Kyaruzi Kajuna
%Department of Electrical Engineering
%Pan Africa University
%December 2017
%Simulation for constant envelope OFDM STSK with MMSE detection
%% ------------------------Configuration of the system--------------------
if Nt == 8
Nr = 8;
elseif Nt == 4
Nr = 4;
else
Nr = 2;
end

%% ------------------------Channel setting-------------------------------

snr= 0:2:30;
CHAN='NO';% NO or MMW
env_condition='LOS';%LOS or NLOS

%% ------------------------Receiver Setting----------------------------

equalizer_type='MMSE';%Equalizer Type: MMSE or ZF
detector='ML';% ML

%% ---------------------------------------%% Modulation and coding parameters---------
if strcmp (coding, 'ON')


M = 4; % 4 for QPSK; 2 for BPSK
modConst = 2; % modulation constant
block_size = log2(Q) + log2(M);
hModulator =  comm.RectangularQAMModulator(M,'BitInput',true);
hDemod = comm.RectangularQAMDemodulator('ModulationOrder', M, 'BitOutput', true);
end

%% ----------------------------------%% Simulation runs ------------ ----------------%
chaniter = 200; % Channel changes every niter iterations
niter = 100;

%% ----------------------------%% load dispersion matrix Q-----------------------
if strcmp (coding, 'ON')
disp('This is coded MIMO CEOFDM STSK system')
load(strcat('Q',num2str(Nt),num2str(Nr),num2str(T),num2str(Q), 'qpsk', '.mat'))
for q = 1:Q
A_q{q} = DM(1:Nt, (q-1)*T+1:q*T);
```

```
end
else
disp('This is MIMO CEOFDM STSK system')
load(strcat('Q',num2str(Nt),num2str(Nr),num2str(T),num2str(Q), 'qpsk', '.mat'))
if Nt == 8
for q = 1:Q
A_q{q} = Q8888(1:Nt, (q-1)*T+1:q*T);
end
elseif Nt == 4
for q = 1:Q
A_q{q} = DM(1:Nt, (q-1)*T+1:q*T);
end
else
for q = 1:Q
A_q{q} = DM(1:Nt, (q-1)*T+1:q*T);
end
end
end
%% ------------------------------Monte Carlo Simulation-----------------------
for cc = 1:chaniter

%% ---------------------------------%% CHANNEL PROPERTIES-------------------------------------%

if strcmp(CHAN, 'MMW')

if strcmp(env_condition, 'NLOS');

addpath('C:\Users\ADMIN\Desktop\Papers\OFDM_Chrianus_working_STSK 2\ChannelFolder_NLOS');
chanMat = strcat('Sampled_delaySpread_73_GHz_Outdoor_ ', num2str(Nt), 'x', num2str(Nr), '_',
num2str(cc), '_CIRs', '.mat');
load(chanMat);
else
addpath('C:\Users\ADMIN\Desktop\Papers\OFDM_Chrianus_working_STSK 2\ChannelFolder_LOS');
chanMat = strcat('Sampled_delaySpread_73_GHz_Outdoor_ ', num2str(Nt), 'x', num2str(Nr), '_',
num2str(cc), '_CIRs', '.mat');
load(chanMat);
end

Hvec = sampled_delaySpread;
CP_len = length(Hvec)+20; % Cyclic prefix
idx_woCP = CP_len+1:Nifft+CP_len;
%
elseif strcmp(CHAN, 'NO') %AWGN
Hvec = 1;
CP_len = 0; % Cyclic prefix
idx_woCP = CP_len+1:Nifft+CP_len;
end
%% ----------------------------------%% Monte Carlo simulation starts here -----------
%
for jj = 1:length(snr)
error_niter_zf = zeros(niter , 1);
error_niter_mmse = zeros(niter , 1);
EsN0_lin = block_size/T.*EbN0_lin;
for ii = 1:niter
%% --------------------------------- %% Coding and modulation----------------------------------
```

```
if strcmp(coding, 'ON')
intial_bits = (randi([0 1], block_size*Nqam, 1));

coded_data = convenc(intial_bits, trellis);
inter = randintrlv(coded_data,str2); % Interleave

QnM = reshape(inter, Nqam, block_size/coderate);
Q_no = QnM(:, 1:log2(Q));

M_stream = QnM(:, log2(Q)+1:end);

mappedSymbol = 1/sqrt(modConst)*step(hModulator, M_stream(:));
else
intial_bits = (randi([0 1], block_size*Nqam, 1));
QnM = reshape(intial_bits, Nqam, block_size);
Q_no = QnM(:, 1:log2(Q));
M_stream = (QnM(:, log2(Q)+1:end));
mappedSymbol = 1/sqrt(modConst)*step(hModulator, M_stream(:));
end
%% ---------------------------------------ST block initialized ----------------------%

st_block = complex(zeros(Nt*Nqam, T)); % ST block initialized

ofdmTxIn = [];

%% --------------------------------%% STSK mapping and OFDM symbol making--------%%
for jj_ifft = 1:Nqam
take_one_col = Q_no(jj_ifft, :);
convert_decimal = bi2de(take_one_col, 'left-msb') + 1; % +1 is to remove 0
st_block(((jj_ifft-1)*Nt+1):(Nt*jj_ifft), :) = mappedSymbol(jj_ifft)*A_q{convert_decimal};
end

for jj_tx = 1:Nt
for  u=1:T
st_block1(:,jj_tx,u) = st_block(jj_tx:Nt:end, u);

[message,norm_factor] = real_valued(st_block1(:,jj_tx,u), Nqam, M, Nt, Nifft,'OFDMA'); %
MYASSUMPTION
message_normalized(:,jj_tx,u)=(message);
% ------------------ %% PHASE MODULATION----------------------------------------------------%
As=1;                                %message amplitude
ifft_ant(:,jj_tx,u)= As/sqrt(Nt) * exp(1i*2*pi*modh*message_normalized(:,jj_tx,u)); % CE-OFDM signal

%% ----------------------------%% ADD CP--------------%
ofdmTxIn(:,jj_tx,u) = [  ifft_ant(Nifft-CP_len+1:Nifft,  jj_tx,u);   ifft_ant(:,jj_tx,u)] ;

%% ----------------------------%% Phase noise and power amplifier-----------------------------%
ofdmTxIdeal = ofdmTxIn(:, jj_tx,u);
papr_t(1, u) = (max(abs(ofdmTxIdeal).^2)/mean(abs(ofdmTxIdeal).^2));
if strcmp(phaseNoise, 'ON')
hPhNoise = comm.PhaseNoise('Level', phn_psd, 'FrequencyOffset', off_vect, 'SampleRate', BW);
end

if strcmp(PowAmp, 'ON')
[ofdmTx(:, jj_tx,u),  cons, clip_noise(jj_tx,u)] = rappModel_CE(ofdmTxIdeal, IBO, Nt, T);
elseif strcmp(PowAmp, 'OFF')
```

```
ofdmTx(:, jj_tx,u) = ofdmTxIdeal ;
cons = 1;
end
end
end

%% ----------------------------------------CHANNEL BLOCK-----------------%

%% MIMO channel modeling & AWGN
faded_noisy_signal = complex(zeros(Nifft+CP_len,  Nr,T));       % Pre-allocations

faded_signal_PN    = complex(zeros(Nifft+CP_len, Nr,T));       % Pre-allocations

chan_FR =ones(Nifft, Nt*Nr, T); % Frequency response of Tx1 to Rx1

if  strcmp(CHAN, 'MMW')
% Millimeter wave channel MIMO Channel is added here
Hvec1=Hvec;
Hvec2=[];
for t = 1:T
kk = 0;

for jj_tx = 1:Nt
for jj_rx = 1:Nr
kk = kk +1;
Hvec2(kk, :) = Hvec1(kk, :)./sqrt(sum(abs(Hvec1(kk, :)).^2));
faded_signal =  filter(transpose(Hvec2(kk, :)), 1, ofdmTx(:, jj_tx, t));
if strcmp (phaseNoise, 'ON')
faded_signal_PN(:, jj_rx,t) = faded_signal_PN(:, jj_rx,t) + step(hPhNoise, faded_signal);
elseif strcmp (phaseNoise, 'OFF')
faded_signal_PN(:, jj_rx,t) = faded_signal_PN(:, jj_rx,t) + faded_signal;
end
% chan_FR(:, kk) = (fft(Hvec.ir{kk}, Nifft, 2)); % Frequency response of Tx1 to Rx1
chan_FR(:, kk,t) = (fft(Hvec2(kk, :), Nifft, 2)); % Frequency response of Tx1 to Rx1
end
end
y_awgn = 1/sqrt(2)*(randn(length(faded_signal), Nr)+1i*randn(length(faded_signal), Nr));
var_sig = Nt/cons;
N0=var_sig/EsN0_lin;
faded_noisy_signal(:, :, t) = faded_signal_PN(:,:,t) + sqrt(N0)*y_awgn;
end
elseif strcmp(CHAN, 'NO')
% MIMO Channel is added her
faded_signal_PN    = complex(zeros(Nifft+CP_len, Nr,T));
chan_FR = ones(Nifft, Nt*Nr, T); % Frequency response of Tx1 to Rx1
for t = 1:T
for jj_tx = 1:Nt
for jj_rx = 1:Nr
%                       if (jj_tx*jj_rx)==2
if (jj_tx~=jj_rx)
faded_signal= zeros(Nifft,1);
else
faded_signal =  filter(1, 1, ofdmTx(:, jj_tx,t));
end
faded_signal_PN(:, jj_rx,t) = faded_signal_PN(:, jj_rx,t) + faded_signal;
end
```

```
end
% Adding noise
y_awgn = 1/sqrt(2)*(randn(length(faded_signal_PN), Nr)+1i*randn(length(faded_signal_PN), Nr));
var_sig= Nt/cons;
N0=var_sig/EsN0_lin;
faded_noisy_signal(:,  :,t) = (faded_signal_PN(:,  :,t)) + sqrt(N0)*y_awgn;
end
end
%% --------------------------------RECEIVER-----------------------------------------------%
%% ----------------------------%% CP removal ------------------------------%
ofdmRx = complex(zeros(Nr, Nqam, T));
for t = 1:T
for jj_rx = 1:Nr
ofdmRx_noCP(:, jj_rx, t) = faded_noisy_signal(idx_woCP, jj_rx,t);
end
end
%% ----------------------------Frequency Domain Equalization ----------------------
if strcmp(CHAN,'MMW')
RX_noCP=fft(ofdmRx_noCP,Nifft,1);
for t=1:T
for n=1:Nifft
Y=transpose(RX_noCP(n,:,t));

H=(reshape(chan_FR(n,:,t),Nr,Nt));

if strcmp(equalizer_type,'ZF')
Y_equalized(n,:,t)=(H'*H)\(H'*Y);
elseif strcmp(equalizer_type,'MMSE')
Y_equalized(n,:,t)=(H'*H+N0.*eye(Nt))\(H'*Y);

end
end

S_equalized(:,:,t)=ifft(Y_equalized(:,:,t),Nifft,1);
%%---------------------------- Phase demodulation --------%
S_unwrap(:,:,t)=(angle(cons.*S_equalized(:,:,t))./(2*pi*modh);

% --------------------------- OFDM demodulation and subcarrier extraction---------%
S_Detect_In(:,:,t)=(sqrt(norm_factor*2*Nqam)/Nifft).*fft(S_unwrap(:,:,t),Nifft,1);
S_wo_Z(:,:,t)=S_Detect_In(2:Nqam+1,:,t);
end
elseif strcmp(CHAN,'NO')
S_unwrap=angle(cons.*ofdmRx_noCP)./(2*pi*modh);
S_Detect_In=(sqrt(norm_factor*2*Nqam)/Nifft).*fft(S_unwrap,Nifft,1);
S_wo_Z=S_Detect_In(2:Nqam+1,:,:);

end

%% ---------------------Prepareing the input of STSK detector ----------------------
St_Detect_In=zeros(Nqam*Nt,T);
for t=1:T
for jj_tx=1:Nt
St_Detect_In(jj_tx:Nt:end,t)=S_wo_Z(:,jj_tx,t);
end
end
```

```
%% ------------------------------------%% Detection----------------------------------%

[Q_error_ml, Est_bit_ml] =MLdetec_CEOFDM( Nt, Nr,St_Detect_In, Nqam, A_q, Q, Q_no, T, M)
if strcmp(coding, 'ON')

% reshaped_Q_error_ml = transpose(Q_error_ml);

Demod_ML = step(hDemod, Est_bit_ml);

concentenated_codedMMSE_bits =  [reshaped_Q_error_ml(:); Demod_ML];

%% ---------------------------------- Deinterleaver ----------------------------------------%

Est_bit_ml_deInterleave =  randdeintrlv(concentenated_codedMMSE_bits, str2); % Deinterleave.

% --------------------------------- Decoder---- ------- -------------------------------%
decodedData_ml = vitdec(Est_bit_ml_deInterleave, trellis, tbl,'trunc','hard');
%%---------------------------------- Calculating error -------%
error_niter_ml(ii, 1) = length(find(decodedData_ml - intial_bits));   % Error calculated
else
Demod_ml = step(hDemod, Est_bit_ml);
Bit_error_ml = length(find(Demod_ml - M_stream(:)));

reshaped_Q_error_ml = transpose(Q_error_ml);
Dispersion_error_ml= length(find(reshaped_Q_error_ml(:) - Q_no(:)));
error_niter_ml(ii, 1)  = Bit_error_ml + Dispersion_error_ml;   % Error calculated
end

end% niter (ii)
if strcmp(detector, 'ML')
BER_ml(jj, cc) = sum(error_niter_ml)/(block_size*Nqam*niter)
end
%
end% snr (jj)
end %chaniter (cc)
%% -------------- drawing----------------------------
if strcmp(detector, 'ML')

BERml_chaniter= [snr' sum(BER_ml, 2)/chaniter];

semilogy(BERml_chaniter(:,1), BERml_chaniter(:,2))
%     filename='4X4_T4MMW_codedceofdmONPA_3.mat';
%     save(filename)
filename = strcat('BERml_chan_coded1.5', num2str(Nt), num2str(Nr), num2str(T), num2str(Q),);
save(filename, 'BERml_chaniter')
elseif strcmp(detector, 'linear')
BERzf_chaniter = [snr' sum(BER_zf, 2)/chaniter];
BERmmse_chaniter = [snr' sum(BER_mmse, 2)/chaniter];
figure
semilogy(BERmmse_chaniter(:,1), BERmmse_chaniter(:,2))
end
```

III. Publication